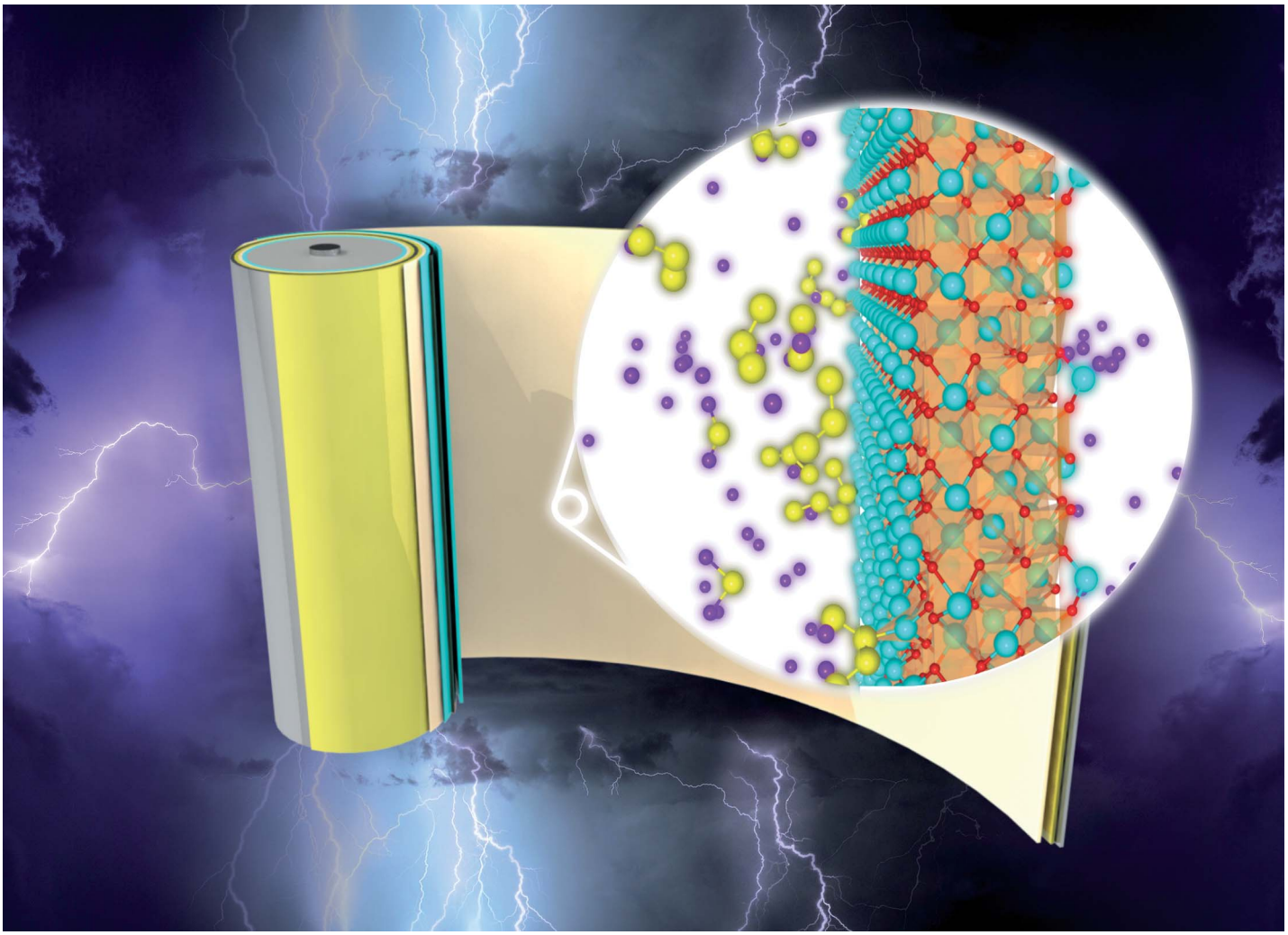

Showcasing research from Professor Rajkumar's laboratory, Integrated Science and Engineering Division, Underwood International College, Yonsei University International Campus, Incheon, South Korea.

Recent advances in modified commercial separators for lithium-sulfur batteries

Conducting polymer are a special class of polymer which are electrically conducting due to the presence of conjugated double bonds. When a separator is modified with conducting polymer it reduces the porosity of the commercial polyolefin separator as a result, lithium polysulfide mobility through the pore reduced drastically. Conducting polymers are synthesized and applied in various applications such as supercapacitor, battery and water splitting etc.

As featured in:

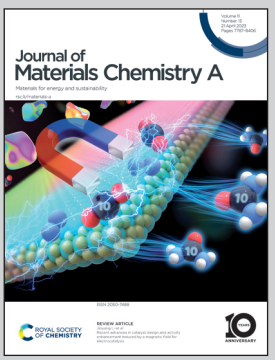

See Rajkumar Patel *et al.*, *J. Mater. Chem. A,* 2023, **11**, 7833.

ROYAL SOCIETY OF CHEMISTRY

rsc.li/materials-a

Registered charity number: 207890

Journal of Materials Chemistry A

REVIEW

View Article Online
View Journal | View Issue

Cite this: J. Mater. Chem. A, 2023, 11, 7833

Recent advances in modified commercial separators for lithium–sulfur batteries

Andrew Kim, [a] Seok Hyeon Oh,[b] Arindam Adhikari, [cd] Bhaskar R. Sathe, [e] Sandeep Kumar[f] and Rajkumar Patel *[g]

Received 29th November 2022
Accepted 27th February 2023

DOI: 10.1039/d2ta09266b

rsc.li/materials-a

Lithium–sulfur batteries (LSBs) are one of the most promising next-generation batteries because they have higher theoretical capacities, lower cost, and smaller environmental impact than lithium-ion batteries (LIBs). However, one of the main issues preventing widespread LSB adoption is its low cycle stability due to the formation and diffusion of intermediate lithium polysulfides (LiPSs). Some of the most cutting-edge advancements of LSBs address this issue by using functional separators modified from commercial polyolefin separators used in most LIBs. Popular and promising modifiers include (a) many functionalized or conducting polymers, (b) different carbon nanostructures like graphene or carbon nanotubes, (c) covalent–organic or metal–organic frameworks, and (d) various inorganic modifiers like metal oxides and MXenes. This review analyzes the latest insights into designing and fabricating modified polyolefin membranes that minimize polysulfide shuttling in LSBs. Other benefits, including enhanced rate capability, specific capacity, sulfur utilization, electrolyte wettability, Li-ion conductivity, thermal resilience, and structural integrity, are also discussed.

1 Introduction

The increasing popularity of electric vehicles, dependence on portable technology, and recent global crises have brought battery technology innovation to the forefront. Increased production in electric vehicles has required major developments in LIB technology, emphasizing energy density, charge rate, and safety.[1,2] The coronavirus disease (COVID-19) pandemic that started in 2020 caused millions of workers and students to become more dependent on phones, laptops, and other portable information technologies powered primarily by LIBs.[3,4] Russia's invasion of Ukraine in 2022 led to many European nations facing energy shortages,[5,6] emphasizing the need to develop energy storage technologies to facilitate renewable energy adoption, including solar,[7–11] thermoelectric,[12] microbial,[13] and hydrogen[14–18] power. LIBs and their derivatives currently dominate the battery market for portable electronics and large-scale energy storage.[19–21] However, new energy storage technologies like supercapacitors[22–24] with high power densities and next-generation batteries[25–28] with large energy densities derived from low-cost and environmentally friendly materials are necessary to meet the exponentially rising energy storage demands.

Among the candidates for next-generation batteries, lithium–sulfur batteries (LSBs) are especially promising for their high theoretical capacity, natural abundance, and safety.[29,30] LSBs have a theoretical energy density of 2600 W h kg^{-1} and a specific capacity of 1675 mA h g^{-1} for a sulfur cathode,[31,32] which is around 5 times higher than that of LIBs (150–220 W h kg^{-1} and 150–200 mA h g^{-1}).[33,34] We do not extensively describe the redox mechanism and battery operation of LSBs because such principles have been described in great detail in more general reviews by Li *et al.*,[35] Zhao *et al.*,[36] Yin *et al.*,[37] and Wild *et al.*[38] The components and construction of an LSB have been excellently summarized by Manthiram *et al.*[39] Briefly, as shown in Fig. 1a, an LSB is discharged when Li-ions from the Li anode diffuses through a porous separator to the sulfur cathode where S_8 is reduced into Li_2S through a series of reactions that produce semi-stable intermediates (Li_2S_x; $2 \leq x \leq 8$) called lithium polysulfides (LiPSs). A typical charge/discharge profile of an LSB is shown in Fig. 1b, and it highlights the two discharge plateaus that correspond to the soluble high-order LiPS (high plateau around 2.3 V) and insoluble low-order LiPS (low plateau around 2.1 V).

LSBs have several drawbacks preventing commercialization, including poor cyclability, self-discharging, Li dendrite

[a]Department of Chemical Engineering, The Cooper Union for the Advancement of Science and Art, New York City, NY, 10003, USA
[b]Nano Science and Engineering, Integrated Science and Engineering Division (ISED), Underwood International College, Yonsei University, 85 Songdogwahak-ro, Yeonsugu, Incheon, 21983, South Korea
[c]Adarsh Innovations, Pune, 411045, Maharashtra, India
[d]Ormecon Pvt. Ltd, CBD Belapur, Navi Mumbai, 400614, Maharashtra, India
[e]Department of Chemistry, Dr Babasaheb Ambedkar Marathwada University, Aurangabad, India
[f]PerkinElmer Inc., 501 Rowntree Dairy Rd, Woodbridge, ON, L4L dH1, Canada
[g]Energy & Environmental Science and Engineering (EESE), Integrated Science and Engineering Division (ISED), Underwood International College, Yonsei University, 85 Songdogwahak-ro, Yeonsugu, Incheon, 21983, South Korea. E-mail: rajkumar@yonsei.ac.kr

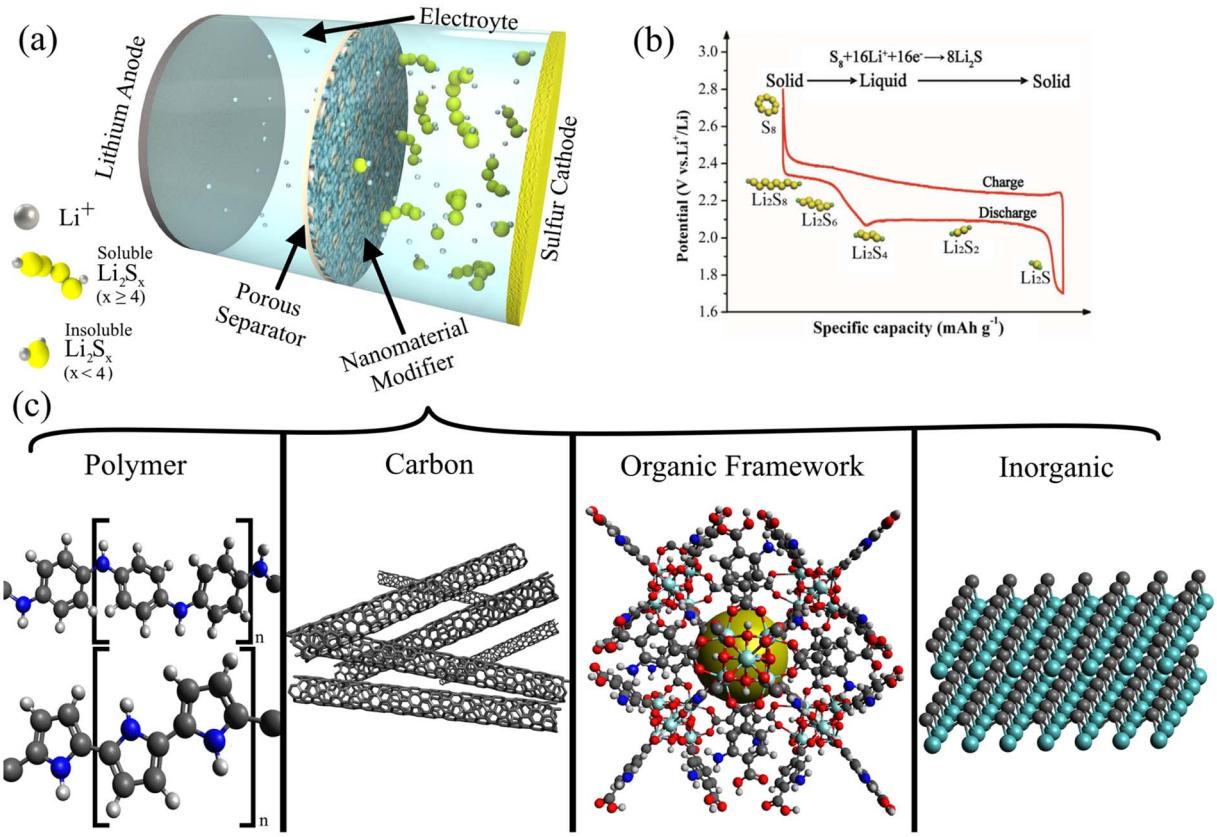

Fig. 1 (a) Schematic of a typical LSB configuration with a Li metal anode, porous separator modified with nanomaterials, electrolyte, and sulfur cathode. The shuttle effect is prevented by the nanocomposite separator. (b) A typical charge/discharge profile of LSBs, highlighting the conversion of sulfur (S_8) into Li_2S *via* various polysulfide species (Li_2S_x; $2 \leq x \leq 8$).[78] (Reproduced with permission from ref. 78 Copyright 2017, the Royal Society of Chemistry). (c) A preview of the common modifications to commercial separators analyzed in this review.

formation, low sulfur loading, and large volume expansion (~80%).[40,41] To address these issues, many recent studies investigated various Li–S cathode materials, cathode modifications, electrolyte combinations, catalyst additives, and other optimizations.[41–56] Promising nanomaterials used in other renewable technologies, such as graphene,[57–59] quantum dots,[60–64] double-layered hydroxides,[65,66] and other nanoparticles,[67–71] have been used to enhance LSBs. Similarly, advanced polymer techniques enabled the fabrication of various polymer blends and composites[72–77] that may be promising to critical LSB components, such as the separator and storage pack.

One of the largest issues with LSBs is the shuttle effect, which severely reduces cycle stability, decreases coulombic efficiency, and increases self-discharging. During the multi-step discharging process (Fig. 1b), the soluble LiPSs (Li_2S_8, Li_2S_6, and Li_2S_4) are solvated by the liquid electrolyte and "shuttled" from the cathode to the anode primarily *via* diffusion. The shuttle effect harms the cathode by decreasing the amount of active material on the cathode side and limiting the sulfur loading in the cathode, reducing the total capacity of the LSB.[79] While some LiPSs may be recovered during the charging process as they shuttle back from the anode to the cathode, most long-chain LiPSs are lost because of parasitic reactions with the Li anode. Specifically, soluble LiPSs bypass the unstable solid–electrolyte interface (SEI), are reduced by the Li metal, and irreversibly precipitate on the Li anode. These parasitic side reactions increase the impedance of the LSB, corrode the Li anode, facilitate LSB self-discharging, and ultimately decrease the total capacity with each battery cycle.[80] Recently, Pai *et al.* made an enormous breakthrough, with their LSB cycling through 4000 cycles without producing soluble polysulfide intermediates. This was due to the formation of a rare and stable γ-monoclinic sulfur on the carbon host material *via* an altered redox mechanism.[81] While cathode improvements can reduce LiPS shuttling by reducing LiPS formation and using catalytic and chemisorptive materials, a significant amount of LiPS still migrates to the anode, resulting in sub-optimal cyclability.[82,83] Others have tried to reduce the parasitic LiPS reactions at the anode by improving the stability of the SEI by adding electrolyte additives like $LiNO_3$ or engineering artificial SEI interlayers.[84] The electrolyte solvent can also be designed to create strong solvation shells that encapsulate long-chain LiPSs, preventing reactions with the Li metal anode.[85] Alternatively, liquid electrolytes may be replaced with solid electrolytes to eliminate the shuttle effect.[86] As shown in Fig. 1c, the separator may also be modified to reject LiPSs.

Another important obstacle to overcome is Li dendrite growth on the anode after repeated cycling. The exact

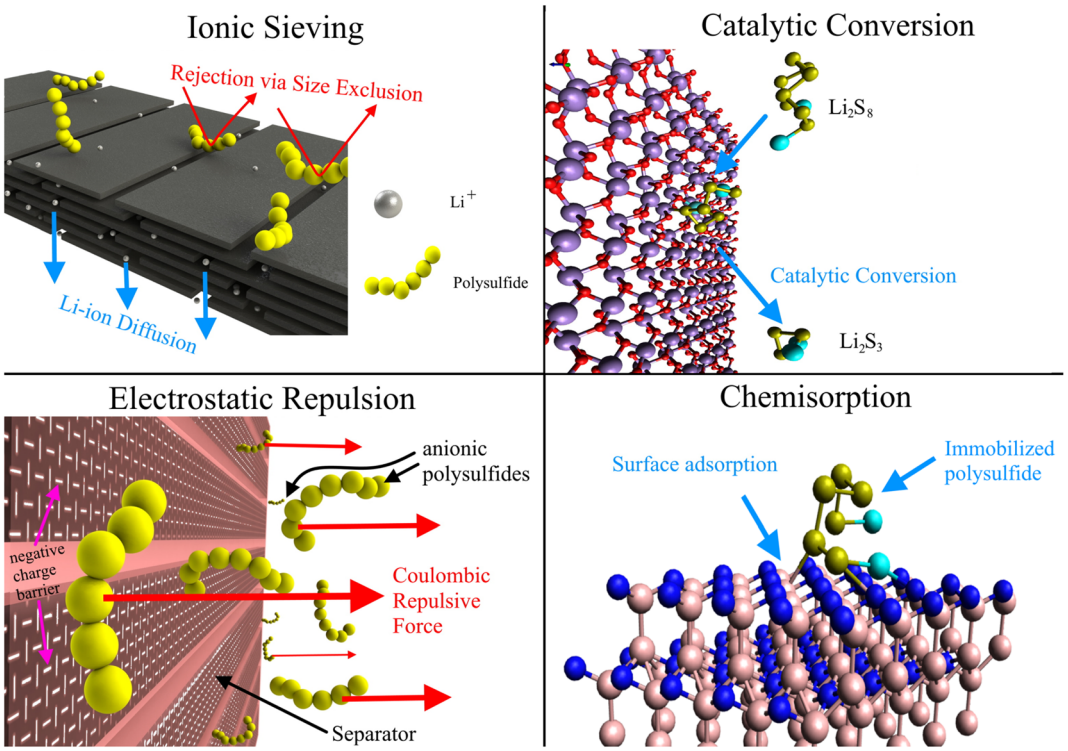

Fig. 2 The primary LiPS rejection mechanisms by modified commercial separators, including ionic sieving (top-left), catalytic conversion (top-right), electrostatic repulsion (bottom-left), and chemisorption (bottom-right).

mechanism behind Li dendrite formation is still under investigation, but the main culprits are generally considered to be the unstable SEI, uneven current density at the anode, and concentration polarization.[87] The Li dendrites reduce coulombic efficiency, consume electrolyte, decrease active material, and can ultimately short-circuit the LSB and become a safety hazard.[27]

One of the most facile methods of reducing LiPS shuttling and Li dendrite formation is to use modified separators. The separator is a critical component in modern batteries that act as a physical barrier between the cathode and anode, preventing short-circuiting while allowing fast ion diffusion *via* the permeating electrolyte.[88] The most widely available separators are microporous polyolefin-based membranes often used in LIBs, which are fabricated from polypropylene (PP), polyethylene (PE), or a blend of both. These separators are sold commercially under brand names like Celgard. However, polyolefin separators are poor options for LSBs, owing to high polysulfide shuttling, poor thermal stability, and low electrolyte wettability.[89] Glass fiber-based separators have recently gained popularity for improving LSB performance but are not as widely used as polyolefin-based separators.[90–94] Various polymer nanofiber separators like polyacrylonitrile (PAN) nanofiber[95–97] and cellulose nanofiber[98] separators have also been developed for LSBs, but these are still in their development stage and are not readily available for commercialization.

Instead of developing new separators for LSBs, we can modify the ubiquitous polyolefin separators to leverage existing manufacturing methods and supply chains for the ubiquitous polyolefin separators. In doing so, we can reduce production costs and smoothly scale up LSBs to market. Various physical and chemical modifications have been made to commercial membranes, resulting in composite separators with improved polysulfide rejection *via* enhanced ionic sieving, catalytic conversion, electrostatic repulsion, and surface chemisorption, as shown in Fig. 2. Ionic sieving occurs when long-chain polysulfides are unable to pass through the small nanopores in the separator due to size exclusion. Complex pore systems like hierarchical pore structures can also trap LiPSs.[99] Catalytic conversion reduces the shuttle effect by facilitating the conversion of soluble LiPSs into insoluble LiPSs. Modifiers promote LiPS redox kinetics by improving electron mobility, increasing Li_2S nucleation, and lowering activation energy.[100,101] Anionic polysulfides are also rejected *via* coulombic repulsion if the surface of the separator is endowed with a net negative charge. The electrostatic shield is often generated with electronegative functional groups on the modified separator surface.[102] Lastly, chemisorption plays a large role in immobilizing LiPSs, with many modifiers selected for their high LiPS adsorption affinity. The sulfur atoms are adsorbed by electron-deficient metal centers while electron-rich functional groups bind to the Li component of LiPSs.[103,104] These modifications may also decrease Li dendrite formation by homogenizing Li-ion flux and distributing local current densities.[105] Functional separators may also provide improved rate capability, sulfur utilization, Li-ion conductivity, and thermal stability, yielding improved specific capacity and battery safety.[106]

Due to the popularity of battery research, thousands of studies have been published on LSBs, followed by numerous summaries and overviews. However, most reviews focus on advances in LSB cathodes,[107–115] electrolytes,[116–124] or other important LSB components, like electrocatalysts[125] or binders.[126] Others present a general overview of improving LSBs, with brief sections on separator modifications.[127–132] The few latest reviews focused on separators for LSBs do not organize developments by materials,[133] do not specialize in modified polyolefin separators,[134] nor focus on specific material composites.[135–139] In contrast, this review primarily focuses on cutting-edge developments in modified polyolefin separators for LSBs organized by additive material: polymer-based, carbon-based, organic framework-based, and inorganic-based composites. There is a heavy focus on popular materials like conducting polymers (polyaniline and polypyrrole), functionalized carbon nanomaterials (graphene and carbon nanotubes), metal oxides (TiO_2), and metal sulfides (MoS_2), amongst many other composites. The advantages of less common yet promising materials like electrically conductive polymers, metal–organic frameworks, and Mxenes are also discussed. We hope this critical review of the latest modified polyolefin separators will guide future work in making LSBs commercially viable.

2 Polymer-based modifications

Polymer-based modifications to commercial membranes are frequently performed *via* surface modification methods, including grafting,[140] surface polymerization,[141] and layer-by-layer techniques.[142] The main goals of polymer-based modifications are to (a) decrease pore sizes for improved polysulfide sieving, (b) endow a negative charge for the coulombic repulsion of anionic polysulfide, (c) improve compatibility between the polyolefin separator and other modifiers, and (d) to increase separator hydrophilicity for improved electrolyte wetting. To achieve this, common polymers, functionalized polymers, and electrically conductive polymers have been investigated as surface modifiers for commercial polyolefin separators in LSBs. The performance of exemplary polymer-modified separators is summarized in Table 1.

2.1 Common polymers

Popular polymers like Nafion, polyethylene glycol (PEG), polydopamine (PDA), polyacrylic acid (PAA), and polyethylenimine (PEI) are easily appended to PP or PE separators *via* graft polymerization or filtration methods.[140] Upon modification, the composite separators may have reduced pore sizes to promote polysulfide sieving. Unlike PP and PE, polymer modifiers have highly electronegative functional groups, like carboxyls, carbonyls, and sulfonates, which endow a net negative surface charge to repel anionic polysulfides.[143] Because various polymers can have strong interactions with polyolefins and polar additives simultaneously, they are useful binders for other modifiers.[142] Hydrophilic functional groups in common polymers also improve electrolyte wettability for improved Li-ion conduction.[144] Despite all the benefits of using polymer modifiers, common polymer modifications alone are usually insufficient in mitigating the shuttle effect and do not significantly

Table 1 Summary of LSB performance and longevity with polymer-modified commercial membranes

Membrane	Specific charge (mA h g^{-1})	C rate (C)	Cycles	% Loss per cycle	Highlights	Ref.
Common polymers						
PP/Nafion/KB	6701	0.2	150	0.06	Filling interparticle gaps in KB	143
PP/PDA/PEI	1250	0.2	100	0.28	Smoother separator surface	144
PP/PAA	562	0.5	600	0.07	UV grafting decreased pore size	166
PP/Nafion/Cu-MOF	680	0.5	300	0.07	Electrostatic shield	153
PP/PDA/g-CN	764	0.5	500	0.05	Improved g-CN adhesion to separator	161
PP/Nafion/super P	807	0.5	250	0.22	Synergized ionic sieving	154
PP/silicone/PDA	982	1.0	1000	0.03	Blocked side reaction of silicone and Li metal	162
PP/Co-carbon/PDDA	872	2.0	1200	0.02	Small size of PDDA increases LiPS contact	167
Functionalized polymers						
PP/SPEEK	1228	0.2	100	0.23	Electrostatic shield	168
SPEI/PEI	1285	0.2	200	0.21	Improved electrolyte uptake and Li-ion conductivity	170
PP/PVDF/super P	1040	0.5	100	0.67	Functionalized PP separator pre-coating	173
Conducting polymers						
PP/PSS	1300	0.05	30	1.00	Minimum PSS loading required	190
PP/PANI/V_2O_5	1132	0.2	100	0.11	Improved electron mobility	182
PP/PE/PEDOT:PSS	985	0.25	1000	0.04	Electrostatic barrier	179
PP/PEDOT:PSS	1096	0.5	500	0.03	PEDOT chelated structures with LiPSs	178
PP/PANI/CFP	723	1.0	100	0.74	PANI used as a binder	183
PP/PPy/GO	809	1.0	1000	0.04	Pyrrolic nitrogen for LiPS chemisorption	185
PP/RPM	947	5.0	700	0.06	Conductive bridge between MoS_2 and rGO	184
PP/PPy-Li-MMT	775	1[a]	600	0.04	Improved thermal stability	189

[a] Current density measured in mA cm^{-2} instead of C rate.

improve the rate capability of LSBs, limiting their charge rate and power density.

Nafion is the brand name of a popular and commercially available sulfonated tetrafluoroethylene-based fluoropolymer-copolymer modified to reduce polysulfide shuttling in LSBs *via* physical and electrostatic mechanisms.[145–150] Although Nafion may be used as a separator directly for its high proton conductivity and good thermal stability,[151] it is a very expensive polymer, so it is better used as a modifier for polyolefin separators to save material cost. Wang *et al.*[152] modified a standard PP separator with Nafion/MXene composite nanosheets *via* vacuum filtration. The Nafion contributed to the electrostatic repulsion of polysulfides and decreased the pore size from 200 nm to 40 nm. MXenes were added to create a stacked pore structure that further improved rejection *via* size exclusion. Recently, Diao *et al.*[153] composited Nafion with a porous Cu-based MOF that mitigated Li dendrite formation by homogenizing Li-ion flux with its negatively charged sulfonate groups. In a Li//Li symmetric cell overpotential test, the Nafion-modified separator had a low overpotential for over 100 h, whereas the pristine PP separator had short-circuited after only 80 h.

While many porous modifiers like porous carbons (Section 3.3) and MOFs (Section 4.1) have excellent adsorptive ability and can trap long-chain LiPSs in their complex pore structure, they have poor adhesion for PP and PE. As a polymer with strong polar groups, Nafion can fill the interparticle gaps and anchor polar additives. As shown in Fig. 3a, Rana *et al.*[143] used Nafion as filler to hold the Ketjen black particles together and reduce the interparticle gaps. The resulting Nafion/Ketjen composite was slurry coated onto a standard PP separator, which showed excellent polysulfide rejection even at high sulfur loadings up to 7.88 mg cm^{-2}. Hao *et al.*[154] similarly synthesized a Nafion/Super P composite and coated it onto a commercial Celgard membrane that enabled polysulfide trapping.

PEG is a low-cost, hydrophilic, and non-toxic polymer frequently used to modify LIB separators due to its excellent electrolyte wettability and ionic conductivity.[155–157] For LSBs, PEG modifications can restrict polysulfide shuttling while maintaining high Li-ion conductivity. However, PEG modifications alone are insufficient to reduce polysulfide shuttling and are often composited with porous materials like MWCNTs or porous carbon that can trap polysulfides. For example, Wang *et al.*[158] coated a Celgard 2400 separator with a PEG/MWCNT composite, resulting in a 67% higher initial specific capacity than a pristine Celgard separator. Moreover, after 500 cycles, the LSB with the PEG/MWCNT membrane had a 4-times-higher specific capacity than with the unmodified membrane. Similar improvements with PEG were reported by Chung *et al.*[159] and Luo *et al.*[160]

PDA is another promising material for LSB separator modification, owing to its hydroxyl groups that may provide an electrostatic barrier and improved Li-ion diffusion. Recently, Pei *et al.*[144] modified a Celgard membrane with a PDA/PEI composite. The significantly increased hydrophilicity resulted in a 75% increase in electrolyte uptake rate, a 13% increase in ionic conductivity, and a 28% higher initial specific capacity. PDA is a particularly useful binding molecule between standard polyolefin separators and other additives. For example, Tong *et al.*[161] coated a Celgard 2500 separator with PDA to anchor graphitic carbon nitride (g-CN) nanofibers to the membrane substrate. The resulting PP/PDA/g-CN membrane showed good physical and thermal stability, with higher PDA content improving thermal stability. Yang *et al.*[162] used a PDA coating to prevent the reaction between silicone nanofilaments and Li anode. Specifically, a Celgard 2400 membrane was modified with silicone nanofilaments to increase electrolyte wettability and physical polysulfide trapping, but the PP/silicone had poor cycling due to its reaction with Li. The PDA coating prevented the silicone–Li reaction and improved the lifespan of the LSB to 20 000 hours, whereas the battery with a Celgard separator lasted 100 h of voltage cycling and PP/silicone lasted 460 h. Similarly, Hu *et al.*[163] prevented CoFe/C nanoparticles from aggregating on the Celgard surface by encapsulating the nanoparticles with PDA. Interestingly, PDA may also be

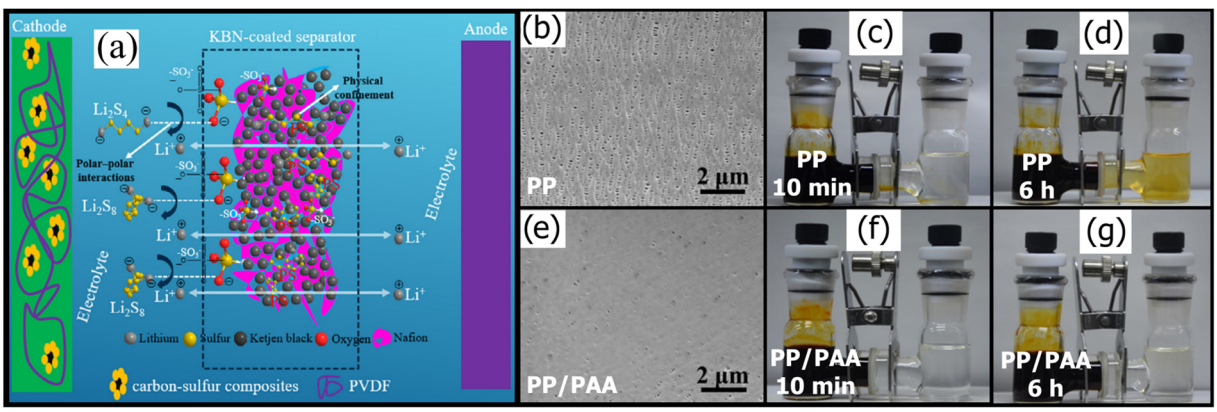

Fig. 3 (a) Schematic of the mechanism of physical confinement of the PS in the porous structure of the KB and polar–polar interaction with $-SO_3^-$, with Nafion filler[143] (Reproduced with permission from ref. 143. Copyright 2020, Elsevier). SEM of (b) PP and (e) PP/PAA. Digital photograph of a polysulfide diffusion test with a PP separator after (c) 10 min and (d) 6 h and PP/PAA after (f) 10 min and (g) 6 h (h)[166] (Reproduced with permission from ref. 166. Copyright 2018, Elsevier).

a precursor to carbon-based core/shell modifications to polyolefin separators.[164,165]

By grafting a polymer layer on the cathode side of mesoporous membranes with various polymers, the pore sizes can be easily controlled to reject polysulfides while allowing high Li-ion diffusion. For example, Song *et al.*[166] used a facile and inexpensive photografting method to append a PAA layer to a standard PP-based Celgard 2325 membrane. As shown in Fig. 3b and e, the pore size decreased from 100 nm for the pristine membrane by more than 50%, and the total number of pores decreased. Increasing the time under UV irradiation increased the grafting rate, resulting in smaller pores and lower pore density, which improved polysulfide rejection. Fig. 3c and d and Fig. 3f and g show how much the PAA layer improved polysulfide diffusion *via* a simple diffusion test with a dark yellow LiPS solution on the left compartment and clear solvent on the right compartment separated by either a pristine PP or PAA-modified separator. The PP separator fails almost immediately, with yellow LiPSs diffusing within 10 minutes and completely turning the right compartment yellow in 6 h. In contrast, the PAA-modified PP separator test showed no noticeable color change even after 6 hours of testing. This kind of visual diffusion method qualitatively shows the improved LiPS rejection ability of the PAA-modified separator. However, a UV-vis absorbance test following the diffusion test would be a non-invasive method of providing quantitative results for LiPS diffusion through the separator. While greater PAA grafting improved LiPS rejection *via* highly selective ionic sieving, the composite membrane exhibited greater hydrophobicity, which decreased electrolyte wettability and, consequently, ionic conductivity. In more recent work, Pei *et al.*[144] similarly found that appending a polydopamine (PDA) layer to a Celgard membrane reduced average pore sizes by 35% (130 nm). However, the PP/PA membrane surface was rough with only PDA. Modifying PDA with PEI yielded a smoother surface finish, which improved Li-ion conductivity. Having multiple layers of PDA/PEI further decreased surface roughness and polysulfide rejection without significantly increasing the LSB's impedance.

Gao *et al.*[167] compared the performance of LSBs with PP/cobalt-doped porous carbon composite separator modified with chenodeoxycholic acid, berberine chloride hydrate, or poly(diallyl dimethyl ammonium chloride) (PDDA). LSBs with the PDDA modification showed one of the highest capacity retentions, with a decay rate of 0.031% per cycle after 1200 cycles at a high current of 4C. The small molecular size of PDDA allowed it to exhibit stronger repulsion against polysulfides and improved ionic sieving than the other organic molecules.

2.2 Functionalized polymers

Polymers may be functionalized prior to their implementation in polyolefin separators to have more hydrophilic and anionic functional groups. Common polymers like PEI (Section 2.1) and other less common polymers like poly(ether ether ketone) (PEEK) can benefit from additional functionalization.[168] Newly appended polar groups like sulfonates and carboxyl/hydroxyl groups increase the polymer's ability to immobilize LiPSs with greater chemisorption and repel LiPSs with a more negative surface charge. These groups can also improve Li-ion conductivity and electrolyte wettability for improved rate capability. While the additional functionalization of various polymer modifiers can improve LiPS rejection, it is unsure whether the added material cost and synthesis time are justified, as the cost-benefit analysis is often overlooked.

Polymers often undergo sulfonation, where sulfonate groups are appended *via* reaction in sulfuric acid. For example, Li *et al.*[168] sulfonated PEEK before modifying a PP separator. Similar to Nafion, the SPEEK separator had abundant sulfonate groups that formed an electrostatic barrier against LiPSs, but SPEEK can be fabricated at a lower cost with eco-friendly and facile one-step synthesis. Similarly, Babu *et al.*[169] used SPEEK and Nafion to modify a commercial Celgard membrane. The SPEEK improved the stability of the LSB, while Nafion improved specific capacity. Liu *et al.*[170] sulfonated PEI, which is known for its excellent thermal, chemical, and mechanical stability. In all aforementioned studies, the sulfonation decreased polysulfide shuttling by increasing electrostatic repulsion against polysulfides. Other sulfonated polymers, such as lithiated poly(diphenylether oxadiazole) sulfonate[171] and sulfonated PEG,[172] have been used in LIBs but have not yet been investigated for LSBs.

Other common functional group modifications to LSB separators include carboxyl and hydroxyl groups. In a recent study, Paniagua-Vásquez *et al.*[173] used plasma treatment to functionalize the PP substrate with hydroxyl and carboxyl groups before coating with polyvinylidene fluoride (PVDF)/super P. The pre-functionalized PP substrate increased compatibility with the PVDF/super P coating, resulting in a smooth coating with no visible cracks and small interparticle gaps. After 100 cycles, the LSB with the modified membrane had a higher specific capacity than the initial capacity of the battery with a pristine membrane. This was due to the PVDF/super P modification enabling improved Li-ion conduction and sulfur utilization. Song *et al.*[166] and Yu *et al.*[174] similarly found that modifying a PP membrane by grafting poly(acrylic acid) (PAA) and hydrolyzed acrylamide, respectively, introduced carboxyl functional groups that provided a highly negative surface charge. The improved hydrophilicity and electrostatic repulsion significantly reduced polysulfide shuttling while improving Li-ion diffusion. Gu *et al.*[175] controlled the ratio of charged amine and carboxylate groups on the surface of a PE/poly(allylamine hydrochloride)/PAA (PE/PAH/PAA) separator by changing the acidity of the electrolyte solution. The microporous PE membrane was modified with alternating layers of PAH and PAA *via* a layer-by-layer technique. Decreasing the pH from 8.5 to 3 increased specific capacity retention due to the increase in charged carboxylate groups that provided an electrostatic barrier against polysulfides.

2.3 Electrically conductive polymers

Conductive polymers are a special class of polymers that are electrically conductive due to their backbones comprising contiguous sp^2 hybridized covalent bonds. The delocalized

electrons in these large polymer structures are free to move, resulting in metallic or semiconducting behavior.[176] Similar to common polymers (Section 2.1) and functionalized polymers (Section 2.2), conductive polymers can reduce the pore sizes of polyolefin separators for improved LiPS sieving. Separators modified with conductive polymers can also exhibit high ionic conductivity because conductive polymers improve electrolyte wettability. Uniquely, the high electrical conductivity of conductive polymers can improve the conversion kinetics of LiPSs and synergize with other modifiers. Despite these benefits, conductive polymers are limited in use due to their difficult processing and have variable conductivities depending on external factors like the presence of other dopants and coating thickness.[177]

Polystyrene sulfonate (PSS) is often applied together with poly(3,4-ethylenedioxythiophene) (PEDOT) to yield an electrically conductive polymer called PEDOT:PSS. PEDOT also helps contain polysulfides by forming chelated structures with LiPSs.[178] Abbas *et al.*[179] spray-coated a layer of PEDOT:PSS onto the cathode side of a Celgard 2500 membrane. Due to the highly negative surface charge of the modified membrane, the separator effectively reduced polysulfide shuffling *via* coulombic repulsion, decreasing the charge decay rate by 67%. While PEDOT:PSS-modified separators have been shown to potentially reduce the kinetics of the battery due to its thickness,[180] the nano-scale thick PEDOT:PSS layer (approx. 800 nm) after spray coating was thin enough to allow high Li-ion conduction.[179] Moreover, the hydrophilicity increased with the PEDOT:PSS modification, resulting in improved electrolyte wettability and decreased the charge transfer resistance of the LSB by 14%. Similarly, Hareendrakrishnakumar *et al.*[178] and Zhong *et al.*[181] reported significant polysulfide rejection due to the negatively charged PEDOT:PSS barrier.

Polyaniline (PANI) is another popular conducting polymer for LSBs with its electrostatically repulsive imine (=N–) groups and excellent conductivity. PANI is particularly useful for providing a conductive coating for other modifiers like metal oxides that have an excellent chemisorption affinity for polysulfides but poor catalytic ability due to their electrically insulating nature. For example, Chen *et al.*[182] coated V_2O_5 nanowires with PANI to enhance the ionic conductivity of Li-ions, electrical conductivity for Li polysulfide conversion, and mechanical strength. After the PANI/V_2O_5 composite was vacuum filtered through a standard PP separator, the resulting LSB exhibited a 19% higher initial capacity and 11% higher capacity retention after 200 cycles at 0.5C than the LSB with a PP/V_2O_5 membrane. This was due to the improved reaction kinetics and sulfur utilization because of the significantly lower charge transfer resistance with PANI. Jo *et al.*[183] found similar improvements to initial capacity and cyclability after coating Co–Fe Prussian Blue analogs (CFPs) with PANI and applying the PANI/CFP to a standard Celgard membrane. The PANI coating on the CFPs allowed more effective binding with the PVDF and NMP binder solution, yielding a more structurally stable surface modification on the PP substrate. Shi *et al.*[184] used PANI as a conductive intermediate between a conductive rGO backbone and highly catalytic and polysulfide-adsorptive MoS_2 nanosheets. Fig. 4a shows the synthesis of the rGO-PANI/MoS_2 (RPM) composite, and Fig. 4b shows the "trapping-interception-conversion" mechanism for LiPS rejection enabled by the RPM composite. While MoS_2 has weak interactions with carbon, PANI interacted with MoS_2 *via* strong Mo–N bonds and rGO *via* strong electrostatic effects. The high electrical conductivity of PANI allowed fast electron transfer from the rGO to MoS_2, unlike other polymer connectors. Hence, when cycled at a high rate of 5C, the LSB with an RPM-modified PP separator showed an excellent 99.7% coulombic efficiency and retained 55% of its initial capacity.

Polypyrrole (PPy) is another excellent conducting polymer for LSB separator modifications due to its adsorptive amine groups and facile synthesis. Li *et al.*[141] modified a Celgard separator on both sides with a thin layer of PPy *via in situ* vapor phase polymerization to reduce Li-dendrite formation on the anode side, with no visible corrosion even after 250 charge/discharge cycles. The improved conductivity and nitrogen functional groups in PPy improved the reversibility of sulfur at the cathode, resulting in a smoother cathode surface. The hydrophilicity of the 15 nm thick PPy coating improved electrolyte wettability, increasing electrolyte uptake from 70% to 108% for higher Li-ion conductivity. Moreover, the rate capability of the LSB was significantly enhanced due to the increased conversion kinetics provided by the conductive PPy (Fig. 4c). While carbon-based modifiers are often modified with a mix of pyridinic, pyrrolic, and graphitic nitrogen atoms, it is possible to modify carbon matrices with mostly pyrrolic nitrogen sites by functionalizing with PPy.[185] This is important because pyrrolic nitrogen sites have shown excellent polysulfide adsorption and catalytic conversion compared to the other nitrogen sites.[186,187] In a recent study, Zhang *et al.*[188] used DFT to show that a composite comprising PANI chains and α-ZrP nanosheets was highly catalytic to polysulfide conversion. The Li polysulfides adsorbed by the α-ZrP nanosheets acted as an electronic switch that allowed electrons to flow between PPy and α-ZrP, which triggered the multiphase conversion of the adsorbed polysulfide. The PPy was also shown to limit excessive polysulfide oxidation by controlling the output of electrons. As shown in Fig. 4d, the relative energy barrier of Li-ion diffusion through α-Zr/PPy is significantly lower than other common materials. Interestingly, PPy composites can also be used to reduce the effects of thermal shrinkage and thermal runaway. Yang *et al.*[189] compared the thermal stability of a PPy-Li-montmorillonite (PPy-Li-MMT)-modified PP separator, acetylene black-modified PP separator, and pristine PP separator. As shown in Fig. 4e, after heating 160 °C, the PP/PPy-Li-MMT retained its shape and had an evenly spread heating profile. In contrast, PP/acetylene black (Fig. 4f) and PP (Fig. 4g) quickly deformed and disintegrated, owing to the generation of hot spots. While MMT is a well-known flame retardant, the addition of PPy improved the uniformity of MMT on the PP surface while allowing the composite to retain high thermal conductivity, resulting in better thermal stability than a PP modified with MMT without PPy.

3 Carbon-based modifications

Carbon-based modifications are most frequently implemented into polyolefin separators *via* vacuum filtration,[103] layer-by-layer techniques,[191] and slurry coating methods.[192] Carbon-based modifications are primarily to (a) improve the LiPS conversion kinetics by improving electron mobility during the redox reaction, (b) decrease Li dendrite formation by decreasing local current density and Li surface reactions, and (c) decrease the charge transfer resistance of the LSB as a whole for improved rate capability (d) decrease pore sizes for improved LiPS sieving, and (e) to improve the performance of other additives.[193] While there is no direct current flow through the separator, increasing the conductivity of the separator reduces the charge transfer resistance of the whole LSB by improving the electron mobility of sulfur in the cathode and polysulfides.[194] Moreover, modifying a separator's anode side with conductive carbon nanostructures can mitigate Li dendrite formation by reducing local current densities at the anode, reducing Li surface reactions, and homogenizing Li-ion flux. A carbon layer can also physically

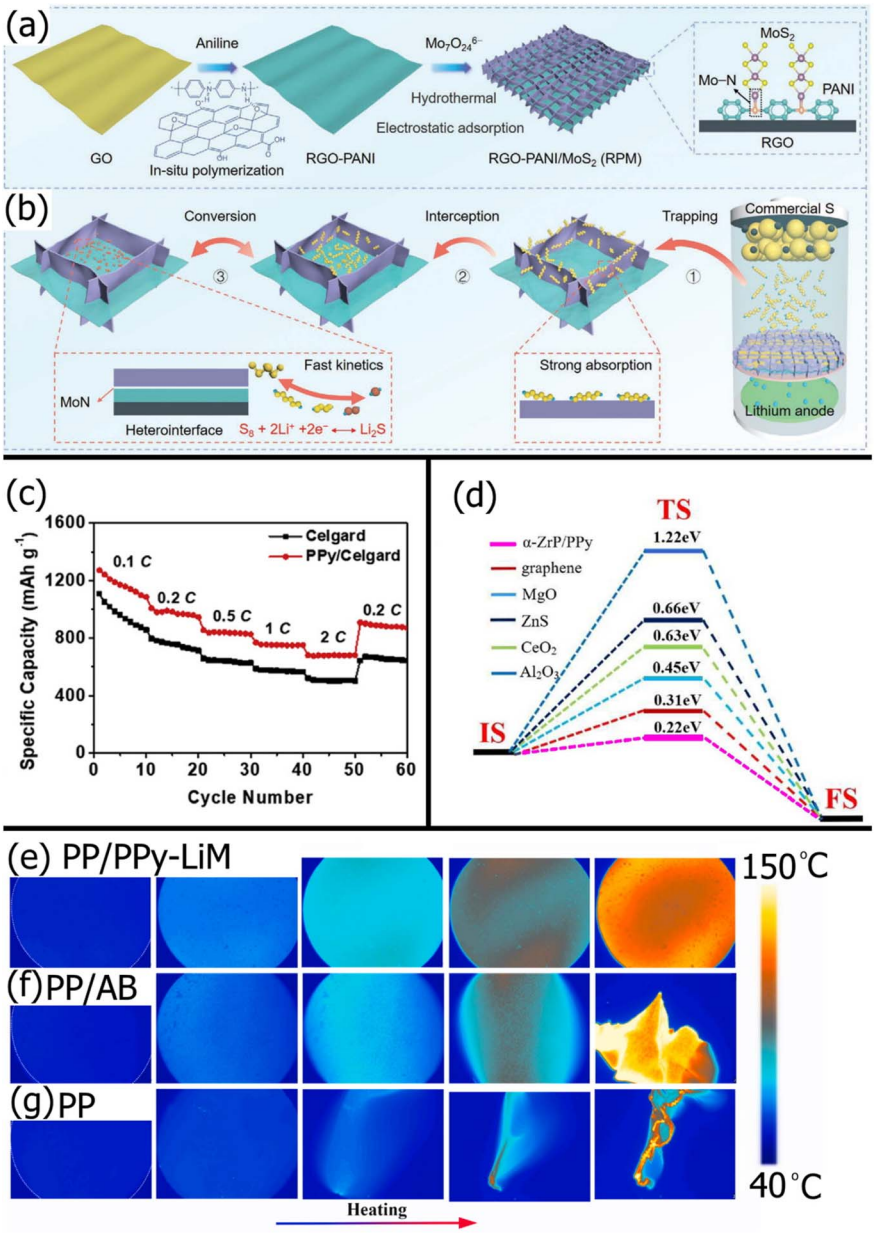

Fig. 4 Schematic showing the (a) synthesis process of RPM and (b) the "trapping-interception-conversion" mechanism of the RPM modification on a PP separator substrate[184] (Reproduced with permission from ref. 184. Copyright 2022, John Wiley and Sons). (c) Rate performance of an LSB with a standard Celgard separator and a PPy-modified Celgard separator[141] (Reproduced with permission from ref. 141. Copyright 2019, Elsevier). (d) Transition state search of lithium ions diffusion in the α-ZrP/PPy interface compared with other materials[188] (Reproduced with permission from ref. 188. Copyright 2022, Elsevier). *In situ* infrared thermography of (e) PP/PPY-LiM, (f) PP/AB, and (g) PP separators[189] (Reproduced with permission from ref. 189. Copyright 2021, Elsevier).

shield the LSB against Li dendrite penetration with its small nanopores.[195] Thus, various forms of carbon, including graphene, CNTs, porous carbons, and other graphitic carbons, have been used as surface modifiers for commercial LSB separators. Unlike most modifiers, carbon-based nanomaterials may be easily synthesized from biomass or waste, making carbon materials excellent options for sustainability-focused manufacturing.[196] The performance of exemplary LSBs with carbon-modified separators is summarized in Table 2.

3.1 Graphene

Graphene is a 2D nanosheet of a monolayer, honeycomb-arranged carbon lattice with excellent electrical conductivity, mechanical strength, thermal stability, and high functionalizability, among other properties.[197] Graphene derivatives, such as graphene oxide (GO) and reduced graphene oxide (rGO), have many or some oxygen functionalization and are much more common in literature as they are easier to prepare while sharing similar properties with perfect graphene.[198] As modifiers for commercially available polyolefin separators, graphene and its derivatives reduce the shuttle effect *via* ionic sieving with controllable pore sizes and enhanced LiPS reduction kinetics owing to increased electron mobility. Because GO has abundant oxygen groups, they can contribute to LiPS rejection *via* chemisorption and electrostatic repulsion. Functionalized graphene moieties are also beneficial for improving electrolyte wettability. However, graphene-based modifiers alone are unable to completely mitigate the shuttle effect and must be co-doped with more adsorptive or catalytic modifiers.

Graphene dopants can control the pore size of the composite membrane to improve LiPS sieving. Ou *et al.*[199] reduced the pore sizes of a PP/PE/PP membrane by transferring a layer of graphene to the Celgard membrane using a wet transfer method. The average pore size of the graphene-modified separator was 2.45 nm, but the pore size was increased to 3.76 nm *via* O_2 plasma treatment for improved Li-ion conductivity while still being small enough to sieve LiPSs. Improved sieving was indicated by a 15% higher specific capacity after 95 cycles with the graphene-modified separator than with the pristine membrane. Nylon-66 was appended to the composite separator *via* interfacial polymerization to decrease pore sizes by clogging larger pores in the graphene sheets. The result was a 10% higher capacity retention than the unclogged graphene-modified separator due to improved size exclusion. While the nylon

Table 2 Summary of LSB performance and longevity with carbon-modified commercial membranes

Membrane	Specific charge (mA h g^{-1})	C rate (C)	Cycles	% Loss per Cycle	Highlights	Ref.
Graphene						
PP/PNCG	1192	0.1	800	0.05	*In situ* formation of PCN on GO	101
PP/NG nanoscroll	950	1.0	800	0.02	Improved electrolyte wettability	195
PP/NG/Ni_3Sn_2	1022	1.0	400	0.07	Nitrogen defects for improved chemisorption	201
PP/rGO/MoS_2	1040	1.0	300	0.08	Increased sulfur utilization	210
PP/GO/CoPc	1092	1.0	400	0.08	Improved thermal stability	219
PP/tungsten-NG	1100	2.0	100	0.05	Adsorptive tungsten metal centers in graphene lattice	207
Carbon nanotubes						
PE/CNT/Ti_4O_7	888	0.5	250	0.1	Mitigated Ti_4O_7 overgrowth	234
PE/MWCNT–OH	1058	0.5	400	0.11	Hydroxyl groups for LiPS immobilization	240
PP/SWCNT/MnS	876	0.5	500	0.07	Thinner modification layer	238
PP/MWCNT/TiO	1527	0.5	1000	0.06	Increased sulfur capacity	229
PP/SWCNT/TB-BAA	880	1.0	500	0.06	Decreased TB-BAA layer thickness	241
PP/MWCNT/CTF	1000	1.0	1000	0.05	Conductive bridging between CTFs	223
PP/NCNT/MoS_2	1173	1.0	1000	0.05	Reduce MoS_2 nanosheet aggregation	236
PP/OCNT/NiFe-LDH	730	2.0	600	0.09	Ozone treatment for oxygen functionalization	239
Porous carbons						
PP/Carbon	1198	0.3	100	0.42	Porous carbon from sucrose and egg white	266
PP/N-doped KB/Co	1058	0.3	500	0.1	Nitrogen heteroatom increased LiPS affinity	252
PP/NC	1098	0.5	600	0.07	Chlorella (algae) powder	265
PP/Carbon	906	1.0	500	0.10	Rice paper plant	264
PP/PC	912	1.0	800	0.06	Lowered redox the activation energy	261
PP/HNPC	1302	1.0	900	0.06	P & N heteroatom doping	260
PP/Co–N-CNT/Carbon	782	2.0	500	0.04	One-step pyrolysis synthesis	262
PP/INC	1151	2.0	500	0.11	I-doped carbon from kelp	263
Graphitic carbon						
PP/CF	1063	0.5	500	0.07	Clogged large PP pores	271
PP/CNP	699	1.0	200	0.08	Low dimensionality for interparticle space filling	269
PP/NSCNP	650	2.0	500	0.09	Nitrogen and sulfur heteroatom doping	270

modification reduced polysulfide shuttling, the charge transfer resistance increased slightly by 8.5%, resulting in a 1% lower initial capacity. Similarly, Lee *et al.*[200] reduced the pore sizes of a commercial PE membrane *via* electrospraying an rGO/PEDOT:PSS mixture. The spray-coated rGO/PEDOT:PSS layer yielded a 2-times-higher specific capacity than the pristine membrane after 100 cycles. Ni_3Sn_2 doping was used to decrease the pore size of NrGO by 32%, improving polysulfide rejection.[201]

Because the ion-sieving mechanism is often insufficient, graphene is usually modified *via* heteroatom doping, yielding nitrogen-doped graphene and sulfur-doped graphene.[202,203] By adding nitrogen defects to the graphene lattice, lone pairs from the graphitic, pyridinic, or pyrrolic nitrogen enable LiPS chemisorption. Recently, Qi *et al.*[201] used the adsorption ability of nitrogen-doped graphene (NG) to reduce the shuttle effect. The LSB with the PP/NG separator had 112% higher capacity retention than the battery with a pristine separator. While nitrogen doping improves polysulfide adsorption, NG does not exhibit significant catalytic ability. The adsorption energy of various polysulfides on different parts of the NGO/Mo_2N composite was calculated with computational simulations and is shown in Fig. 5d.[204] As expected, the strongest binding energies with all polysulfide forms were by pyridinic and pyrrolic nitrogen groups on the NGO. Still, the nitrogen heteroatoms usually have lower binding energies for LiPSs than metal centers like Mo.

Thus, graphene derivatives are usually paired with various inorganic modifiers for LiPS adsorption. The properties and benefits of different inorganic modifiers are discussed in detail in Section 5. In this section, we focus on graphene's role in supporting the inorganic modifier. Gai *et al.*[205] slurry coated a Celgard separator with nitrogen-doped rGO (NrGO) and Co nanoparticles. The NrGO was responsible for ion-sieving and polysulfide adsorption, while the Co nanoparticles enhanced the reversible conversion of polysulfides. Similarly, Jing *et al.*[206] used vanadium nitride (VN) nanoparticles to enhance the reduction and oxidation kinetics of the polysulfides. Fig. 5a shows that adding VN yielded clear redox peaks for the conversion of polysulfides in both directions, whereas NG alone did not have any distinct redox peaks. The NG/VN also promoted Li_2S nucleation and growth, yielding higher specific capacity than pristine NG (Fig. 5b). Likewise, Wang *et al.*[207] doped a graphene lattice with tungsten metal centers to improve polysulfide adsorption and catalytic conversion. Recently, Jing *et al.*[208] sandwiched SrF_2 between graphene nanosheets (Fig. 5c) before vacuum filtration onto a commercial PP membrane. The graphene provided ion-sieving effects as expected but also improved electron transfer for faster polysulfide conversion kinetics. In another study by Jing *et al.*,[209] a standard PP membrane was modified with CaF_2-decorated rGO. A 1 : 3 ratio between adsorptive and catalytic CaF_2 and conductive rGO was the best compromise between cycle stability from CaF_2 and specific capacity from rGO.

Graphene plays a significant role in sulfur utilization. This was exemplified by Cheng *et al.*[210] who modified a Celgard separator with MoS_2-doped rGO nanosheets. The highly conductive rGO enabled a high sulfur utilization as high as 80 wt%. Similar synergies have been reported between graphene derivatives and metal oxides like CeO_2,[211] Fe_3O_4,[212] MoO_2,[213]

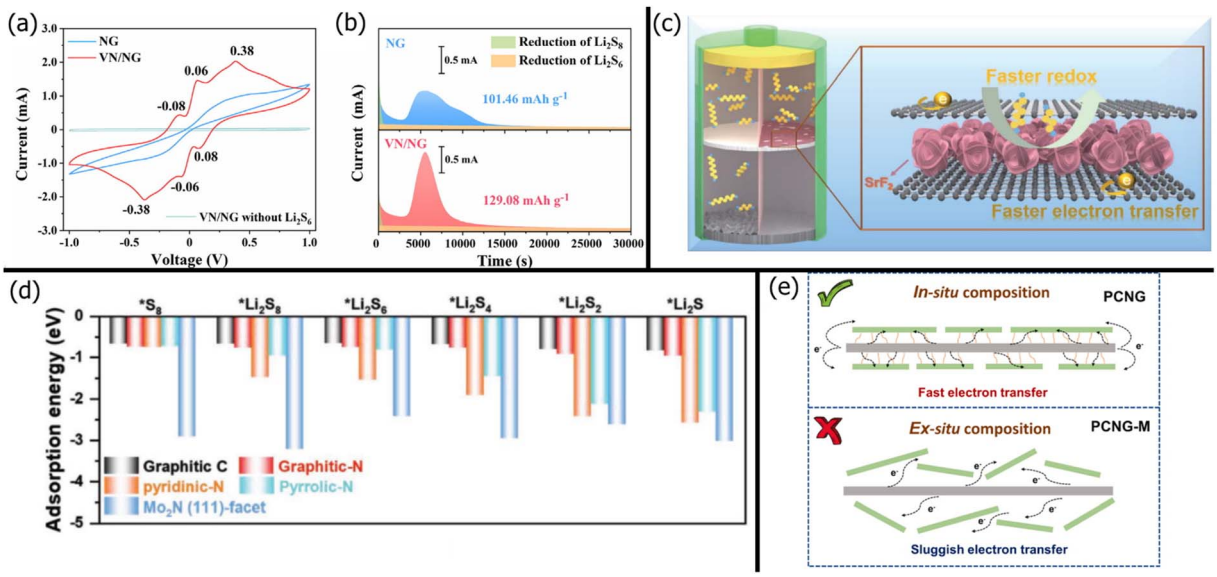

Fig. 5 (a) Cyclic voltammetry curves of Li_2S_6 symmetric cells with an NG/VN separator in a voltage range between −1.0–1.0 V and a scan rate of 1 mV s^{-1}. (b) Potentiostatic discharge profiles at a voltage of a cell with an NG/VN separator at 2.05 V[206] (Reproduced with permission from ref. 206. Copyright 2021, Elsevier). (c) Schematic of a battery with a PP/graphene/SrF_2 separator in LSBs, showing faster redox of polysulfides and electron transfer through graphene.[208] (Reproduced with permission from ref. 208. Copyright 2022, The Royal Society of Chemistry). (d) Comparison of adsorption energies between polysulfides and Mo_2N (111) surface[204] (Reproduced with permission from ref. 204. Copyright 2022, John Wiley and Sons). (e) Schematic diagram of electron transfer path across PCNG and PCNG-M[101] (Reproduced with permission from ref. 101. Copyright 2022, Elsevier).

$BaTiO_3$,[214] and defect-rich and amorphous Fe_3O_{4-x}.[215] Studies involving transition metal nanoparticles like cobalt,[216] tungsten,[207] iron,[217] and nickel[218] on graphene have also reported similar benefits.

The synergy between graphene derivatives and inorganic nanoadditives may also improve heat dispersion. Shen *et al.*[219] improved the thermal stability of a PP separator *via* modification with GO/cobalt phthalocyanine (GO/CoPc). Due to the large thermal capacity of GO/CoPc and the thermally conductive GO, the separator was able to dissipate heat more readily and withstand prolonged heating at 130 °C. Improved thermal stability and heat dissipation will help mitigate battery thermal runaway.

When modifying graphene with other nanoparticles, the distribution and adhesion of the nanoparticles play a significant role in the specific capacity of the LSB. For example, Zhang *et al.*[101] compared the performance of a modified Celgard separator prepared with *in situ* and *ex situ* methods. In the *in situ* process, phenyl-modified carbon nitride (PCN) was directly formed on GO (referred to as PCNG) *via* pyrolysis of a freeze-dried mixture of 2,4-diamino-6-phenyl-1,3,5-triazine (DPT) and GO. In the *ex situ* process, DPT was calcined into g-C_3N_4 and mechanically mixed with GO (referred to as PCMG-M). Fig. 5e illustrates the difference in the microstructural bonding between PCN and GO. Because the PCN was uniformly distributed on GO with strong covalent bonding in PCNG, the PCN layer could adsorb polysulfides without deforming and provide direct conductive pathways for improved polysulfide conversion. In contrast, the *ex situ* synthesized PCN layer was loosely held with random arrangements, resulting in longer conductive pathways. Thus, the *in situ* synthesis of nanoparticles is recommended for composition with graphene.

Other than modifying graphene with other nanoparticles, graphene morphology has been altered for improved polysulfide rejection. Li *et al.*[220] synthesized hollow graphene spheres (HGS) to block the pores of a Celgard membrane. The hollow spheres exhibited both physical blocking and adsorption mechanisms, resulting in a 55% higher capacity retention than the pristine separator. Interestingly, the HGS seemed to exhibit stronger adsorption effects than regular graphene, indicated by a decent but relatively high decay rate of 0.15% per cycle compared to other graphene composite membranes presented in Table 2. However, the adsorption effects were limited as graphene itself has weak adsorption properties. Changing the morphology of graphene may also add functionality. Zhang *et al.*[195] synthesized nitrogen-doped graphene nanoscrolls (rolled-up sheets of NG nanosheets) that wrapped around Co_3O_4 nanoparticles. Compared to an LSB with a PP membrane modified with planar NG/Co_3O_4, the battery with a nanoscroll-modified membrane retained a 10% higher coulombic efficiency (99.5%) after double the number of cycles (800 cycles). The nanoscroll membrane also reduced lithium dendrite formation on the anode. The benefits stemmed from the nanoscroll morphology promoting better electrolyte wetting, homogenous Li-ion diffusion, and lower overpotentials than NG nanosheets.

3.2 Carbon nanotubes

Single-walled carbon nanotubes (SWCNTs) and multi-walled carbon nanotubes (MWCNTs) are 1D tubes with nanoscale diameters and are often thought of as rolled-up tubes of graphene. Thus, they share many of the same properties as graphene (Section 3.1) and consequently have great potential as modifiers in LSBs because of their excellent electrical conductivity, thermal conductivity, functionalizability, and compatibility with other additives.[221] This was clearly demonstrated by Raja *et al.*,[106] who found that MWCNTs on the cathode side of a Celgard separator improved polysulfide reaction kinetics. This allowed more efficient charge/discharge at higher charge rates with around a 20% higher initial charge capacity. The effect of MWCNTs on sulfur was only effective on the cathode side. An LSB with MWCNTs on the anode side (Li side) of the separator yielded similar performance to an LSB with a pristine Celgard membrane.

As a popular upper current collector material, CNTs may promote electron transfer to hasten LiPS conversion, but CNTs alone do not adsorb LiPSs effectively. Hence, CNT-based modifications employ catalytic compounds that provide chemisorption. Recently, Fan *et al.*[222] used a poly(diallyl di-methyl ammonium) bis(trifluoromethanesulfonyl)imide (PDDA-TSFI) layer on the CNTs to increase polysulfide adsorption and induced interfacial charge distribution, resulting in a 67% higher capacity retention after 300 cycles. Other polysulfide trapping compounds, such as COFs,[223] MOFs,[224] MXenes,[225] metal dichalcogenides,[226] metal nitrides,[227] and metal phosphides,[228] have also been composited with CNTs for similar benefits.

CNTs have been frequently paired with various metal oxides (Section 5.1) that boast excellent polysulfide trapping properties for higher sulfur utilization and redox kinetics. Li *et al.*[229] fabricated a PP/MWCNT/TiO separator that enabled a high sulfur utilization of 62%. While TiO alone limits polysulfide conversion due to its insulating nature, limiting the discharge capacity, adding conductive MWCNTs improved the specific capacity by about 50% more than the pristine membrane. Essentially, adding MWCNTs made TiO a viable modifier for LSB separators, allowing an astoundingly low capacity fade rate of 0.057% per cycle. Similarly, recent studies combined various CNTs with oxygen-rich MnO nanoflakes,[230] TiO_2,[231] Nb_2O_5,[232] MnO,[233] and Ti_4O_7 [234]to enhance specific capacity while also significantly improving polysulfide rejection. Wang *et al.*[235] sandwiched 1D SWCNTs between 2D V_2C/V_2O_5 nanosheet layers to prevent the nanosheets from agglomerating, resulting in a maximum number of active sites for polysulfide adsorption. Moreover, the interstacked SWCNTs created a conductive network that improved LiPS conversion kinetics. Similarly, Gong *et al.*[236] used N-doped CNTs (NCNTs) to provide a porous structure that reduced MoS_2 aggregation and consequently greatly increased polysulfide adsorption and sulfur re-utilization. Liu *et al.*[237] synthesized 2D WS_2 nanosheets interwoven with 1D SWCNTs that formed a porous 3D structure that provided abundant active sites for polysulfide adsorption and conversion. In another example, Kannan *et al.*[238] slurry coated

a PP membrane with SWCNTs functionalized with MnS nanoparticles. The SWCNTs provided conductive pathways for polysulfide redox reactions while also physically blocking polysulfide shuttling.

CNTs are easily functionalizable with various groups that improve adhesion with other modifiers. For example, Liu *et al.*[239] modified MWCNTs with NiFe layered double hydroxides (NiFe-LDH) by first functionalizing the MWCNTs with carboxyl and hydroxyl groups *via* ozone treatment (OCNTs). The NiFe-LDHs were subsequently grown on the functionalized MWCNTs *via* an *in situ* hydrothermal method. The electronegative oxygen functionalization was necessary for the homogeneous distribution of Ni^{2+} and Fe^{2+} in solution, yielding a uniform distribution of NiFe-LDHs. The ability of NiFe-LDH/OCNT/PP separator to reject LiPSs was supported by *in situ* Raman spectroscopy with a custom-designed Raman battery shown in Fig. 6a. The resulting Raman spectra showed no obvious peaks for any LiPS species during charge and discharge of the battery. This was due to the good chemisorption and electrocatalytic conversion afforded by the NiFe-LDHs on the OCNTs.

Moreover, CNTs functionalized with electronegative groups that repel polysulfides and can form porous nanostructures that physically obstruct polysulfide shuttling. Ponraj *et al.*[240] functionalized MWCNTs with abundant hydroxyl functional groups (MWCNT–OH) *via* a hydrothermal method and used vacuum filtration to coat a standard PE separator with a uniform layer of MWCNT–OH. The MWCNT–OH adsorbed polysulfides, which reduced the shuttling effect. This was observed when stirring MWCNT–OH in a vial of Li_2S_4 solution turned the yellow solution to a nearly clear solution. In contrast, adding pristine MWCNTs did not show any significant adsorption characteristics. As shown in Fig. 6b, the Li anode with a pristine PE separator suffered from large deposits of inactive sulfur. In contrast, the LSB with a MWCNT-OH–modified separator had a smooth Li anode surface even after 100 cycles at 0.5C. The hydroxyl functionalization of the MWCNTs enabled efficient polysulfide chemisorption, resulting in a nearly perfect coulombic efficiency of 99.5%. The MWCNT–OH also reduced the charge transfer resistance, which resulted in enhanced rate performance and increased re-utilization of sulfur during charge/discharge cycles, indicated by a 52% higher initial charge capacity. Because the MWCNT–OH separator reduced the deposition of inactive sulfur on the Li anode, electrolyte resistance and interfacial resistance decreased. NCNTs have also demonstrated their ability to adsorb polysulfides.[236]

MWCNTs coatings can also act as a gutter layer that reduces the thickness of highly polysulfide-rejecting layers. A gutter layer prevents the selective material from clogging the support layer's holes and enables a thin, uniform coating of the selective material.[241] Sun *et al.*[242] used SWCNTs as a gutter layer between a Celgard 2500 separator support and zwitterionic microporous polymer (TB-BAA) selection layer (Fig. 6c). Without the gutter layer, TB-BAA infiltrated deep into the PP pores (6.5 μm thick layer) while leaving some large microporous holes, leaving pathways for polysulfide shuttling. In contrast, longer SWCNTs were smoothly coated onto the PP substrate and allowed the TB-BBA to be thinly and uniformly coated (400 nm thick layer) on top of the SWCNTs, resulting in a 50% higher specific capacity retention.

3.3 Porous carbons

3D porous carbons are also promising modifiers for commercial LSB separators, owing to their high ionic conductivity, electrical

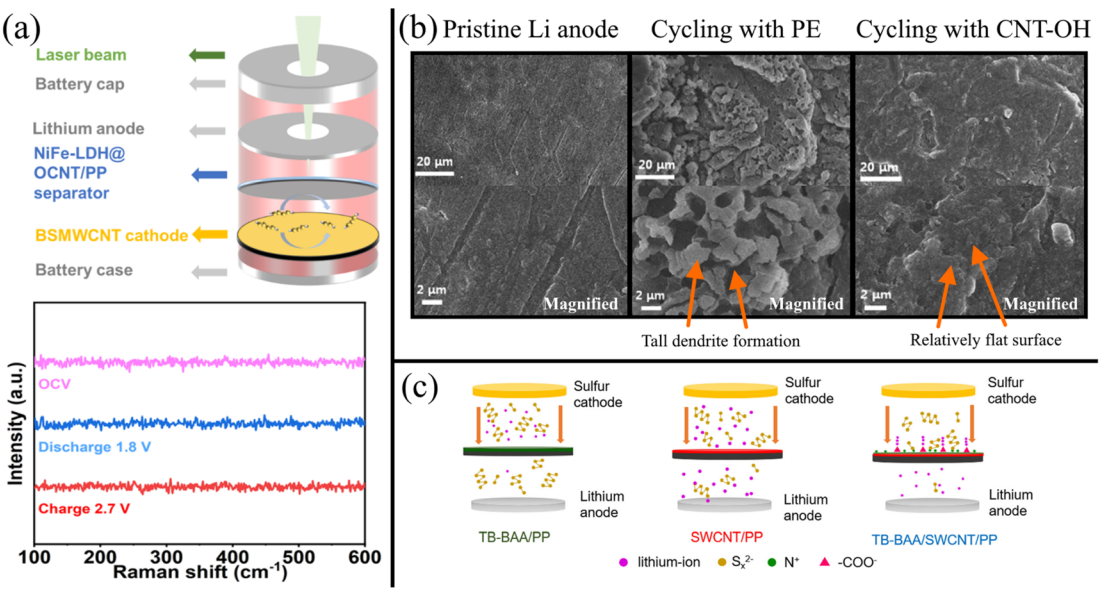

Fig. 6 (a) Schematic illustrating a standard cell design for *in situ* Raman spectroscopy and the corresponding Raman spectra for an LSB with a NiFe-LDH/OCNT-modified PP separator[239] (Reproduced with permission from ref. 239. Copyright 2022, John Wiley and Sons). (b) SEM of a Li anode surface before cycling at 1.8–2.6 V at 0.5C for 100 cycles, and after cycling in an LSB with a PE separator *versus* MWCNT–OH modified separator. The magnified view of the anode surface is shown in the bottom row[240] (Reproduced with permission from ref. 240. Copyright 2017, American Chemical Society). (c) Schematic showing the implementation of an SWCNT/TB-BAA gutter layer *via* modification of a PP separator[242] (Reproduced with permission from ref. 242. Copyright 2022, Elsevier).

conductivity, and surface area. By controlling their pore size, volume, and density, porous carbon modifications physically block polysulfides with their complex pore structures while allowing high Li-ion diffusion.[243] Porous carbons are frequently synthesized starting with a variety of carbon sources *via* template methods or by using chemical activators followed by pyrolysis at high temperatures.[244] The most common implementation of porous carbons to commercial separators is *via* slurry coating, yielding micrometer-thick, flexible selective layers against polysulfides. Unlike graphene (Section 3.1) and CNTs (Section 3.2) that require more complex processing, porous carbons are readily available as byproducts of industrial processes or as pyrolyzed biowastes, making porous carbon implementations easily scalable and sustainable.

Commercially abundant carbon blacks are common modifiers for standard LSB separators. Acetylene black (AB) is produced in large volumes as a byproduct of incomplete coal and oil combustion and is mixed with other porous carbons like graphite to form hybrid 3D structures.[245] Similarly, Ketjen black (KB) is a commonly available and popular carbon black frequently used to modify commercial LSB membranes. Its high porosity and excellent electrical conductivity make it an excellent polysulfide sieve and upper current collector that improves sulfur utilization.[246] Super P is already one of the most common conductive additives for lithium-based batteries, and super P-modified separators are already commercially available for LSB applications.[247,248] Between the many commercially available porous carbons, acetylene black may exhibit the best polysulfide rejection with high ionic conductivity, owing to it having the smallest pore size and pore volume.[249] This was shown by Huang *et al.*,[249] who compared LSBs with a PP separator slurry coated with acetylene black, Ketjen black, super P, lamp black, Vulcan black, activated carbon, activated charcoal, and carbon Black Pearls. The main difference between the carbons came down to pore size and pore volume. Non-porous carbons like acetylene black and super P formed closely connected carbon networks that physically blocked polysulfides and limited liquid electrolyte adsorption. However, porous carbons like Ketjen black and activated carbon had large pore volumes that blocked fewer polysulfides and disrupted Li-ion diffusion due to their higher electrolyte uptake. Hence, the separator with non-porous acetylene black, which had the second smallest pore size and second smallest pore volume outperformed the other carbon-modified separators that had mixed rankings of pore size and volume. Still, every carbon-modified separator had at least a 40% capacity retention (acetylene had 64%), which outperformed the pristine separator that had less than 10% retention after 200 cycles at 0.1C.

However, commercial porous carbon modifications alone are not sufficient for polysulfide rejection. Jin *et al.*[247] showed this by comparing the performance of an LSB with a standard PE separator, a commercial super P-modified PE separator, and a Co–N–C powder/super P-modified PE separator. The battery with the PE/super P separator had a 30% higher initial capacity than the pristine separator and lost 73% of its capacity after 200 cycles. Interestingly, the battery with the pristine separator lost only 79% of its initial capacity under the same conditions, suggesting that super P did not significantly stop polysulfide diffusion due to its large pores and minimal electrostatic interactions. However, the addition of Co–N co-doped carbon nanocages to super P increased the initial capacity by 28% and capacity retention by 21%. Hence, carbon blacks are frequently mixed with more catalytic compounds. Because porous carbons have high surface areas and conductivities, they can adsorb a large amount of additives that have high affinities for polysulfides and provide conductive pathways for fast reaction kinetics.

Porous carbons often need to be combined with metal nanoparticles like Ni, Co, Fe, V, Cr, Mo, Nb, and Mn and catalytic metals like Pt and Au to maximize LiPS adsorption and catalytic conversion.[247,250,251] For example, Zhen *et al.*[252] found that adding Co nanoparticles to Ketjen black improved capacity retention from 54% to 69% after 300 cycles at 0.3C. Fig. 7a shows the modification of Ketjen black with nitrogen and Co. The nitrogen groups were necessary for the adhesion of Co nanoparticles into the Ketjen pores. The highly adsorptive Co and nitrogen centers embedded in the porous carbon were then able to efficiently adsorb and immobilize LiPSs. Similarly, highly polar metal salts like metal oxides,[253–255] sulfides,[256,257] fluorides,[258] and selenides,[259] exhibit good adsorption for polysulfides. While not the most effective against polysulfide rejection, porous carbons have also been composited with doped graphene and CNTs. In such instances, the porous carbons provide high surface areas with large pores to adsorb polysulfides, while the doped graphene or CNTs provide high electron mobility for fast LiPS conversion.

Heteroatom doping with nitrogen, phosphorous, and sulfur improves porous carbon's ability to reject polysulfides by endowing electrostatic and chemisorption effects. The most common doping is with nitrogen atoms, owing to increased electrical conductivity, interlayer spacing, and interaction with polysulfides. Zhang *et al.*[104] synthesized pyridinic N-doped carbon *via* the calcination of GO with NH_4HCO_3 at 600 °C. Compared to a pristine Celgard separator or an rGO-modified Celgard separator, the N-doped porous carbon-modified separator reported a higher initial capacity (indicating better sulfur utilization) and lower decay rate per cycle. The improved chemisorption of polysulfides was due to the abundant pyridinic nitrogen groups combined with effects from pyrrolic nitrogen, graphitic nitrogen, and oxygen functional groups in the N-doped porous carbon separator. The reduction of the shuttle effect was determined using time-resolved *in situ* Raman spectroscopy, wherein significantly lower intensity peaks for soluble LiPSs were detected with the N-doped carbon-modified separator than with the pristine PP separator. Zeng *et al.*[260] synthesized honeycomb-like N, P dual-doped carbon (HNPC) powder by pyrolyzing a mixture of glucose, urea, $NH_4H_2PO_4$, and SiO_2 nanoparticles and applied it to a Celgard membrane *via* slurry coating. LSBs with an N and P-doped separator exhibited better cycle stability, specific capacity, and rate capability than an only N-doped separator. This was due to the P atoms exhibiting excellent bonding with sulfur atoms in the polysulfides that improved polysulfide adsorption, reaction kinetics, and sulfur loading. Kong *et al.*[261] similarly found that

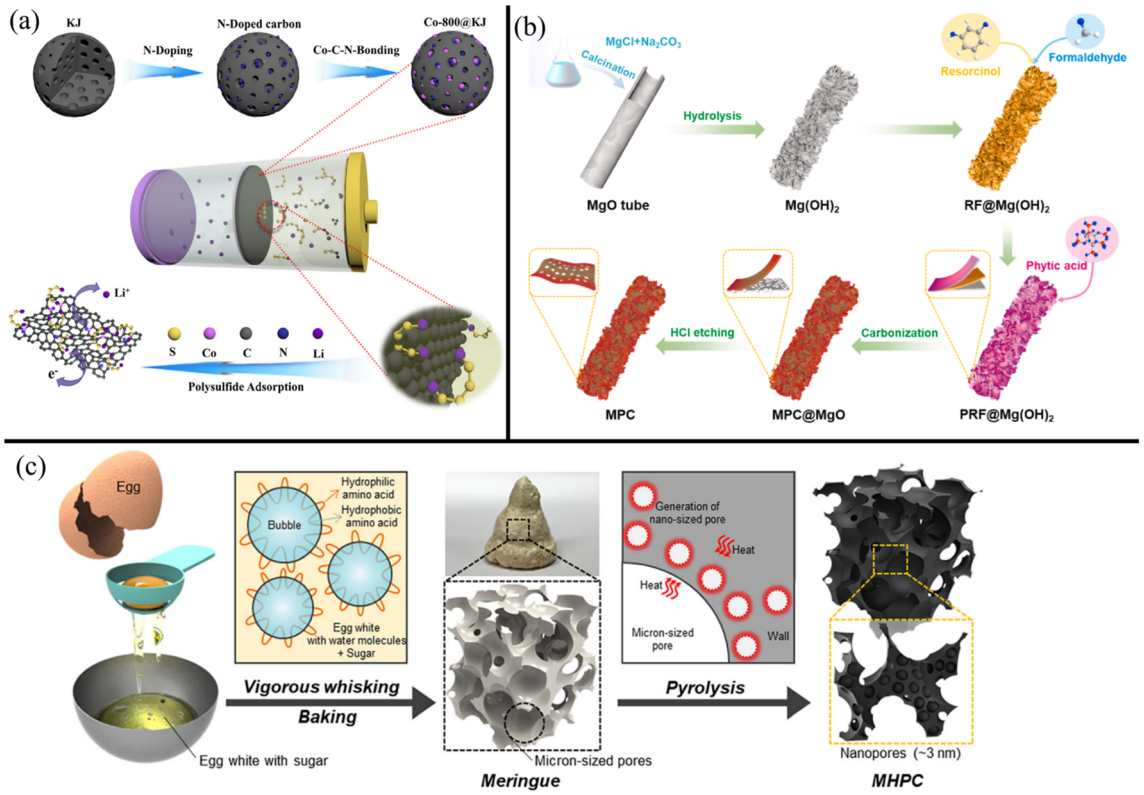

Fig. 7 (a) Schematic showing the N and Co modification of Ketjin black to improve LiPS adsorption[252] (Reproduced with permission from ref. 252. Copyright 2021, John Wiley and Sons). (b) Schematic showing the formation of P-doped hierarchical porous carbon with flower petal-like protrusions for increased surface area[261] (Reproduced with permission from ref. 261. Copyright 2022, Elsevier). (c) Schematic showing the synthesis of porous carbon derived from egg whites and sugar[266] (Reproduced with permission from ref. 266. Copyright 2022, Elsevier).

strong P–S and P–Li bonds significantly reduced polysulfide shuttling. Fig. 7b outlines the synthesis of a hierarchically porous P-doped carbon nanosheet structure using MgO as an initial template. HCl etching was used to remove the MgO nanoparticles, leaving uniform pores around 4 nm for effective LiPS sieving. The improved adsorption also lowered the reaction energy barrier for Li_2S precipitation, resulting in faster liquid–solid conversion between the polysulfides and Li_2S. Metallic dopants like Co were shown by Liu *et al.*[262] to exhibit bi-directional catalytic activity for the redox of polysulfides.

The most promising carbon sources are biomaterials and biowastes, which make porous carbons greener alternatives than other carbon-based modifiers. Yang *et al.*[263] turned supermarket kelp into I and N co-doped carbon powder (INC). While other carbon materials like graphene and CNTs require additional chemicals during synthesis for heteroatom doping, biologically derived porous carbons naturally have abundant atoms like nitrogen, phosphorous, and sulfur in their structure. This makes their synthesis significantly more facile and cost-effective for large-scale production. Recently, Zhu *et al.*[264] carbonized rice paper plant pith commonly used in traditional Chinese pharmacies into a light carbon powder with honeycomb-like pores. Li *et al.*[265] pyrolyzed chlorella (algae) powder to yield N-doped carbon powder (NC). Choi *et al.*[266] used egg whites with sucrose as pore-forming agents, yielding hierarchically porous carbon (Fig. 7c). Wang *et al.* synthesized heteroatom-doped porous carbon from Ginko leaves.[267] *In situ* Raman spectroscopy showed that the Ginko leaf-derived carbon layer mitigated the shuttle effect, with unchanging LiPS peak intensities at the PP separator surface even after 300 min. Recycling such biowaste materials should be encouraged for a more sustainable future. Biologically derived porous carbons are often mixed with small quantities of commercial powders like super P, Ketjen black, and acetylene black as fillers before application to commercial LSB separators.

3.4 Graphitic carbons

While not as popular as graphene, CNTs, and porous carbons modifications, some recent works have been done on modifying commercial separators with other graphitic carbon materials—in particular, carbon nanoparticles (CNPs) and graphitic flakes. As with the other carbon-based materials, graphitic carbon has high conductivity for improved sulfur utilization and the ability to sieve polysulfides.[268] Since the primary role of carbon-based modifications in rejecting LiPSs is to improve LiPS conversion kinetics with high electron mobility, lower-dimensional CNPs may be more efficient than 1D CNTs and 2D graphene. Zhang *et al.*[269] compared the performance of LSBs with PP membranes modified with CNPs, CNTs, and graphene nanosheets fabricated *via* vacuum filtration. Fig. 8 shows SEMs of CNP, CNT, and

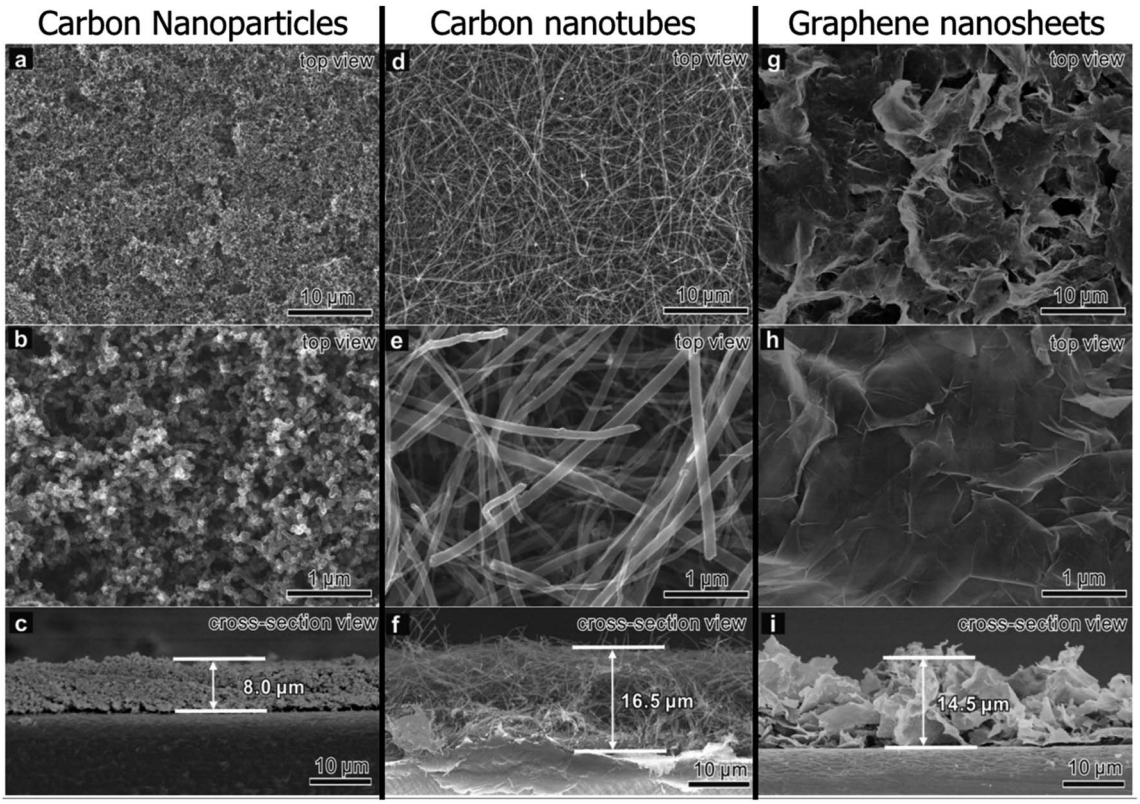

Fig. 8 SEM of PP separators coated with a layer of (a–c) CNPs, (d–f) CNTs, and (g–i) graphene nanosheets. An unmagnified and magnified view from the top is shown in the first two rows, respectively. A cross-view of the modified separator is shown in the last row, with the average thickness of the carbon layer labeled[269] (Reproduced with permission from ref. 269. Copyright 2021, Elsevier).

graphene-coated separators. The 0D CNPs were more densely packed than the intertwined CNTs and flaky graphene, resulting in smaller pore sizes that limited polysulfide shuttling while still having a high pore volume for electrolyte and polysulfide adsorption. Moreover, the charge transfer resistance of the cell with the CNPs was lower than the CNTs and graphene flakes, resulting in better rate capability even at 3C charge/discharge rate. Due to their low dimensionality, CNPs acted as conductive bridges that decreased interparticle gaps between the catalytic modifiers and LiPSs compared to higher dimensional carbon morphologies. The polysulfide rejection was respectable despite the commercial separator having only carbon modifications, with the LSB having a small 0.08% decay per cycle after 200 cycles at 1C. This work shows the potential of CNPs as potential modifiers.

CNPs may undergo heteroatom doping with nitrogen or sulfur to improve their interaction with polysulfides. Diez *et al.*[270] co-doped nitrogen and sulfur in CNPs (NSCNPs) by using polypyrrole as a carbon precursor and reaction with sodium sulfate during activation. Having the NSCNP modification resulted in a 23% higher initial capacity of 1020 mA h g^{-1}. Moreover, the cell with the modified separator retained 82% of its initial capacity after 100 cycles at 0.2C (0.089% decay per cycle for 500 cycles at a higher rate of 2C), whereas the cell with the pristine separator retained only 56% after 100 cycles. The superior conductivity and polysulfide adsorption ability of doped CNPs caused the increase in capacity and cyclability.

Graphitic carbon flakes (CFs) are also potential modifiers that exhibit excellent conductivity. Zheng *et al.*[271] synthesized CFs by directly carbonizing sodium citrate and embedded the CFs into a PP separator *via* vacuum filtration. The CFs clogged the large pores in the PP separator while leaving enough space for Li-ion diffusion. Due to the abundant carboxyl, carbonyl, and hydroxyl groups in the CFs, the CFs had significantly improved electrolyte wettability, indicated by an almost 0° electrolyte contact angle. The rate performance of a battery with PP/CF separators was better than that of a battery with a PP separator, with a 54% higher initial capacity at 0.2C (1207 mA g^{-1}) and 99% coulombic efficiency even after 200 cycles. The capacity fading rate was 0.071% per cycle for 500 cycles at 0.5C.

4 Organic framework-based modifications

Metal–organic frameworks (MOFs) and covalent–organic frameworks (COFs) are highly porous compounds with highly organized crystal structures consisting of metal or organic nodes and organic linkers. Organic frameworks provide polyolefin separators with (a) a highly organized cage structure with controllable pore sizes for highly selective sieving, (b) catalytic metal or

Table 3 Summary of LSB performance and longevity with organic framework-modified commercial membranes

Membrane	Specific charge (mA h g^{-1})	C rate (C)	Cycles	% Loss per cycle	Highlights	Ref.
MOFs						
PE/UiO-66/Nafion	1127	0.1	200	0.11	Nafion helped bind MOFs to PE	287
PP/ZIF-8/KB	1235	0.1	100	0.29	High LiPS chemisorption	279
PP/aMIL-88	1249	0.2	100	0.10	Amorphous MIL-88 better than crystalline MIL-88	102
PP/ZIF-8/MWCNT	1588	0.2	100	0.45	91% sulfur utilization	278
PP/UiO-66	855	0.5	500	0.03	Improved thermal stability	274
PE/ZnO/N/KB	868	0.5	400	0.10	ZIF-8 carbonization	283
PP/Ce–UiO-66/super P	891	1.0	300	0.09	Super P conductivity required for catalysis	281
PP/Ce-MOF-808	955	1.0	500	0.03	Homogeneous Li platting/stripping	273
PP/FJU-90	1047	1.0	500	0.04	Pore-space partitioning increased active sites	285
PP/ZIF-8/PDA	750	2.0	500	0.01	PDA increased MOF density	286
PP/CSUST-1/CNT	976	2.0	1200	0.04	Multi-valent Ce metal centers	282
COFs						
PP/COF	864	1.0	500	0.05	Lithiophilic properties of the SO_3H groups	290
PP/CTF/MWCNTs	1156	1.0	1000	0.05	Decreased overall LSB resistance	223
PP/CTF/PEDOT:PSS	1205	1.0	1000	0.05	Improve adhesion with negatively charged PEDOT:PSS	293
PP/COF	666	2.5	1000	0.05	Electrophilic carboranyl groups	289
PP/COF	633	4.0	400	0.04	Improved Li-ion conductivity	294
PP/TAPP-ETTB/graphene	1350	0.5[a]	400	0.08	Decreased square resistance by 99%	292

[a] Current density measured in A g^{-1} instead of C rate.

organic centers for high LiPS adsorption, and (c) lithiophilic groups that improve Li-ion conductivity. Commercial membranes are often modified with organic frameworks *via* slurry coating[272] but may also be directly crystallized on polyolefin separators.[273] The performance of exemplary MOF and COF composite polyolefin separators for LSBs is summarized in Table 3.

4.1 Metal–organic framework (MOF)

MOFs are highly organized, porous, crystalline networks assembled with inorganic metal centers connected with organic ligands. Due to MOFs' easily tunable pore sizes and chemisorptive metal centers, they have been used to reduce polysulfide shuttling *via* physical and adsorptive mechanisms. While the advantages of MOFs are clear, recent improvements to MOFs involve improving the electrical conductivity of MOFs for higher sulfur utilization and tuning pore sizes for high Li-ion diffusion with minimal polysulfide shuttling. MOFs used to modify commercial LSB separators include[274] UiO-66 and ZIF-67.[275] More obscure MOFs include Ni_3(2,3,6,7,10,11-hexaiminotriphenylene)$_2$ (Ni_3(HITP)$_2$)[276] and HKUST-1.[277]

One of the most common MOFs is the zeolitic imidazolate framework (ZIF-8), owing to its facile synthesis and easily controllable pore size. Carbon materials (Section 3) are often composited with ZIF-8 to increase the MOF's catalytic ability. Wu *et al.*[278] composited ZIF-8 with MWCNTs. The ZIF-8/MWCNTs slurry-coated PP separator exhibited a high sulfur utilization of 95% due to the combined effects of Lewis acid–base chemisorption effects of the ZIF-8 and reduced charge transfer and internal resistance due to the MWCNTs. More recently, Ma *et al.*[279] coated a PP separator with a slurry mixture of ZIF-8 and Ketjen black. The capacity retention of the PP separator with ZIF-8 and KB was 57%, much higher than the 45% for PP/KB and 36% for pristine PP. While adding ZIF-8 to PP/KB increased the charge-transfer resistance by 8%, the LSB with the PP/ZIF-8/KB had a 9% higher initial capacity. This suggests that the benefits of adding ZIF-8 outweighed the potential loss in conductivity.

Cerium-based MOFs have also recently gained popularity, owing to their excellent hydrophilicity and larger pore sizes compared to ZIF-8 and ZIF-67 MOFs.[280] Recently, Dang *et al.*[273] grew cerium-based MOF-808 crystals directly on both sides of a commercial PP separator *via* a room temperature *in situ* growth method. The Ce-based MOF-modified separator exhibited a 60% lower charge transfer resistance than a pristine PP separator, owing to the enhanced electrolyte wettability from the hydrophilicity of the Ce-based MOF (Fig. 9c). Moreover, the 1.8 nm pore sizes allowed fast Li-ion diffusion while sieving polysulfides and provided a large surface area for faster redox kinetics, evidenced by the significantly higher, indicated by the small ratio between the steady state current to the initial current shown in Fig. 9d. Ce-based MOFs have also been composited with carbon materials to enhance their electrical conductivity. Recently, Su *et al.*[281] modified a standard Celgard separator with Ce-based UiO-66-MOF and super P, resulting in a composite separator with a higher initial capacity and significantly improved capacity retention compared to the separator modified with only super P. Similarly, Jin *et al.*[282] composited a Ce-based MOF with CNTs before slurry coating the composite onto a commercial PP separator. As shown in Fig. 9a, the mixed-valence Ce-based MOFs were derived from Ce-based UiO-66, referred to as CSUST-1. Compared to the UiO-66-modified, CNT-modified, and un-modified Celgard separators, the CSUST-1/CNT-modified separator exhibited higher overall capacity and superior rate performance shown in Fig. 9b. This was due to the

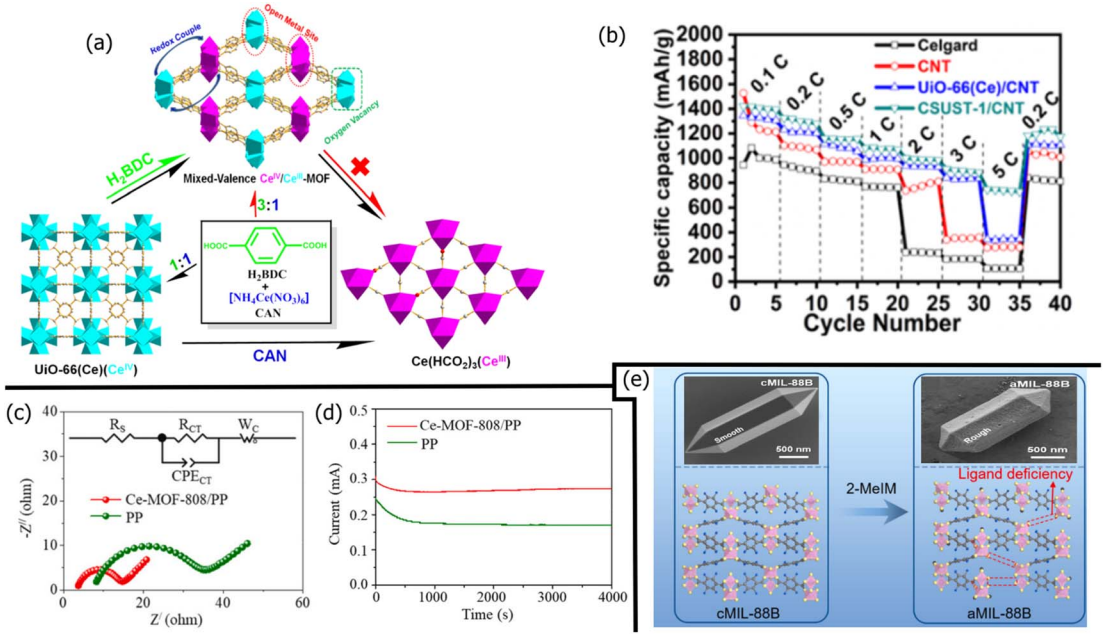

Fig. 9 (a) Synthesis and conversion among Ce-based UiO-66, CSUST-1, and $Ce(HCO_2)_3$. (b) Comparison of rate performances at various C-rates for a pristine Celgard *versus* CNT-modified, UiO-66/CNT-modified, and CSUST-1/CNT-modified Celgard separators[282] (Reproduced with permission from ref. 282. Copyright 2021, The American Chemical Society). (c) Electrochemical impedance spectrum (EIS) and (d) Current *vs.* Time plots of a Ce-based MOF-808 modified separator and pristine PP separator[273] (Reproduced with permission from ref. 273. Copyright 2022, Elsevier). (e) Schematic diagram of crystalline and amorphous MIL-88. SEMs of crystalline and amorphous MIL-88 are also shown[102] (Adapted with permission from ref. 102. Copyright 2021, Elsevier).

abundant oxygen vacancies stabilized by Ce(IV) metal sites, excellent catalytic properties of the open Ce(III) sites, and the Ce(IV)/Ce(III) redox couple (Fig. 9a).

MOFs can be used as templates that undergo carbonization to increase electrical conductivity while preserving small pore sizes. In a recent study, Qian *et al.*[283] carbonized a ZIF-8/KB composite to yield a porous ZnO/N/KB composite. Similarly, Zeng *et al.*[181] carbonized a ZIF-8/PAN composite to yield a network of carbon nanofibers. In another example, Qian *et al.*[284] derived Ni-doped porous carbon structures using a Ni-based MOF precursor. Such composites are discussed more fully in our discussion of porous carbons (Section 3.3).

Besides carbon-based improvements to MOF conductivity, amorphous MOFs with abundant defects have exhibited improved conductivity while retaining their catalytic ability. Zhang *et al.*[102] compared the performance of crystalline and amorphous MIL-88 MOF as modifications to a commercial separator. As shown in Fig. 9e, the amorphous MIL-88 MOF (aMIL-88) was rougher and more porous than the crystalline MIL-88 MOF (cMIL-88). The more abundant activation sites with the amorphous MOF improved sulfur utilization and polysulfide rejection, increasing the initial capacity and capacity retention. The amorphous MIL-88 MOF also had a lower charge transfer resistance and interface resistance, owing to the formation of Li-ion transport channels during amorphization.

The ability to control the porosity of MOF-modified commercial separators has been heavily investigated. Jeon *et al.*[99] used rigorous molecular dynamics simulations to show that a nanosheet layer of Cu_3(benzene-1,3,5-tricarboxylate)$_2$ MOF was highly selective against polysulfides but favorable for high Li diffusion. Chen *et al.*[285] fabricated pore-space-partitioned FJU-90 MOFs with pore sizes optimized to around 9 Å for a balance between fast Li-ion diffusion, uniform Li-ion electrodeposition, and high polysulfide rejection. Moreover, the pore structure was modified to expose the Co and Ni metal centers for polysulfide adsorption and catalytic conversion. MOFs may also be used to increase the porosity of other separator modifiers.

One of the limitations of MOF modifications to standard PP or PE separators is the low density and adhesion of MOFs to commercial separators. To improve MOF compatibility, intermediate materials like polydopamine (PDA) may be used. For example, Wu *et al.*[286] used PDA as a glue between PP and ZIF-8. The zinc centers in the MOF had strong interactions with the catechol groups in the PDA for improved adhesion to the PP substrate. The PDA interlayer also increased the number of nucleation sites for ZIF-8 growth, resulting in a denser packing of MOFs that closed the larger PP pores more effectively. Similarly, Kim *et al.*[287] could not coat a pristine PE separator completely with UiO-66 MOFs *via* vacuum filtration due to the weak interactions between the PE and MOF. To overcome this, a Nafion layer was added, which interacted strongly with both the PE separator and the MOF additive.

4.2 Covalent–organic framework (COF)

COFs are highly nanoporous crystalline materials formed by strong covalent links between organic building blocks.[288] COF-based modifications have excellent potential in LSBs used in

portable technologies like electric vehicles and smart devices, owing to the low density and high thermal stability.[289] While they are not yet under intense study due to their difficult synthesis and instability, their tunable pore sizes and excellent functionalizability leave much room for further development.

COFs are promising in LSB separators because of their highly tunable pore size and low density. Zhao *et al.*[290] recently modified a PP separator with a 1,3,5-triformylphloroglucinol (Tp) and 2,5-diaminobenzene sulfonic acid (TpPa–SO_3H) COF *via* interfacial polymerization. The PP/COF exhibited regular pore channels and improved electrolyte wettability to its high polarity, resulting in a 157% higher ionic conductivity than pristine PP. The lithiophilic sulfonic groups in the TpPa–SO_3H COF helped block polysulfides *via* coulombic repulsion, resulting in a low 25% decrease in initial capacity after 500 cycles at 1C. Moreover, having the TpPa–SO_3H increased lithium conductivity by 158% than PP (Fig. 10a), while the COF with –SO_3H groups showed an 11% higher Li-ion transference than the COF with –COOH groups (Fig. 10b). This was due to the lithiophilic interaction from –SO_3H and more regular pore structure for the COF with –SO_3H groups.

Zhu *et al.*[289] modified a Celgard separator with a carborane-based COF that exhibited a 72% higher initial capacitance and 27% lower % decay per cycle than a pristine Celgard separator. Fig. 10d shows the binding energies between the COF and LiPSs of various chain lengths. The high polysulfide rejection was attributed to the electrophilic boron centers in the COF that easily adsorbed the polysulfides. Work by Sahu *et al.*[291] has also shown the efficacy of boron atoms as adsorptive centers for sulfur. Moreover, the small 1.2 nm pore sizes sieved the large polysulfides while allowing high Li diffusion.

Because COFs suffer from low electrical conductivity, COFs are often combined with conducting materials such as carbon nanomaterials or conductive polymers before modification to commercial battery membranes. For example, Sun *et al.*[292] combined a COF with graphene. 5,10,15,20-tetrakis(4-aminophenyl)porphyrin cores and 4,4′,4″,4‴-(ethene-1,1,2,2-tetrayl) tetrabenzaldehyde linkers were reacted to form a COF called TAPP-ETTB (Fig. 10c). The COF was mixed with graphene in a *n*-methyl-2-pyrrolidone (NMP) solution and combined with a commercial PP *via* vacuum filtration. Adding graphene to the COF decreased the square resistance from over 20 000 Ω square^{-1} to 33 Ω square^{-1}. Compared to a PP/graphene separator, the PP/COF/graphene separator exhibited about 55% higher specific capacitance at a range of current densities, owing to improved sulfur utilization, decreased polysulfide shuttling, and diffusion during lithiation/delithiation. Similarly, Shi *et al.*[223] modified a COF with MWCNTs before coating

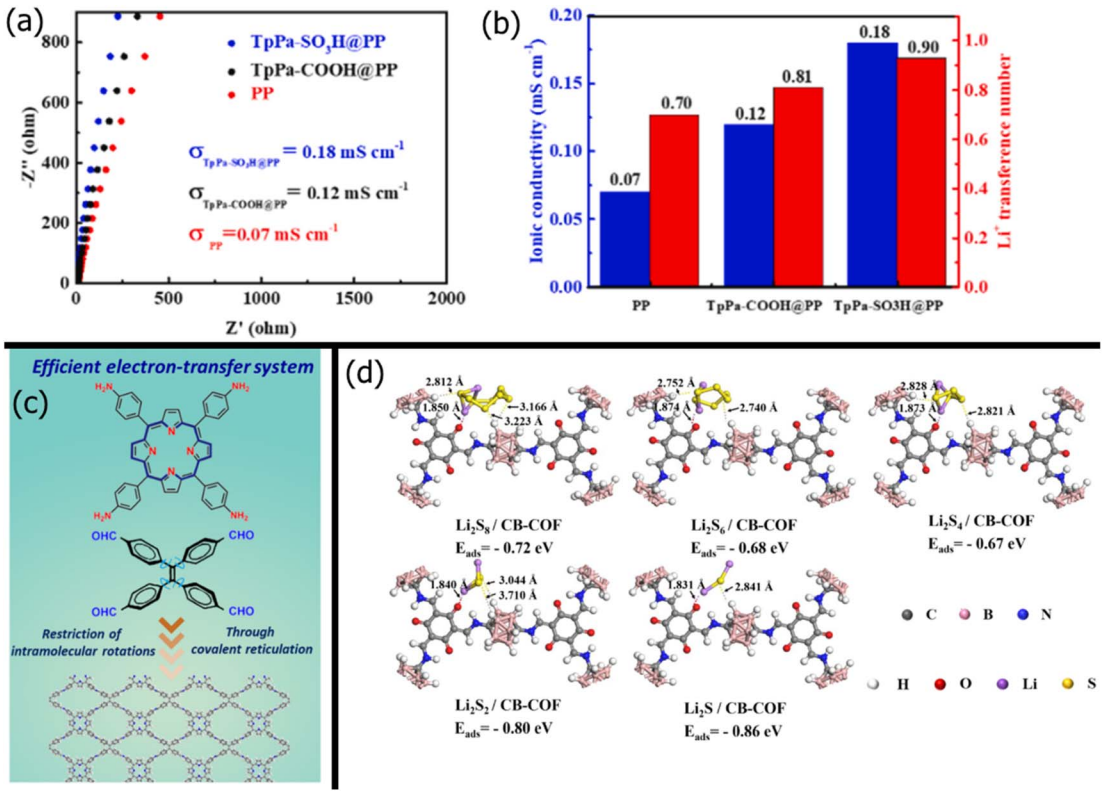

Fig. 10 (a) Ionic conductivity of the TpPa–SO_3H@PP, TpPa–COOH@PP, and PP separators; (b) bar graph of ionic conductivity and Li-ion transference number of the TpPa–SO_3H, TpPa–COOH, and PP separators[290] (Reproduced with permission from ref. 290. Copyright 2022, Elsevier). (c) Schematic showing the rigid structure of the TAPP-ETTB COF with an optimally designed electron transfer system *via* the porphyrin[292] (Reproduced with permission from ref. 292. Copyright 2022, The American Chemical Society). (d) Adsorption energies between the CB-COF molecule and various sulfur species (Li_2S_x, $1 \leq x \leq 8$) based on DFT calculation[289] (Reproduced with permission from ref. 289. Copyright 2021, The American Chemical Society).

a Celgard separator. A 2D covalent triazine framework (CTF) was mixed with MWCNTs in NMP and slurry coated onto a Celgard separator. The CTF/MWCNTs-modified separator exhibited a 42% lower decay per cycle than an MWCNT-modified separator, owing to the abundant pyridinic nitrogen groups in the CTF adsorbing the polysulfides. Interestingly, the PP/CTF/MWCNT separator exhibited a lower total resistance than a PP/MWCNT separator, resulting in the highest rate capability for the CTF/MWCNT separator. CTFs have also been combined with conductive PEDOT:PSS *via* a layer-by-layer technique onto a Celgard separator.[293] The Celgard separator was pretreated with Nafion for stable layer-by-layer assembly. Likewise, the CTF was functionalized with poly(diallyl dimethyl ammonium chloride) (PDDA) to have a positive charge before layering with negatively charged PEDOT:PSS. Ionic conductivity increased by 14% than a pristine separator, and the composite had a low 33 Ω interfacial resistance due to the higher electrolyte wettability and conductivity of the CTF/PEDOT:PSS composite.

While not in direct contact, a conductive interlayer between the modified separator and cathode can significantly improve rate capability. Cao *et al.*[294] fabricated a PP/TpPa–SO_3Li COF separator that could not sustain capacity at a current density above 2C. However, adding a CNT interlayer enabled a low 0.039% decay per cycle to a respectable 632.7 mA h g^{-1} even after 400 cycles at 4C. This was because the CNTs lowered the charge transfer resistance of the sulfur-loaded cathode, which decreased the build-up of inert LiS/S.

5 Inorganic modifications

The most common inorganic modifications to LSB separators include transition metal oxides, metal sulfides, and MXenes. Other promising inorganic modifiers include metal nitrides, borides, phosphides, and fluorides. Inorganic modifiers specialize in effective LiPS rejection *via* (a) immobilization through strong chemisorption, (b) rapid catalytic conversion with their multi-valent metal component (c) sieving or trapping when using 1D or 2D morphologies.[295] Inorganic modifiers are often implemented in commercial polyolefin separators *via* vacuum filtration.[296] However, they often require other

Table 4 Summary of LSB performance and longevity with inorganic-modified commercial membranes

Membrane	Specific charge (mA h g^{-1})	C rate (C)	Cycles	% Loss per cycle	Highlights	Ref.
Metal oxides						
PP/$MgAl_2O_4$/MWCNT	1370	0.1	50	0.61	Only impacted cathode side	106
PP/CeO_2/graphene	1039	0.5	200	0.12	High sulfur loading	211
PP/TiO_2/MWCNT	1104	0.6	900	0.07	Increased separator surface area	231
PP/MnO/NCNTs	929	1.0	500	0.07	Upper current collector	230
Mn_3O_4/PP	572	2.5	2000	0.03	Oxygen vacancies for selective catalyst	306
PP/V_2O_5/graphene	2028	1.0[a]	100	0.62	Increased Li-ion insertion/extraction capacity	299
Metal sulfides						
PP/ZnS	967	0.5	200	0.04	Quantum dots with abundant active sites	314
PP/CoS/KB/C_3N_4	810	1.0	500	0.03	Capacity retention plateaused after 200 cycles	256
PP/C–SnS_2/AB	919	1.0	500	0.06	Chemical etching for defects	257
PP/WS_2/SWCNT	1069	1.0	1000	0.04	Porous 3D layer	237
PP/CuS/graphene	1029	1.0[a]	200	0.19	Increased electrolyte wettability	311
MXenes						
PP/V_2C/SWCNT/V_2O_5	1240	0.2	500	0.17	MWCNTs reduced V_2C nanosheets aggregation	235
PP/Ti_3C_2	849	0.5	500	0.06	Decreased charge transfer resistance	316
PP/$Ti_3C_2T_x$	852	1.0	600	0.06	CNTs prevented MXene restacking	225
PP/Ti_2C/Nafion	920	1.0	1000	0.03	Decreased pore size	152
Other inorganic modifiers						
PP/purified BNNT	1429	0.3	200	0.12	Li dendrite suppression	326
PP/Ni–Co–P/carbon	961	0.5	1000	0.06	High rate capability at high sulfur loadings	338
PP/CaF_2/rGO	1005	0.5	420	0.06	LiF formation mitigated dendrites	209
PP/SrF_2/graphene	1140	0.5	350	0.05	SrF_2 lithophilicity suppressed dendrites	208
PP/TiN–Si_3N_4	1243	0.5	500	0.09	Molten salt process reduced synthesis cost	327
PP/Sb_2Se_3/rGO	945	1.0	500	0.03	Defect engineering increased conductivity	342
PP/ZnSe/carbon	1026	1.0	1000	0.04	MOF-derived ZnSe nanoparticles	341
PP/VN/NG	1082	1.0	300	0.07	Dual redox catalysis	206
PP/f-BN	1194	1.0	1000	0.01	Amino and carboxyl functionalization	323
PP/$Ni_{0.2}Mo_{0.8}N$/MWCNT	1421	1.0	1400	0.05	Bimetallic synergy in metal nitride	332
PP/Ni_3B/rGO	572	2.0	500	0.06	Electron deficient adsorbent	334
PP/Mo–MoB	671	2.0	500	0.06	Heterogeneous catalyst for multi-step LiPS reduction	335
PP/CoN/CNT	901	2.0	250	0.11	Nitrogen vacancies	227

[a] Current density measured in A g^{-1} instead of C rate.

conductive materials like carbon-based nanomaterials (Section 3) or conductive polymers (Section 2.3) for practical applications due to their poor electrical conductivity. The performance of LSBs with inorganic/polyolefin composite separators is summarized in Table 4.

5.1 Metal oxides

Transition metal oxides comprise a broad class of nanomaterials that boast abundant active sites, multiple valence states, and low preparation costs. Their use as modifiers for commercial LSB separators is primarily due to their ability to immobilize and catalyze polysulfides *via* Lewis acid–base interactions and oxygen vacancies.[297] Wang *et al.*[298] recently modified a standard PP separator with MnO_2 *via* a self-assembly method from $KMnO_4$. The aforementioned properties of transition metal oxides resulted in a low decay rate of 0.058% per cycle after 500 cycles at 0.5C. Cheng *et al.*[299] used V_2O_5 microspheres on graphene to increase the specific capacity of the LSB. Because V_2O_5 has a large electrochemical window that can match with the sulfur cathode, it can theoretically act as a secondary cathode for Li-ion insertion/extraction, increasing the cathode-side capacity of the LSB.[300] Hence, Cheng *et al.*[299] reported one of the highest initial discharge capacities at 2028 mA h g^{-1} at 1 A g^{-1} current. Fig. 11a shows a special LSB cell designed for *in situ* XRD analysis. The disappearance of α-S_8 during discharge and reappearance during the charging process showed the excellent reversibility of the LiPS redox reaction (Fig. 11b). No Li_2S was observed during the charge/discharge, suggesting incomplete LiPS reduction. The consistent presence of long-chain LiPS signals also indicated that the soluble LiPSs remained on the cathode side without any significant diffusion to the anode.

In another study, a PP separator modified with Eu_2O_3 and Ketjen Black yielded a low 0.05% decay per cycle for 500 cycles at 1C, primarily due to the adsorption and catalytic conversion by Eu_2O_3.[297] The KB supplemented the poor electrical conductivity of Eu_2O_3, boosting its rate capability. A similar synergy was reported between Ti_4O_7 and KB.[301] Both Ti_4O_7 and KB outperformed the pristine separator and KB-modified separator in low and high sulfur loadings, indicated by the higher initial capacity and longer cycle life. Other conductive nanomaterials have been used to improve the charge transfer between insulating polysulfides and metal oxides, including porous carbons,[302] CNTs,[303] carbon coatings,[304] and conductive polymers like PANI.[182]

While often doped as nanoparticles into conductive hosts, transition metal oxides may have 1D or 2D morphologies that may be directly layered onto standard polyolefin separators. For example, Huang *et al.*[305] synthesized a layered structure of sodium-containing TiO_2 nanowires and TiO_2 nanosheets *via* a hydrothermal process. The mixed structure composite was vacuum filtered through PP to yield a composite separator. The polar TiO_2 increased electrolyte wettability and decreased the shuttling effect, as expected. Compared to a separator with only TiO_2 nanowires, the nanowire/nanosheet mixed-structure

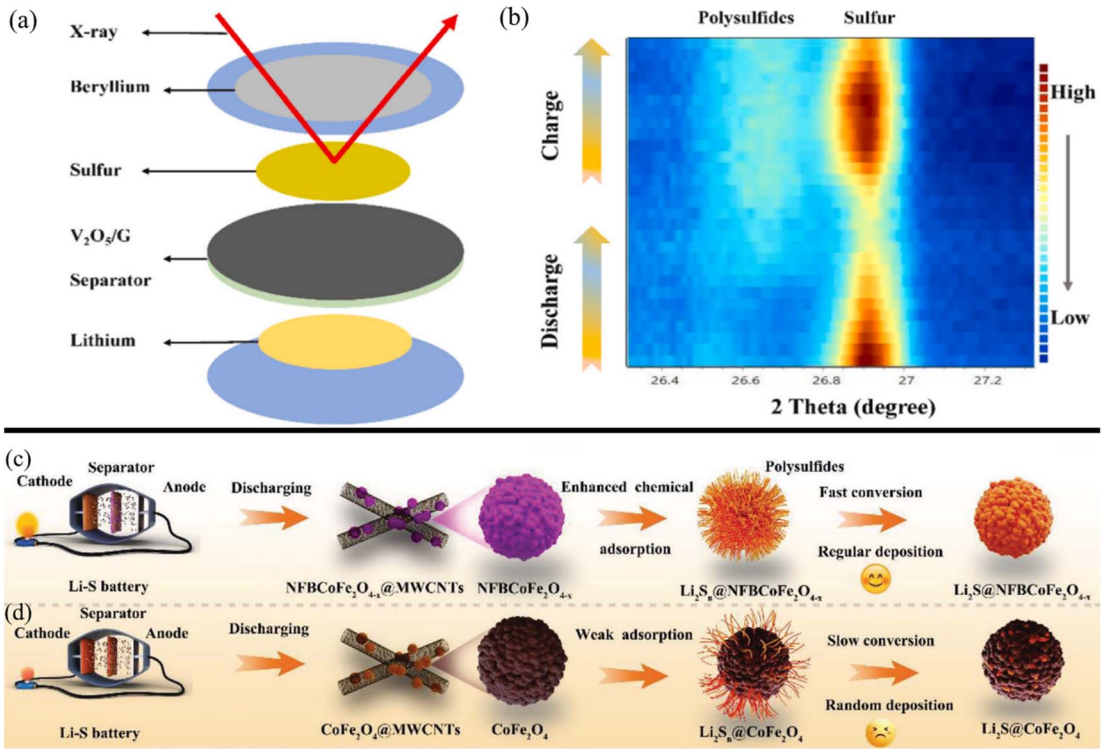

Fig. 11 (a) Schematic showing the configuration of an LSB used for *in situ* XRD test with a V_2O_5-modified separator and (b) *in situ* XRD contour plot of the LSB with a V_2O_5-modified separator[299] (Reproduced with permission from ref. 299. Copyright 2021, Elsevier). Schematic of the LiPS transformation on the surface of (c) N, F, B-doped $CoFe_2O_4$–x on MWCNTs and (d) $CoFe_2O_4$ on MWCNTs[303] (Reproduced with permission from ref. 303. Copyright 2022, John Wiley and Sons).

composite had an approximately 40% higher initial capacity at 0.2C, with better rate capability for charge densities between 0.2 to 2C. This was partly due to the thinner deposition of the mixed-structure TiO_2 than pure TiO_2 nanowires, higher Li-ion diffusion rate, and improved polysulfide rejection capability. Other transition metal oxides like V_2O_5 are commonly used as nanowires.[182]

Surface engineering has been used to improve the catalytic activity for multiple LiPS species instead of specific LiPSs. Zhu *et al.*[306] created oxygen vacancies in Mn_3O_4 to reduce the activation energy of converting soluble long-chain LiPS into insoluble short-chain LiPS. Due to the oxygen vacancies, strong Mn–S bonds were formed between the catalyst and long-chain LiPS, whereas short-chain LiPS formed more Li–O bonds. Moreover, the binding energy calculated by DFT was significantly lower for oxygen-vacant Mn_3O_{4-x} (−2.7 eV) than pristine Mn_3O_4 (−2.2 eV). The strong chemisorption of soluble LiPS reduces the shuttle effect, while the favorable Li–O bonds for insoluble LiPS free the sulfur for faster redox kinetics. *In situ* XRD supported these findings, with fast disappearance of Li_2S_8 peaks and rapid appearance of Li_2S peaks during discharge, with MnS and Li_y-Mn_zO_{4-x} intermediate peaks.

Multi-metal oxide heterostructures are promising for LiPS adsorption owing to their abundant defects providing oxygen vacancies. Hu *et al.*[303] decorated MWCNTs with N, F, and B co-doped $CoFe_2O_{4-x}$ and coated a Celgard separator (Fig. 11c). The resulting separator exhibited an astoundingly low capacity decay of 0.016% decay per cycle over 1000 cycles at 1C. The excellent rejection was partly due to the heteroatoms increasing polysulfide affinity, resulting in more physiochemical trapping. Moreover, there was more uniform LiPS adsorption with heteroatom doping than without, as illustrated in Fig. 11d. The oxygen vacancies also improved polysulfide conversion kinetics, resulting in decreased shuttling. Liu *et al.*[307] found a low 0.065% decay per cycle over 1000 cycles at a high current density of 2C using $NiFe_2O_4$ bimetallic oxides. Multiphase and multi-component $NiFe_2O_4$–NiO heterostructures attached to CNTs were directly grown on a PP substrate yielding uniform and crystalline heterostructure interfaces. This minimized electrical impedance and maximized ionic conductivity, resulting in a high capacity of 1350 mA h g^{-1} at 0.1C.

5.2 Metal sulfides

Transition metal sulfide nanosheets have abundant metal centers for polysulfide adsorption. Fig. 12a shows the adsorption energies of various LiPSs on MoS_2 nanosheets,[236] respectively. Compared to the nearly non-existent adsorption energy of

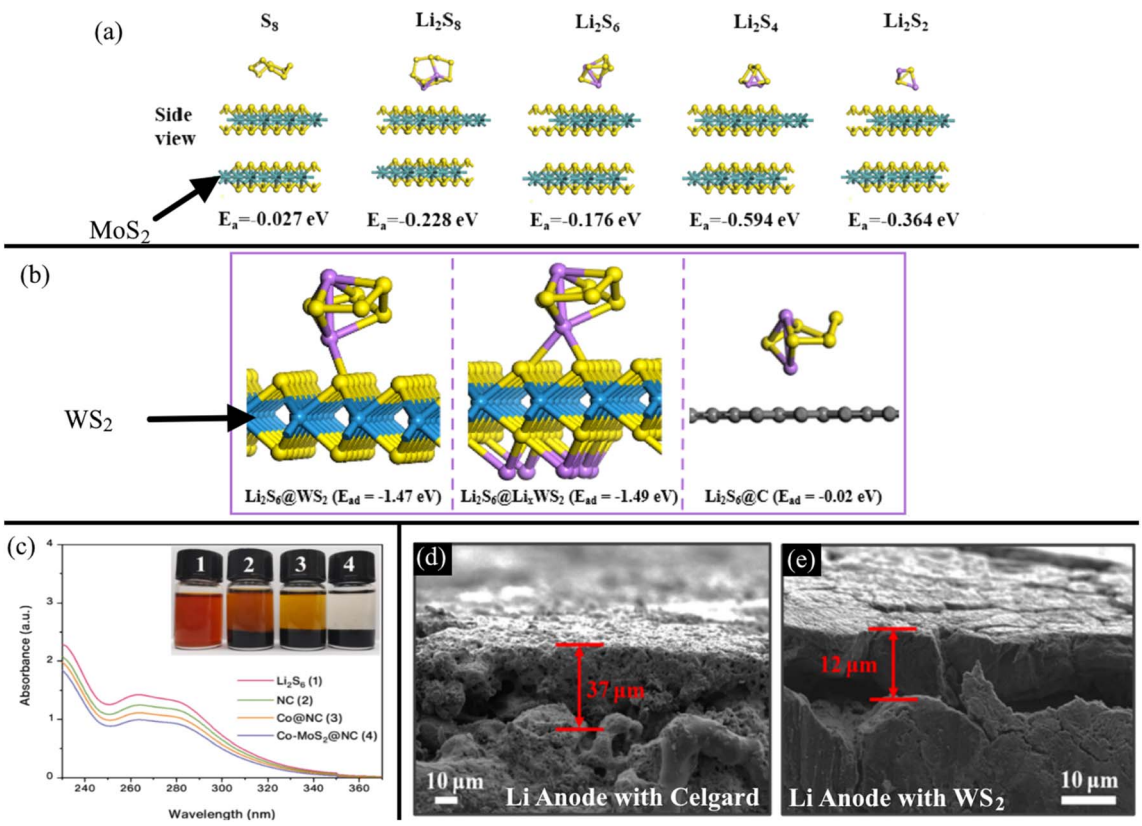

Fig. 12 (a) Adsorption energy of S_8 and Li_2S_x ($2 < x < 8$) on a slab of MoS_2.[236] (Adapted with permission from ref. 236. Copyright 2022, Elsevier). (b) Adsorption energy of Li_2S_6 on a slab of WS_2 without lithiation (left) and with lithiation (center). The adsorption energy of Li_2S_6 on graphene (right)[237] (Adapted with permission from ref. 237. Copyright 2021, American Chemical Society). (c) UV-vis spectra of Li_2S_6 solutions upon the adsorption by different sorbents (inset: photograph of the corresponding Li_2S_6 solutions).[236] (Adapted with permission from ref. 236. Copyright 2022, Elsevier). Li anode after 100 cycles at 1C of an LSB with a (d) pristine Celgard separator and (e) WS_2-modified separator[237] (Adapted with permission from ref. 237. Copyright 2021, American Chemical Society).

LiPS on graphene (Fig. 12b), the metal sulfides have a high affinity for LiPSs, indicated by their highly negative adsorption energies. Liu *et al.*[308] used MoS_2 nanosheets, which are known to have excellent Li conductivity, to coat a standard PP separator. An LSB with the modified separator exhibited a 51% higher initial capacitance at a low current density of 0.1C and maintained a high 752 mA h g^{-1} capacity at 2C. The excellent adsorptive properties of the MoS_2 nanosheets resulted in a 93% capacity retention after 500 cycles at 1C. The LSB with a MoS_2-modified separator had a low 0.083% decay per cycle due to a mix of excellent polysulfide adsorption and physical blocking. Cheng *et al.*[210] found that sulfur-deficient MoS_2 nanoflowers exhibited excellent chemisorption and catalytic conversion of polysulfides but required efficient electron transfer from rGO to increase LiPS conversion rates.

Other metal sulfide nanosheets like SnS_2,[309] VS_2,[310] and WS_2 [237] have reported improved LiPS adsorption and conversion, improving LSB cycle stability and initial capacity. For example, Li *et al.*[311] found that adding CuS nanoflowers greatly increased electrolyte wettability, with an astounding electrolyte contact angle of 0°. Adding WS_2 to a Celgard separator decreased the growth of inactive Li, indicated by the smoother and thinner Li anode surface shown in Fig. 12e (WS_2) than in Fig. 12d (Celgard).[237] As shown in Fig. 12b, the WS_2 had much higher affinities for LiPS adsorption, resulting in the reduction of parasitic polysulfide reactions at the anode. Compositing metal sulfide nanosheets with conductive carbon nanomaterials can produce a synergistic effect that improves the catalytic conversion of polysulfides. For example, Gong *et al.*[236] covered nitrogen-doped Co-CNTs with MoS_2 nanosheets, resulting in excellent Li-ion diffusion and electrical conductivity shown in the high 610 mA h g^{-1} capacity at 4C. As shown in Fig. 12c, the vial containing a Li_2S_6 solution that was dark red initially became nearly transparent after 2 hours with MoS_2/Co-CNTs added to the vial. In contrast, with only N-doped CNTs and N-doped Co-CNTs, the vials had much higher absorptions, indicated by their visually brown hues. Ghazi *et al.*[312] found that vacuum filtration of MoS_2 through a Celgard membrane yielded a composite separator with a high Li-ion conductivity of 0.2 mS cm^{-1} (5.4 times higher than with a GO-modified separator).

Metal sulfide nanoparticles have also been used to modify commercial LSB separators. However, the 0D nanoparticles are often used as dopants for carbon-based modifiers (Section 3). Liu *et al.*[256] added CoS nanoparticles to graphitic carbon nitride and KB. The CoS provided Lewis acid–base interactions that immobilized the polysulfide and hastened its conversion. Li *et al.*[313] embedded ZnS nanoparticles on N-doped carbon nanosheets and subsequently carbonized the composite, yielding unsaturated Zn metal centers that formed strong coordinate bonds with polysulfides. ZnS[314] quantum dots have shown excellent adsorption and catalytic properties.

5.3 MXenes

MXenes are 2D nanomaterials composed of transition metal carbides, nitrides, or carbonitrides that are electrically conductive with good electrocatalytic properties. In particular, the abundant metal centers may adsorb polysulfides[315] (Fig. 13b) and hasten their conversion.[315] Fig. 13a shows the high binding energies (>2 eV) of various MXenes for all stable LiPSs. Song *et al.*[316] coated a PP separator with Ti_3C_2 MXenes *via* vacuum filtration. Due to the high electronic conductivity of MXene nanosheets, the charge transfer resistance decreased from 101.2 Ω for the pristine PP separator to 45.06 Ω. The Ti metal centers in the modified separator exhibited increased LiPS chemisorption, resulting in a low capacity decay rate of 0.062% per cycle at 0.5C. Moreover, the Mxenes increased sulfur utilization and rate capability, resulting in a 72% higher initial capacity at 1C than with a pristine PP membrane. Mxenes have also been used to increase electrolyte wettability with their abundant functional groups and enhance ionic conductivity.[152]

MXenes are also highly compatible with other materials that can provide functionality, such as increased electrocatalytic ability and faster Li-ion diffusion *via* ionic channels. Gu *et al.*[29] added Co nanoparticles to MXenes to improve polysulfide conversion kinetics. As shown in Fig. 13c and d, adding Co nanoparticles increased LiS_2 deposition in the cathode, suggesting faster conversion from Li_2S_8 to Li_2S and a smaller loss of sulfur due to a reduced shuttle effect. Liu *et al.*[317] fabricated an asymmetric separator with MXenes facing the cathode side and Cu-TCPP MOFs on the anode side. As shown in Fig. 13e, the pristine separator and MOF/PP separator had a greater self-discharge, owing to the inability to suppress soluble LiPSs on the cathode side. In contrast, the addition of MXenes with almost 50% improved self-discharge resistance than with a standard PP separator. Wang *et al.*[152] used a layer-by-layer to combine MXene with Nafion onto a commercial PP substrate. The composite membrane had a 50% higher initial capacitance than with a pristine PP separator of 1234 mA h g^{-1}, with a low 0.03% decay per cycle for 1000 cycles at 1C. MXenes have also been modified with CNTs to prevent the aggregation of MXene nanosheets while maintaining excellent electrical conductivity.[225] Li *et al.*[318] combined a Ti_3C_2 MXene with guanidinium-based ionic-covalent organic nanosheets (iCON) to suppress the shuttle effect with fast catalytic conversion. While Ti_3C_2 had decent redox capabilities at low cyclic voltammetry (CV) scan rates (Fig. 13f) but failed at high CV scan rates (Fig. 13g). In contrast, the Ti_3C_2/iCON composite showed excellent redox capabilities at both CV scan rates, with little change to its shape. The sustainably high catalytic ability of the Ti_3C_2/iCON composite was due to the high electron mobility afforded by iCON.

5.4 Other inorganic modifiers

Other inorganic modifiers, including nitrides, borides, phosphides, fluorides, and selenides, have been studied for their catalytic abilities as LSB cathodes.[319–321] Recently, various catalytic inorganic compounds have also been implemented as modifiers for polyolefin separators. Like the inorganic modifiers discussed previously, these inorganic compounds improve LiPS rejection *via* strong chemisorption and improve the conversion of soluble LiPSs into insoluble Li_2S_2 and Li_2S. In addition, the materials discussed in this section have unique

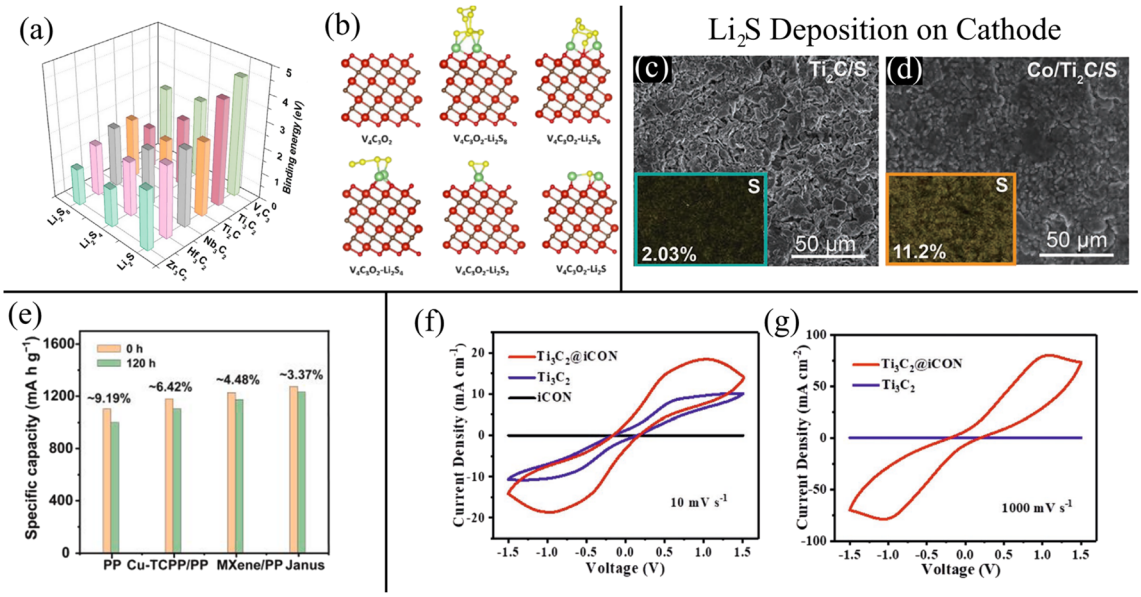

Fig. 13 (a) Three-dimensional columnar contrasts of the binding energy of several transition metal carbides for LiPSs. (b) Theoretical structure of $V_4C_3O_2$ and optimized configurations of Li_2S_n ($n = 1, 2, 4, 6, 8$) adsorption on $V_4C_3O_2$[315] (Reproduced with permission from ref. 315. Copyright 2022, Elsevier). SEM images and the corresponding sulfur distribution map of the (c) Ti_2C and (d) Co/Ti_2C cathodes after Li_2S deposition[29] (Reproduced with permission from ref. 29. Copyright 2022, John Wiley and Sons). (e) Self-discharge tests of the LSBs with standard PP, Cu-TCPP-modified, MXene-modified, and Janus (Cu-TPP/MXene) separator configurations after resting for 120 h[317] (Reproduced with permission from ref. 317. Copyright 2023, Elsevier). *CV* curves of symmetric cells at a scan rate of (f) 10 mV s^{-1} and (g) 1000 mV s^{-1} for the Ti_3C_2@iCON and Ti_3C_2-modified PP separators[318] (Reproduced with permission from ref. 318. Copyright 2021, John Wiley and Sons).

structures that make them promising for LSB separator modification.

Boron nitride (BN), sometimes called inorganic graphite, has recently gained popularity due to its structural similarity with graphene, high thermal conductivity, and chemical stability.[322] While the nitrogen groups in BN can bind to the Li in LiPSs, additional functionalization is usually required for improved LiPS chemisorption. Fan *et al.*[323] functionalized BN nanosheets (fBN) with amino and carboxyl groups and vacuum-filtered the modified BN nanosheets through a Celgard separator. The functional groups immobilized LiPSs *via* chemisorption, resulting in an exceptional 83% capacity retention after 1000 cycles at 3C, whereas an LSB with a Celgard separator retained only 27%. BN coatings on the anode side of the separator can reduce Li dendrite formation. Its high thermal conductivity creates a uniform thermal distribution on the Li anode during charge/discharge, stabilizing the SEI and homogenizing Li plating/stripping.[324] Kim *et al.*[325] tested a BN-modified separator through a Li plating/stripping test and found that the BN-modified separators retained a high coulombic efficiency above 85% with no decay even after 100 cycles. SEM analysis showed flat Li granules with a large 1 μm diameter grew on the anode surface with a BN separator, whereas sharp pillars of Li nanowires were formed with a carbon-modified PP separator. BN can also be made into nanotubes (BNNTs) with uniform pore structures for LiPS sieving. Standard synthesis yields impurities such as hexagonal or amorphous boron nitrides, which reduce the BNNT's Li conductivity. In recent work, Kim *et al.*[326] synthesized purified BNNTs of defects before composition with a PP separator *via* slurry coating. The Li diffusion coefficient was 58% higher for the LSB with purified BNNTs than standard BNNTs and PP. SEM and Li plating/stripping tests showed that purified BNNTs reduced Li dendrite growth and Li inactivation. Purified BNNTs also had strong adsorption for LiPSs, indicated by an 85% decrease in UV-vis absorbance during a simple diffusion test.

Unlike BN, metal nitrides have excellent conductivity and greater adsorption affinity for LiPS due to their abundant metal centers. TiN has shown excellent LiPS adsorption ability and catalytic conversion; however, the high cost, harmful byproducts, and complex synthesis have limited its application.[327] To circumvent this, Shen *et al.*[328] devised a one-step solid–state reaction for the growth of TiN on graphene. Zhou *et al.*[327] used a molten salt method (Fig. 14a) to synthesize TiN coated Si_3N_4 core–shell nanoparticles. Unlike typical high-temperature synthesis, the molten salt process did not require harmful solvents and could be largely recycled, improving the safety and economic viability of TiN. The TiN shell had a dendritic structure that provided a greater surface area for LiPS adsorption.

Vacancy engineering may also be employed to improve chemisorption and catalytic properties. In recent work, Luo *et al.*[227] synthesized nitrogen-deficient CoN grown on MWCNTs (Fig. 14b) to improve LiPS adsorption and catalytic conversion. As shown in Fig. 14c, DFT calculations confirmed that nitrogen vacancies improved the binding energy, which makes sense as more metal centers are exposed to adsorb the bulky polysulfides. Moreover, the catalytic properties of nitrogen-vacant CoN improved due to its decreased band gap between the d-

band in Co and p-band in nitrogen, resulting in improved electron mobility. Fig. 14d shows how nitrogen-vacant CoN/CNTs had smaller energy barriers for Li_2S_4 diffusion, which would improve LiPS reduction kinetics as LiPS diffusion is critical for the reaction pathway. Yao *et al.*[329] created Te vacancies in a P-doped $NiTe_{2-x}$ electrocatalyst. The bi-metal catalyst was anchored to biologically-derived carbon nanosheets and used to modify a PP separator. With a standard PP separator, *in situ* Raman spectroscopy showed the formation of soluble LiPSs on the Li anode side during LSB discharge, which remained during recharge. In contrast, no noticeable Raman peaks were detected for the LSB using the electrocatalyst-modified separator. Similarly, selenium vacancies in bimetallic Co_9S_{8-x}/$FeSe_{2-y}$ significantly reduced the shuttle effect *via* excellent chemisorption and electrocatalytic conversion.[330] The bimetallic selenide was crystalized onto CNTs before modifying a PP separator. The conversion of soluble LiPSs were detected using *in situ* XRD, which showed the evolution of α-S_8 turning into Li_2S during discharge and into β-S_8 during recharge. The formation of $Se_{1.1}S_{6.9}$ was also detected, suggesting the formation of strong chemical bonds between Se from the bimetallic Co_9S_{8-x}/$FeSe_{2-y}$ and S from the LiPSs.

Quantum dots are newer but promising additives that boast excellent adsorption properties with high surface area and catalytic abilities. In a recent study by Ma *et al.*,[204] Mo_2N quantum dots were also used to improve the Li-ion conduction of nitrogen-doped GO (NGO) by a factor of 3. While the smaller pore sizes of the NGO layer deposited on the PP separator decreased Li-ion conductivity by 56%, the addition of lithiophilic Mo_2N supplied attractive forces that improved Li-ion conductivity by 48% more than pristine PP. The excellent polysulfide adsorption resulted in an LSB with one of the highest reported capacity retentions, indicated by a low 0.039% decay per cycle for 800 cycles at a high current of 2C. Similarly, Nitrogen-doped nanodots like NbN[331] have been used to increase the rate of LiPS conversion. *In situ* Raman spectroscopy was performed on a uniquely designed test battery during the charge/discharge process to determine the presence of LiPSs on the Li anode side. During the first charge/discharge, Raman signals for the soluble Li_2S_8, Li_2S_6, and Li_2S_4 were detected for LSBs using a standard PP separator and N-graphene/PP separator. In contrast, no Raman signals were found when employing an NbN/N-graphene/PP nanocomposite separator.

Multi-metal nitrides can also be designed to overcome the limitations of specific metals. For example, Zhang *et al.*[332] synthesized bimetallic $Ni_{0.2}Mo_{0.8}N$ on MWCNTs to overcome the Mo leaching by polysulfides in Mo_2N and the low conductivity of Ni_3N. Consequently, the LSB with the bimetallic nitride exhibited a 6% and 50% lower capacity decay rate than an LSB with Mo_2N and Ni_3N-modified separators, respectively.

Metal borides are especially promising for LiPS adsorption because boron atoms have empty orbitals that have a high affinity for polysulfides. Unlike metal oxides, sulfides, nitrides, and MXenes that depend on their metal centers for chemisorption with S atoms, metal borides have both metal and boron components binding to the long sulfur chains.[333] Fig. 14e

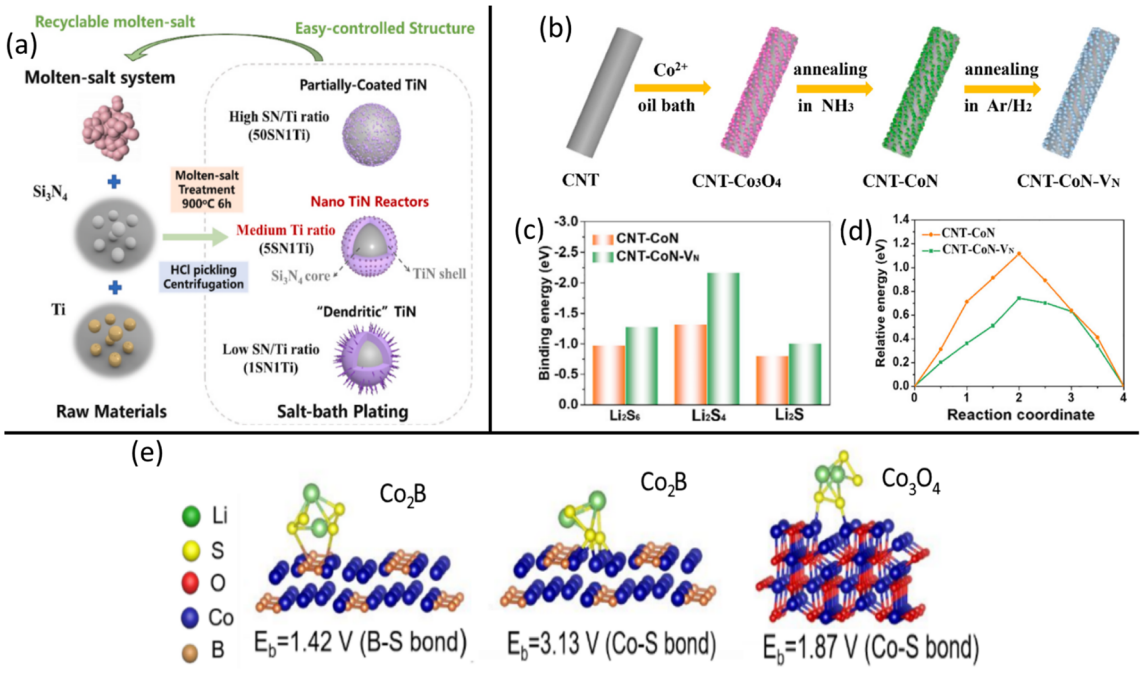

Fig. 14 (a) Schematic of a molten-salt process for synthesizing TiN/Si_3N_2 core/shell structures with dendritic TiN[327] (Reproduced with permission from ref. 327. Copyright 2023, Elsevier). (b) Schematic illustrating the synthesis of nitrogen-vacant CoN (CoN-Vs) grown on CNT to yield CNT-CoN-Vs. (c) Binding energies of Li_2S_6, Li_2S_4, and Li_2S on pristine and nitrogen-vacant CoN/CNTs. (d) Diffusion energy barriers of Li_2S on pristine and nitrogen-vacant CoN/CNTs.[227] (Reproduced with permission from ref. 227. Copyright 2022, Elsevier). (e) Binding energies of Li_2S_4 on Co_2B with boron and cobalt sites, and the binding energy of Li_2S_4 on Co_3O_4 [333](Reproduced with permission from ref. 333. Copyright 2019, American Chemical Society).

shows that the binding energy between the sulfur atom in Li_2S_4 and boron in Co_2B is only slightly lower than the binding energy between Co and S in Co_3O_4. Moreover, the binding energy is 68% higher between Co and S in Co_2B than in Co_3O_4. In recent work, Shrshr *et al.*[334] synthesized Ni_3B nanoparticles uniformly distributed on rGO, which were subsequently slurry coated onto a PP separator. A simple diffusion test showed that Ni_3B had less adsorptive ability than Ni_3B/rGO, suggesting synergistic properties between the metal boride and conductive carbon host. This was further supported by a self-discharge test wherein Ni_3B/rGO lost 2.2% capacity while bare Ni_3B lost 4.0% and bare rGO lost 18.8% of its initial capacity. Guo *et al.*[335] improved the catalytic properties of MoB by synthesizing a metallic Mo and MoB heterostructure *via* a molten salt method. Metallic Mo had a lower Gibbs free energy (ΔG) of 0.31 eV for the reaction of soluble Li_2S_4 into insoluble Li_2S_2, whereas MoB had a high ΔG of 1.42 eV. Then, for the subsequent reaction from Li_2S_2 into Li_2S, the reverse happened where metallic Mo had a large ΔG of 0.76 eV, whereas MoB had a lower ΔG of 0.005 eV. The heterogenous composition of the modifier enabled efficient bidirectional catalysis by having the different components favor different steps of LiPS reduction.

While metal fluorides, like other ionic salts, have a good affinity for LiPS adsorption, they have the unique ability to react with Li to form LiF, which may be used to mitigate Li dendrite growth.[336] Jing *et al.*[209] found that during cycling, the fluorine in CaF_2 and Li in lithium bis(trifluoromethanesulfonyl)imide (LiTFSI) electrolyte formed a layer of LiF. The LiF promoted fast and uniform Li-ion diffusion and deposition. Plating/stripping tests and SEM analysis showed a low and steady overpotential, suggesting minimal dendrite formation. In a more recent study by Jing *et al.*[208] found that SrF_2 also reduced Li dendrite formation due to the lithiophilicity of SrF_2. The sandwich structure comprising SrF_2 and graphene minimized local current densities at the Li anode to further suppress Li dendrites.

Metal phosphides benefit from a similar affinity for LiPSs but have greater electrical conductivities than metal oxides and sulfides.[337] The greater electron mobility allows metal phosphides to potentially have great catalytic ability for improved LiPS rejection. Metal phosphides also boast greater thermal and chemical stability for improved battery safety. Wu *et al.*[338] found that Ni and Co-phosphide-modified carbon nanocages promoted faster Li-ion diffusion and improved catalytic conversion of LiPS. Still, the binding energy to LiPSs can be improved. Wang *et al.*[339] recently used defect engineering to increase the electrical conductivity of Mo_3P. Mo_3P was modified with MoO_2 and MoP to create dangling bonds and oxygen vacancies that decreased the formation energy for generating electron holes. Moreover, the defects exposed more metal active sites for LiPS chemisorption.

Like metal sulfides, metal selenides have similar crystal structures, polar characteristics, and adsorption capacity for LiPSs. However, metal selenides boast greater electrical conductivity due to looser valence electrons and greater defect density.[340] Zhang *et al.*[341] synthesized ZnSe nanoparticles using ZIF-8 MOF as a template. The highly structured ZnSe nanoparticles showed excellent chemisorption of LiPSs, indicated by nearly transparent UV-vis absorbance. Tian *et al.*[342] used defect engineering to increase the conductivity and catalytic properties of Sb_2Se_3. Defects were introduced *via* chemical reduction and thermal shark in an Ar atmosphere. Sb_2Se_3 with abundant Se vacancies had a 5-times-higher electrical conductivity. When combined with rGO, the Sb_2Se_{3-x} maintained stable voltage curves even at a high current rate of 8C. DFT analysis also showed that Se vacancies increased the binding affinity of S–Sb and Li–Se. Consequently, the LSB with Sb_2Se_{3-x}-modified separator had a 25% great capacity retention than with a pristine Sb_2Se_3-modified separator.

6 Future prospects

Various nanocomposite separators have successfully lowered polysulfide shuttling to raise the stability of LSBs to commercially viable standards, withstanding more than 1000 cycles and holding specific capacities above 1300 mA h g^{-1}.[343] Composite separators have also improved Li anode stability, decreasing parasitic LiPS reactions and Li dendrite formation. Moreover, the Li-ion diffusion rates, sulfur utilization, thermal stability, and rate capability of LSBs have been greatly enhanced. Still, there is more to be done before LSBs are commercially viable.

Firstly, LSBs with modified separators are limited by their polyolefin base. Modifying widely available Li-ion battery separators, such as Celgard membranes, will be important for the initial industrial scale-up and commercial production, but novel separators based on nanofibers may be necessary for competitive performance with LIBs. Nanofiber-based separators have better thermal stability, Li-ion conductivity, electrolyte wettability, flexibility, modifiability, and LiPS adsorption ability than standard polyolefin separators.[344] Nonwoven membranes are often made from poly(vinylidene) fluoride (PVDF)[345] or polyimide,[346] and electrospun membranes can be made from various polymers like polyacrylonitrile (PAN)[347] and polyvinylpyrrolidone (PVP).[348] However, such membranes tend to have limited LiPS rejection capabilities and high cost of fabrication.[349] More work into optimizing fiber roughness,[350,351] polymer blend ratios,[352] fiber coating,[353,354] and nanomaterial doping[355–357] may open up solutions to improved fiber-based separators for LSBs.

The complex reaction pathways of LSBs, especially involving the solid–liquid–solid conversion of LiPSs, need to be better understood using improved characterization techniques. *Ex situ* methods like UV-vis spectroscopy of penetrate experiments and SEM/TEM of electrodes show the macroscopic consequences of using different modifiers. However, the reaction pathways (especially involving catalytic materials) are still unclear and can be improved by designing analysis setups for *in situ* spectroscopic techniques like Infrared, UV-vis, and Raman spectroscopy and XRD analysis.[358] Other *in situ* analytical techniques used in LIB research, like *in situ* SEM,[359] EDX,[360] and mass spectroscopy[361] should be employed in LSB investigations to better understand the reactions occurring at the Li anode and modified separator. These *in situ* tests will require uniquely designed LSBs for testing.

LSBs still require much more development in their overall design before becoming commercially viable. While specific capacities are the primary measure for LSB performance that account for the weight of the electrode, this measure does not account for the weight of the whole battery. The weight contributed by thick modification layers may become significant, especially for smaller devices like drones. For weight-dependent applications like EVs or portable electronics, the energy density of the whole device needs to be accounted for. Similarly, volumetric energy densities are almost never reported but are critical for small form-factor applications. The effect of the modified separator on power densities could also be investigated along side performance measures at varying C rates. The tested cells in laboratory settings also most often use Li metal anodes in coin cell configurations. However, the battery industry has shifted away from Li metal anodes due to safety, cost, and ethical concerns in favor of lithiated carbon-based anodes that have lower capacities.[362] Other battery configurations like pouch cells and winding-type cells require LSBs to consider other factors like volume expansion, binder strength, and electrolyte volume, amongst other electrochemical changes. Improvements to the sulfur cathode must also be made for LSBs to sustain higher power densities and greater sulfur loadings.[363]

The cost and processing complexity of most modifiers are considered before beginning investigations. Hence, many studies design composite separators using cheap, sustainable, or easily processible materials like common polymers, porous carbons, and metal oxides. Studies involving more obscure materials like MOFs and MXenes test the viability of the composite membranes and help answer the question of whether industrial-level production would be worth the cost. Overall, the industrial scale-up of lab-scale composite separator fabrication has still not matured and will be a critical bridge to cross before LSB commercialization. The optimal battery form factor for LSBs has also yet to be tested. Moreover, novel separators for LSBs with highly uniform pores or hierarchically porous structures have also been fabricated *via* templating methods,[364,365] anodic oxidation,[366] and advanced polymerization techniques.[367] While such fabrication techniques are popular and well-published for membranes used in nanofiltration and wastewater treatment,[368] these techniques may be tested for LSB separators.

Lastly, the maintenance and longevity of LSBs still need to be examined. Because the primary focus of LSB research has been on reducing the shuttle effect for higher cycling stability, there is much room for improvement regarding thermal stability, physical stress resistance, and volume expansion resistance, especially at high current rates. As with LIBs, thermal stability is critical if LSBs are to be used in EVs and mobile devices with fast charge/discharge requirements that result in overheating.[369] Separators coated with heat-resistant materials like ethylene-vinyl acetate copolymer[370] or separators fabricated from thermally stable polymers like polyimide[371] should be investigated more to improve LSB safety. With portable and wearable electronics being ubiquitous in society, flexible batteries have become more important due to better resistance against physical stress. Few recent investigations have fabricated highly flexible LSBs,[372,373] with many studies using novel separators.[374,375] Battery expansion due to gas build-up, volume expansion, and separator swelling is an issue prevalent in Li-ion batteries[376] that has not been addressed much for LSBs, despite facing similar problems. Such tests for stability are critical before LSBs may be commercially available.

7 Conclusion

LSBs are one of the most promising next-generation batteries that may displace LIB's dominance in portable technology, electric vehicles, and other energy storage applications. LSBs boast a 5-times-higher theoretical capacity than LIBs and use more affordable, environmentally friendly, safer, and abundant materials than LiBs. However, current LSB materials and designs are not yet commercially viable due to low conductivity, dendrite formation, and the polysulfide shuttle effect. Much development in LSBs in recent years involves reducing LiPS shuttling by modifying polyolefin separators, which are used in most LIBs. Polymer/polyolefin composites have facile preparation methods with easily tunable pore sizes and various functional groups that help repel or immobilize polysulfides. Carbon-modified separators have significantly higher conductivity, allowing fast LiPS conversion, enhanced rate capability, and Li dendrite suppression. The uniform and controllable pore structure of organic framework/polyolefin composites provide selective ion channels for high Li-ion diffusion with limited LiPS shuttling. Inorganic, metal-based additives provide catalytic active sites that promote the adsorption and conversion of soluble LiPS to insoluble Li_2S. Modifying polyolefin separators is essential in bringing LSBs to market because it leverages the infrastructure of LIBs' polyolefin separators to lower production costs. However, separator modifications alone are likely insufficient for fully commercializing LSBs, and more work needs to be done in refining the cathode, anode, and electrolyte. Novel separators based on nanofiber technology, graphene sheets, xerogels, or other materials may be required to reach higher efficiencies closer to the theoretical limit of LSBs. With the exponentially growing demand for new energy storage technologies and the potential of LSBs to meet those demands, it is an exciting time to investigate LSBs.

Conflicts of interest

There are no conflicts to declare.

References

1 A. A. Tidblad, K. Edström, G. Hernández, I. de Meatza, I. Landa-Medrano, J. Jacas Biendicho, L. Trilla, M. Buysse, M. Ierides, B. P. Horno, Y. Kotak, H. G. Schweiger, D. Koch and B. S. Kotak, *Energies*, 2021, **14**, 4223.
2 M. Khalid, F. Ahmad, B. K. Panigrahi and L. Al-Fagih, *J. Energy Storage*, 2022, **53**, 105084.
3 L. Jonnatan, C. L. Seaton, K. L. Rush, E. P. H. Li and K. Hasan, *Int. J. Environ. Res. Public Health*, 2022, **19**, 8231.

4 S. Katsumata, T. Ichikohji, S. Nakano, S. Yamaguchi and F. Ikuine, *Comput. Hum. Behav. Rep.*, 2022, **5**, 100168.
5 C. Kuzemko, M. Blondeel, C. Dupont and M. C. Brisbois, *Energy Res. Soc. Sci.*, 2022, **93**, 102842.
6 C. Sturm, *J. Ind. Bus. Econ.*, 2022, **49**, 835–878.
7 G. D. Scholes, M. Jones and S. Kumar, *J. Phys. Chem. C*, 2007, **111**, 13777–13785.
8 A. Kim, J. K. Dash, P. Kumar and R. Patel, *ACS Appl. Electron. Mater.*, 2022, **4**, 27–58.
9 S. Günes, K. P. Fritz, H. Neugebauer, N. S. Sariciftci, S. Kumar and G. D. Scholes, *Sol. Energy Mater. Sol. Cells*, 2007, **91**, 420–423.
10 S. Kumar and G. D. Scholes, *Microchim. Acta*, 2007, **160**(3), 315–325.
11 S. P. Gupta, B. A. Kakade, B. R. Sathe, Q. Qiao, D. J. Late and P. S. Walke, *ACS Appl. Energy Mater.*, 2020, **3**, 11398–11409.
12 A. Kim, P. Kumar, P. K. Annamalai and R. Patel, *Adv. Mater. Interfaces*, 2022, 1–27, DOI: **10.1002/admi.202201659**.
13 A. Kim and A. Simson, *Int. J. Energy Environ. Eng.*, 2022, DOI: **10.1007/s40095-022-00524-2**.
14 X. Zou, X. Huang, A. Goswami, R. Silva, B. R. Sathe, E. Mikmeková and T. Asefa, *Angew. Chem.*, 2014, **126**, 4461–4465.
15 S. S. Narwade, S. M. Mali, P. D. Tanwade, P. P. Chavan, A. V. Munde and B. R. Sathe, *New J. Chem.*, 2022, **46**, 14004–14009.
16 S. Kumaravel, E. Kim, B. B. Kale, A. Adhikari, R. Patel and S. Kundu, *ChemElectroChem*, 2022, **9**, e202200724.
17 H. Jung, A. Karmakar, A. Adhikari, R. Patel and S. Kundu, *Sustainable Energy Fuels*, 2022, **6**, 640–663.
18 S. S. Narwade, S. M. Mali and B. R. Sathe, *New J. Chem.*, 2021, **45**, 3932–3939.
19 B. Dunn, H. Kamath and J. M. Tarascon, *Science*, 2011, **334**, 928–935.
20 J. B. Goodenough and K. S. Park, *J. Am. Chem. Soc.*, 2013, **135**, 1167–1176.
21 M. Winter, B. Barnett and K. Xu, *Chem. Rev.*, 2018, **118**, 11433–11456.
22 S. A. Mane, A. A. Kashale, G. P. Kamble, S. S. Kolekar, S. D. Dhas, M. D. Patil, A. V. Moholkar, B. R. Sathe and A. V. Ghule, *J. Alloys Compd.*, 2022, **926**, 166722.
23 R. Chavan, G. Kamble, A. Kashale, S. Kolekar, B. Sathe and A. Ghule, *ChemistrySelect*, 2022, **7**, e202202166.
24 G. P. Kamble, A. A. Kashale, S. S. Kolekar, I. W. P. Chen, B. R. Sathe and A. V. Ghule, *J. Mater. Sci. Mater. Electron.*, 2021, **325**(32), 5859–5869.
25 S. H. Chung and A. Manthiram, *Adv. Mater.*, 2019, **31**, 1901125.
26 X. Yu and A. Manthiram, *Adv. Funct. Mater.*, 2020, **30**, 2004084.
27 H. Hao, T. Hutter, B. L. Boyce, J. Watt, P. Liu and D. Mitlin, *Chem. Rev.*, 2021, **122**, 8053–8125.
28 H. J. Peng, J. Q. Huang and Q. Zhang, *Chem. Soc. Rev.*, 2017, **46**, 5237–5288.
29 Q. Gu, Y. Qi, J. Chen, M. Lu and B. Zhang, *Small*, 2022, **18**, 2204005.
30 Y. Lin, Y. Zhou, S. Huang, M. Xiao, D. Han, J. Qin, S. Wang and Y. Meng, *Adv. Energy Mater.*, 2022, **12**, 2201912.
31 D. Xiong, S. Huang, D. Fang, D. Yan, G. Li, Y. Yan, S. Chen, Y. Liu, X. Li, Y. Von Lim, Y. Wang, B. Tian, Y. Shi and H. Y. Yang, *Small*, 2021, **17**, 1–10.
32 M. Zhao, X. Chen, X. Y. Li, B. Q. Li and J. Q. Huang, *Adv. Mater.*, 2021, **33**, 1–9.
33 A. Eftekhari, *ACS Sustainable Chem. Eng.*, 2019, **7**, 3684–3687.
34 Q. H. Nguyen, V. T. Luu, S. N. Lim, Y. W. Lee, Y. Cho, Y. S. Jun, M. H. Seo and W. Ahn, *ACS Appl. Mater. Interfaces*, 2021, **13**, 28036–28048.
35 C. Li, Z. Xi, D. Guo, X. Chen and L. Yin, *Small*, 2018, **14**, 1–21.
36 E. Zhao, K. Nie, X. Yu, Y. S. Hu, F. Wang, J. Xiao, H. Li and X. Huang, *Adv. Funct. Mater.*, 2018, **28**, 1–21.
37 Y. X. Yin, S. Xin, Y. G. Guo and L. J. Wan, *Angew. Chem., Int. Ed.*, 2013, **52**, 13186–13200.
38 M. Wild, L. O'Neill, T. Zhang, R. Purkayastha, G. Minton, M. Marinescu and G. J. Offer, *Energy Environ. Sci.*, 2015, **8**, 3477–3494.
39 A. Manthiram, Y. Fu, S. H. Chung, C. Zu and Y. S. Su, *Chem. Rev.*, 2014, **114**, 11751–11787.
40 R. Cheng, Y. Guan, Y. Luo, C. Zhang, Y. Xia, S. Wei, M. Zhao, Q. Lin, H. Li, S. Zheng, F. Rosei, L. Sun, F. Xu and H. Pan, *J. Mater. Sci. Technol.*, 2022, **101**, 155–164.
41 Q. Li, Z. Ma, J. Zhao, K. Shen, T. Shi, Y. Xie, Y. Fan, X. Qin and G. Shao, *J. Power Sources*, 2022, **521**, 230929.
42 Y. C. Huang, H. I. Hsiang and S. H. Chung, *ACS Sustainable Chem. Eng.*, 2022, **10**, 9254–9264.
43 C. Y. Zhang, C. Zhang, J. L. Pan, G. W. Sun, Z. Shi, C. Li, X. Chang, G. Z. Sun, J. Y. Zhou and A. Cabot, *eScience*, 2022, **2**, 405–415.
44 X. Liang, Y. Zhang, Y. Ning, D. Huang, L. Lan, S. Li and S. Brutti, *Nanomater*, 2022, **12**, 2614.
45 F. Schmidt, S. Ehrling, K. Schönherr, S. Dörfler, T. Abendroth, H. Althues and S. Kaskel, *Energy Technol.*, 2022, **10**, 2100721.
46 X. Zhong, D. Wang, J. Sheng, Z. Han, C. Sun, J. Tan, R. Gao, W. Lv, X. Xu, G. Wei, X. Zou and G. Zhou, *Nano Lett.*, 2022, **22**, 1207–1216.
47 D. Guo, X. Zhang, M. Liu, Z. Yu, X. Chen, B. Yang, Z. Zhou and S. Wang, *Adv. Funct. Mater.*, 2022, **32**, 2204458.
48 X. Lang, T. Wang, Z. Wang, L. Li, C. Yao and K. Cai, *Electrochim. Acta*, 2022, **403**, 139723.
49 Z. Xiong, J. Li, Y. Sun, Y. Lin, L. Du, Z. Wei, M. Wu, K. Shi and Q. Liu, *J. Alloys Compd.*, 2022, **899**, 163245.
50 R. Chu, T. T. Nguyen, Y. Bai, N. H. Kim and J. H. Lee, *Adv. Energy Mater.*, 2022, **12**, 2102805.
51 K. Shi, Y. Lin, Z. Xiong, J. Li, S. Zhang and Q. Liu, *Chem. Eng. J.*, 2022, **430**, 132692.
52 Y. Wu, D. Li, J. Pan, Y. Sun, W. Huang, M. Wu, B. Zhang, F. Pan, K. Shi and Q. Liu, *J. Mater. Chem. A*, 2022, **10**, 16309–16318.
53 J. Liu, Y. Ding, Z. Shen, H. Zhang, T. Han, Y. Guan, Y. Tian and P. V. Braun, *Adv. Sci.*, 2022, **9**, 2103517.

54 T. Tonoya, Y. Matsui, H. Hinago and M. Ishikawa, *Electrochem. Commun.*, 2022, **140**, 107333.
55 V. Marangon, E. Scaduti, V. F. Vinci and J. Hassoun, *ChemElectroChem*, 2022, **9**, e202200374.
56 D. Li, H. Li, S. Zheng, N. Gao, S. Li, J. Liu, L. Hou, J. Liu, B. Miao, J. Bai, Z. Cui, N. Wang, B. Wang and Y. Zhao, *J. Colloid Interface Sci.*, 2022, **607**, 655–661.
57 S. S. Narwade, S. M. Mali, A. K. Tapre and B. R. Sathe, *New J. Chem.*, 2021, **45**, 20266–20271.
58 A. V. Munde, B. B. Mulik, P. P. Chavan, V. S. Sapner, S. S. Narwade, S. M. Mali and B. R. Sathe, *J. Phys. Chem. C*, 2021, **125**, 2345–2356.
59 V. S. Sapner and B. R. Sathe, *New J. Chem.*, 2021, **45**, 4666–4674.
60 M. Wang, M. Zhang, J. Li, S. Kumar, G. C. Walker, G. D. Scholes and M. A. Winnik, *ACS Appl. Mater. Interfaces*, 2010, **2**, 3160–3169.
61 M. Wang, S. Kumar, A. Lee, N. Felorzabihi, L. Shen, F. Zhao, P. Froimowicz, G. D. Scholes and M. A. Winnik, *J. Am. Chem. Soc.*, 2008, **130**, 9481–9491.
62 L. Vijaya, S. Suresh, R. Patel and E. B. Gowd, *ACS Macro Lett.*, 2022, **11**, 1272–1277.
63 L. Shen, A. Pich, D. Fava, M. Wang, S. Kumar, C. Wu, G. D. Scholes and M. A. Winnik, *J. Mater. Chem.*, 2008, **18**, 763–770.
64 A. Kim, A. Hosseinmardi, P. K. Annamalai, P. Kumar and R. Patel, *ChemistrySelect*, 2021, **6**, 4948–4967.
65 A. Kim, I. Varga, A. Adhikari and R. Patel, *Nanomaterials*, 2021, **11**, 2809.
66 R. Patel, J. T. Park, M. Patel, J. K. Dash, E. B. Gowd, R. Karpoormath, A. Mishra, J. Kwak and J. H. Kim, *J. Mater. Chem. A*, 2017, **6**, 12–29.
67 M. Subhramannia, B. K. Balan, B. R. Sathe, I. S. Mulla and V. K. Pillai, *J. Phys. Chem. C*, 2007, **111**, 16593–16600.
68 I. Uddin, S. M. Abzal, K. Kalyan, S. Janga, A. Rath, R. Patel, D. K. Gupta, T. R. Ravindran, H. Ateeq, M. S. Khan and J. K. Dash, *ACS Omega*, 2022, **46**, 42438–42445.
69 B. A. Kakade, S. S. Shintri, B. R. Sathe, S. B. Halligudi and V. K. Pillai, *Adv. Mater.*, 2007, **19**, 272–275.
70 G. D. Scholes, J. Kim, C. Y. Wong, V. M. Huxter, P. S. Nair, K. P. Fritz and S. Kumar, *Nano Lett.*, 2006, **6**, 1765–1771.
71 J. Kim, C. Y. Wong, P. S. Nair, K. P. Fritz, S. Kumar and G. D. Scholes, *J. Phys. Chem. B*, 2006, **110**, 25371–25382.
72 S. Jafarzadeh, E. Thormann, T. Rönnevall, A. Adhikari, P. E. Sundell, J. Pan and P. M. Claesson, *ACS Appl. Mater. Interfaces*, 2011, **3**, 1681–1691.
73 S. Jafarzadeh, A. Adhikari, P. E. Sundall and J. Pan, *Prog. Org. Coat.*, 2011, **70**, 108–115.
74 S. Radhakrishnan and A. Adhikari, *J. Power Sources*, 2006, **155**, 157–160.
75 S. Radhakrishnan, B. T. S. Ramanujam, A. Adhikari and S. Sivaram, *J. Power Sources*, 2007, **163**, 702–707.
76 S. Patil, H. Ghadi, N. Ramgir, A. Adhikari and V. R. Rao, *Sens. Actuators, B*, 2019, **286**, 583–590.
77 S. H. Oh and R. Patel, *Membr. J.*, 2020, **30**, 228–241.
78 R. Fang, S. Zhao, Z. Sun, D. W. Wang, H. M. Cheng and F. Li, *Adv. Mater.*, 2017, **29**, 1–25.
79 M. Rana, M. Li, X. Huang, B. Luo, I. Gentle and R. Knibbe, *J. Mater. Chem. A*, 2019, **7**, 6596–6615.
80 J. Zheng, M. Gu, H. Chen, P. Meduri, M. H. Engelhard, J. G. Zhang, J. Liu and J. Xiao, *J. Mater. Chem. A*, 2013, **1**, 8464–8470.
81 R. Pai, A. Singh, M. H. Tang and V. Kalra, *Commun. Chem.*, 2022, **5**(1), 1–11.
82 M. C. Li, Z. Liu, L. Tan, Q. Y. Zhou, J. J. Zhang, P. P. Hou, X. J. Jin, T. B. Lv, Z. Q. Zhao, Z. Zeng, S. Deng and G. P. Dai, *ACS Sustainable Chem. Eng.*, 2022, **10**, 10223–10233.
83 X. Sun, D. Tian, X. Song, B. Jiang, C. Zhao, Y. Zhang, L. Yang, L. Fan, X. Yin and N. Zhang, *Nano Energy*, 2022, **95**, 106979.
84 N. Akhtar, X. Sun, M. Yasir Akram, F. Zaman, W. Wang, A. Wang, L. Chen, H. Zhang, Y. Guan and Y. Huang, *J. Energy Chem.*, 2020, **52**, 310–317.
85 L. P. Hou, Z. Li, N. Yao, C. X. Bi, B. Q. Li, X. Chen, X. Q. Zhang and Q. Zhang, *Adv. Mater.*, 2022, **2205284**, 1–9.
86 S. Li, W. Zhang, J. Zheng, M. Lv, H. Song and L. Du, *Adv. Energy Mater.*, 2021, **11**, 1–24.
87 Y. Luo, L. Guo, M. Xiao, S. Wang, S. Ren, D. Han and Y. Meng, *J. Mater. Chem. A*, 2020, **8**, 4629–4646.
88 Q. Huang, J. Xu, M. Fang, L. Ma, Y. Cao, C. Fan, S. Hu, X. Zhang and D. Niu, *ChemistrySelect*, 2022, **7**, e202201484.
89 A. Liu, S. Li, Z. Jiang, J. Du, Y. Tao, J. Lu, Y. Cheng and H. Wang, *J. Power Sources*, 2022, **521**, 230947.
90 J. Zhu, M. Yanilmaz, K. Fu, C. Chen, Y. Lu, Y. Ge, D. Kim and X. Zhang, *J. Membr. Sci.*, 2016, **504**, 89–96.
91 J. Chen, T. Kang, Y. Cui, J. Xue, H. Xu and J. Nan, *J. Power Sources*, 2021, **496**, 229862.
92 S. Ponnada, M. S. Kiai, D. B. Gorle and A. Nowduri, *Nanoscale Adv.*, 2021, **3**, 4492–4501.
93 B. Dang, Q. Li, Y. Luo, R. Zhao, J. Li and F. Wu, *J. Alloys Compd.*, 2022, **915**, 165375.
94 J. Chen, T. Kang, Y. Cui, J. Zhao, J. Xue, H. Xu and J. Nan, *Energy Technol.*, 2022, **10**, 2101040.
95 S. Jia, K. Huang, J. Long, S. Yang, Y. Liang, N. Yang and J. Xiao, *J. Appl. Polym. Sci.*, 2021, **138**, 1–11.
96 N. Yang, Y. Liang and S. Jia, *Macromol. Mater. Eng.*, 2021, **306**, 2100300.
97 C. Liu, J. Hu, Y. Zhu, Y. Yang, Y. Li and Q.-H. Wu, *Materials*, 2022, **15**, 7527.
98 Z. Zhang, Z. Fang, Y. Xiang, D. Liu, Z. Xie, D. Qu, M. Sun, H. Tang and J. Li, *Carbohydr. Polym.*, 2021, **255**, 117469.
99 T. Jeon and S. C. Jung, *J. Mater. Chem. A*, 2021, **9**, 23929–23940.
100 S. Huang, Z. Wang, Y. Von Lim, Y. Wang, Y. Li, D. Zhang and H. Y. Yang, *Adv. Energy Mater.*, 2021, **11**, 2003689.
101 H. Zhang, Q. Liu, S. Ruan, C. Ma, X. Jia, W. Qiao, L. Ling and J. Wang, *Appl. Surf. Sci.*, 2022, **578**, 152022.
102 X. Zhang, G. Li, Y. Zhang, D. Luo, A. Yu, X. Wang and Z. Chen, *Nano Energy*, 2021, **86**, 106094.
103 G. Wang, J. Li, Z. Du, Z. Ma and G. Shao, *Membranes*, 2022, **12**, 134.
104 J. Zhang, Q. Zhang, X. Qu, G. Xu, B. Fan, Z. Yan, F. Gui and L. Yang, *Appl. Surf. Sci.*, 2022, **574**, 151559.

105 K. Xie, K. Yuan, K. Zhang, C. Shen, W. Lv, X. Liu, J. G. Wang and B. Wei, *ACS Appl. Mater. Interfaces*, 2017, **9**, 4605–4613.
106 M. Raja, S. Suriyakumar, N. Angulakshmi and A. Manuel Stephan, *Inorg. Chem. Front.*, 2017, **4**, 1013–1021.
107 M. Wang, Z. Bai, T. Yang, C. Nie, X. Xu, Y. Wang, J. Yang, S. Dou and N. Wang, *Adv. Energy Mater.*, 2022, **12**, 2201585.
108 S. F. Ng, M. Y. L. Lau and W. J. Ong, *Adv. Mater.*, 2021, **33**, 2008654.
109 K. Liu, H. Zhao, D. Ye and J. Zhang, *Chem. Eng. J.*, 2021, **417**, 129309.
110 Q. Xiao, J. Yang, X. Wang, Y. Deng, P. Han, N. Yuan, L. Zhang, M. Feng, C. an Wang and R. Liu, *Carbon Energy*, 2021, **3**, 271–302.
111 Y. C. Jiang, H. M. U. Arshad, H. J. Li, S. Liu, G. R. Li and X. P. Gao, *Small*, 2021, **17**, 2005332.
112 H. Li, Y. Li and L. Zhang, *SusMat*, 2022, **2**, 34–64.
113 X. Liu, J. Q. Huang, Q. Zhang and L. Mai, *Adv. Mater.*, 2017, **29**, 1601759.
114 H. J. Peng, J. Q. Huang, X. B. Cheng and Q. Zhang, *Adv. Energy Mater.*, 2017, **7**, 1700260.
115 J. Zhang, H. Huang, J. Bae, S. H. Chung, W. Zhang, A. Manthiram and G. Yu, *Small Methods*, 2018, **2**, 1700279.
116 Y. Liu, Y. Elias, J. Meng, D. Aurbach, R. Zou, D. Xia and Q. Pang, *Joule*, 2021, **5**, 2323–2364.
117 J. Guo, H. Pei, Y. Dou, S. Zhao, G. Shao and J. Liu, *Adv. Funct. Mater.*, 2021, **31**, 2010499.
118 G. Liu, Q. Sun, Q. Li, J. Zhang and J. Ming, *Energy Fuels*, 2021, **35**, 10405–10427.
119 X. Q. Zhang, Q. Jin, Y. L. Nan, L. P. Hou, B. Q. Li, X. Chen, Z. H. Jin, X. T. Zhang, J. Q. Huang and Q. Zhang, *Angew. Chem., Int. Ed.*, 2021, **60**, 15503–15509.
120 Q. Pang, X. Liang, C. Y. Kwok and L. F. Nazar, *Nat. Energy*, 2016, **1**(9), 1–11.
121 A. Manthiram, X. Yu and S. Wang, *Nat. Rev. Mater.*, 2017, **24**(2), 1–16.
122 H. Shin, M. Baek, A. Gupta, K. Char, A. Manthiram and J. W. Choi, *Adv. Energy Mater.*, 2020, **10**, 2001456.
123 X. Yang, J. Luo and X. Sun, *Chem. Soc. Rev.*, 2020, **49**, 2140–2195.
124 A. Miura, N. C. Rosero-Navarro, A. Sakuda, K. Tadanaga, N. H. H. Phuc, A. Matsuda, N. Machida, A. Hayashi and M. Tatsumisago, *Nat. Rev. Chem.*, 2019, **33**(3), 189–198.
125 J. He and A. Manthiram, *Energy Storage Mater.*, 2019, **20**, 55–70.
126 F. Zou and A. Manthiram, *Adv. Energy Mater.*, 2020, **10**, 2002508.
127 G. Zhou, H. Chen and Y. Cui, *Nat. Energy*, 2022, **7**, 312–319.
128 R. Deng, M. Wang, H. Yu, S. Luo, J. Li, F. Chu, B. Liu and F. Wu, *Energy Environ. Mater.*, 2022, **5**, 777–799.
129 S. H. Chung, C. H. Chang and A. Manthiram, *Adv. Funct. Mater.*, 2018, **28**, 1801188.
130 J. Zhu, P. Zhu, C. Yan, X. Dong and X. Zhang, *Prog. Polym. Sci.*, 2019, **90**, 118–163.
131 Z. W. Seh, Y. Sun, Q. Zhang and Y. Cui, *Chem. Soc. Rev.*, 2016, **45**, 5605–5634.
132 Y. Huang, L. Lin, C. Zhang, L. Liu, Y. Li, Z. Qiao, J. Lin, Q. Wei, L. Wang, Q. Xie and D. L. Peng, *Adv. Sci.*, 2022, **9**, 1–35.
133 B. W. Zhang, B. Sun, P. Fu, F. Liu, C. Zhu, B. M. Xu, Y. Pan and C. Chen, *Membranes*, 2022, **12**, 790.
134 M. Chen, M. Shao, J. Jin, L. Cui, H. Tu and X. Fu, *Energy Storage Mater.*, 2022, **47**, 629–648.
135 X. Long, S. K. Zhu, Y. Song, M. Zheng, J. J. Shao and B. Shi, *New Carbon Mater.*, 2022, **37**, 527–543.
136 J. Kang, X. Tian, C. Yan, L. Wei, L. Gao, J. Ju, Y. Zhao, N. Deng, B. Cheng and W. Kang, *Small*, 2022, **18**, 2104469.
137 S. Huang, R. Guan, S. Wang, M. Xiao, D. Han, L. Sun and Y. Meng, *Prog. Polym. Sci.*, 2019, **89**, 19–60.
138 J. Lopez, D. G. Mackanic, Y. Cui and Z. Bao, *Nat. Rev. Mater.*, 2019, **45**(4), 312–330.
139 S. Dutta, A. Bhaumik and K. C. W. Wu, *Energy Environ. Sci.*, 2014, **7**, 3574–3592.
140 H. Yu, M. Bi, C. Zhang, T. Zhang, X. Zhang, H. Liu, J. Mi, X. Shen and S. Yao, *Int. J. Energy Res.*, 2022, **46**, 24565–24577.
141 Y. Li, W. Wang, X. Liu, E. Mao, M. Wang, G. Li, L. Fu, Z. Li, A. Y. S. Eng, Z. W. Seh and Y. Sun, *Energy Storage Mater.*, 2019, **23**, 261–268.
142 L. L. Chiu and S. H. Chung, *Polymers*, 2021, **13**, 535.
143 M. Rana, M. Li, Q. He, B. Luo, L. Wang, I. Gentle and R. Knibbe, *J. Energy Chem.*, 2020, **44**, 51–60.
144 C. Pei, J. Li, Z. Lv, H. Wang, W. Dong and Y. Yao, *Int. J. Energy Res.*, 2022, **46**, 10099–10110.
145 M. Li, J. Yang, Y. Shi, Z. Chen, P. Bai, H. Su, P. Xiong, M. Cheng, J. Zhao and Y. Xu, *Adv. Mater.*, 2022, **34**, 2107226.
146 Q. Jin, K. Zhao and X. Zhang, *J. Power Sources*, 2021, **489**, 229500.
147 I. Bauer, S. Thieme, J. Brückner, H. Althues and S. Kaskel, *J. Power Sources*, 2014, **251**, 417–422.
148 A. Mentbayeva, S. Sukhishvili, M. Naizakarayev, N. Batyrgali, Z. Seitzhan and Z. Bakenov, *Electrochim. Acta*, 2021, **366**, 137454.
149 Y. Chen, G. Zhou, W. Zong, Y. Ouyang, K. Chen, Y. Lv, Y. E. Miao and T. Liu, *Compos. Commun.*, 2021, **25**, 100679.
150 Y. Hao, Y. Xing, H. Kong and Y. Jiao, *ChemElectroChem*, 2021, **8**, 2329–2335.
151 X. Yu, J. Joseph and A. Manthiram, *J. Mater. Chem. A*, 2015, **3**, 15683–15691.
152 J. Wang, P. Zhai, T. Zhao, M. Li, Z. Yang, H. Zhang and J. Huang, *Electrochim. Acta*, 2019, **320**, 1–11.
153 W. Diao, D. Xie, D. Li, F. Tao, C. Liu, H. Sun, X. Zhang, W. Li, X.-L. Wu and J.-P. Zhang, *J. Colloid Interface Sci.*, 2022, **627**, 730–738.
154 Z. Hao, L. Yuan, Z. Li, J. Liu, J. Xiang, C. Wu, R. Zeng and Y. Huang, *Electrochim. Acta*, 2016, **200**, 197–203.
155 A. J. Manly and W. E. Tenhaeff, *Electrochim. Acta*, 2022, **425**, 140705.
156 F. Z. Chafi, R. X. Qi, L. Ma, Y. J. Cheng and Y. Xia, *Energy Fuels*, 2021, **35**, 18746–18755.
157 H. Yang, X. Shi, S. Chu, Z. Shao, Y. Wang, H. Yang, X. Shi, S. Chu, Z. Shao and Y. Wang, *Adv. Sci.*, 2021, **8**, 2003096.

158 G. Wang, Y. Lai, Z. Zhang, J. Li and Z. Zhang, *J. Mater. Chem. C*, 2015, **3**, 10715–10722.
159 S. H. Chung and A. Manthiram, *Adv. Mater.*, 2014, **26**, 7352–7357.
160 L. Luo, S. H. Chung and A. Manthiram, *J. Mater. Chem. A*, 2016, **4**, 16805–16811.
161 Z. Tong, L. Huang, H. Liu, W. Lei, H. Zhang, S. Zhang and Q. Jia, *Adv. Funct. Mater.*, 2021, **31**, 1–10.
162 Y. Yang, W. Wang, L. Li, B. Li and J. Zhang, *J. Mater. Chem. A*, 2020, **8**, 3692–3700.
163 Y. Hu, C. Cheng, T. Yan, G. Liu, C. Yuan, Y. Yan, Z. Gu, P. Zeng, L. Zheng, J. Zhang and L. Zhang, *Chem. Eng. J.*, 2021, **421**, 129997.
164 J. He, L. Luo, Y. Chen and A. Manthiram, *Adv. Mater.*, 2017, **29**, 1–5.
165 Z. Li, J. Zhang, B. Guan, D. Wang, L. M. Liu and X. W. Lou, *Nat. Commun.*, 2016, **7**, 1–11.
166 S. Song, L. Shi, S. Lu, Y. Pang, Y. Wang, M. Zhu, D. Ding and S. Ding, *J. Membr. Sci.*, 2018, **563**, 277–283.
167 H. Gao, S. Ning, J. Lin and X. Kang, *Energy Storage Mater.*, 2021, **40**, 312–319.
168 Z. Li, Y. Han, J. Wei, W. Wang, T. Cao, S. Xu and Z. Xu, *ACS Appl. Mater. Interfaces*, 2017, **9**, 44776–44781.
169 D. B. Babu, K. Giribabu and K. Ramesha, *ACS Appl. Mater. Interfaces*, 2018, **10**, 19721–19729.
170 J. Liu, Z. Hong, F. Zhu, Q. Li, J. Li, M. Liu, C. Wang, F. Song, L. Bai and F. Zeng, *Ionics*, 2021, **27**, 4749–4759.
171 D. Li, H. Wang, L. Luo, J. Zhu, J. Li, P. Liu, Y. Yu and M. Jiang, *ACS Appl. Energy Mater.*, 2021, **4**, 879–887.
172 L. Ma, P. Nath, Z. Tu, M. Tikekar and L. A. Archer, *Chem. Mater.*, 2016, **28**, 5147–5154.
173 I. Paniagua-Vásquez, C. C. Zuluaga-Gómez, S. Chacón-Vargas, A. L. Calvo, G. Sáenz-Arce, R. S. Katiyar and J. J. Saavedra-Arias, *Energies*, 2022, **15**, 2183.
174 X. Yu, J. Joseph and A. Manthiram, *Mater. Horizons*, 2016, **3**, 314–319.
175 M. Gu, J. Lee, Y. Kim, J. S. Kim, B. Y. Jang, K. T. Lee and B. S. Kim, *RSC Adv.*, 2014, **4**, 46940–46946.
176 C. Zhan, G. Yu, Y. Lu, L. Wang, E. Wujcik and S. Wei, *J. Mater. Chem. C*, 2017, **5**, 1569–1585.
177 K. Namsheer and C. S. Rout, *RSC Adv.*, 2021, **11**, 5659–5697.
178 H. Hareendrakrishnakumar, R. Chulliyote and M. G. Joseph, *Ionics*, 2021, **27**, 1087–1099.
179 S. A. Abbas, M. A. Ibrahem, L. H. Hu, C. N. Lin, J. Fang, K. M. Boopathi, P. C. Wang, L. J. Li and C. W. Chu, *J. Mater. Chem. A*, 2016, **4**, 9661–9669.
180 H. Li, M. Sun, T. Zhang, Y. Fang and G. Wang, *J. Mater. Chem. A*, 2014, **2**, 18345–18352.
181 S. Z. Zeng, Y. Yao, J. Tu, Z. Tian, J. Zou, X. Zeng, H. Zhu, L. B. Kong and P. Han, *Ionics*, 2021, **27**, 3887–3893.
182 K. Chen, G. Zhang, L. Xiao, P. Li, W. Li, Q. Xu and J. Xu, *Small*, 2021, 1–12, DOI: **10.1002/smtd.202001056**.
183 H. Jo, Y. Cho, T. Yoo, Y. Jeon, H. Hong and Y. Piao, *ACS Appl. Mater. Interfaces*, 2021, **13**, 47593–47602.
184 M. Shi, Z. Liu, S. Zhang, S. Liang, Y. Jiang, H. Bai, Z. Jiang, J. Chang, J. Feng, W. Chen, H. Yu, S. Liu, T. Wei and Z. Fan, *Adv. Energy Mater.*, 2022, **12**, 1–12.
185 Z. Yu, M. Liu, D. Guo, J. Wang, X. Chen, J. Li, H. Jin, Z. Yang, X. Chen and S. Wang, *Angew. Chem., Int. Ed.*, 2020, **59**, 6406–6411.
186 J. Cai, Y. Song, X. Chen, Z. Sun, Y. Yi, J. Sun and Q. Zhang, *J. Mater. Chem. A*, 2020, **8**, 1757–1766.
187 Y. Zhou, H. Gao, S. Ning, J. Lin, J. Wen and X. Kang, *ChemElectroChem*, 2021, **8**, 1798–1806.
188 W. Zhang, Y. Liu, A. Wu, L. Ling, Z. Wang, X. Hao and G. Guan, *Electrochim. Acta*, 2022, **403**, 139609.
189 M. Yang, J. Nan, W. Chen, A. Hu, H. Sun, Y. Chen and C. Wu, *Electrochem. Commun.*, 2021, **125**, 106971.
190 J. Conder, A. Forner-Cuenca, E. M. Gubler, L. Gubler, P. Novák and S. Trabesinger, *ACS Appl. Mater. Interfaces*, 2016, **8**, 18822–18831.
191 Y. Li, X. Zhang, Q. Zhang, J. Cui, X. Liang, J. Yan, J. Liu, H. H. Tan, Y. Yu and Y. Wu, *ACS Appl. Mater. Interfaces*, 2022, **14**, 18634–18645.
192 J.-H. Shin, Y.-Y. Park, S.-H. Moon, J.-H. Kim, J.-S. Jang, S.-B. Kim, S.-N. Lee and K.-W. Park, *Energies*, 2022, **15**, 7961.
193 X. Wang, L. Yang, Q. Li, Y. Wang, Y. Zhong, Y. Song, Y. Chen, Z. Wu, B. Zhong and X. Guo, *Ind. Eng. Chem. Res.*, 2022, **61**, 1761–1772.
194 H. Yao, K. Yan, W. Li, G. Zheng, D. Kong, Z. W. Seh, V. K. Narasimhan, Z. Liang and Y. Cui, *Energy Environ. Sci.*, 2014, **7**, 3381–3390.
195 Z. Zhang, Y. Dong, Y. Gu, P. Lu, F. Xue, Y. Fan, Z. Zhu, J. Lin, Q. Li and Z. S. Wu, *J. Mater. Chem. A*, 2022, **10**, 9515–9523.
196 A. Benítez, J. Amaro-Gahete, Y. C. Chien, Á. Caballero, J. Morales and D. Brandell, *Renewable Sustainable Energy Rev.*, 2022, **154**, 111783.
197 X. Liu, Q. He, J. Liu, R. Yu, Y. Zhang, Y. Zhao, X. Xu, L. Mai and L. Zhou, *ACS Appl. Mater. Interfaces*, 2023, **15**, 9439–9446.
198 L. Li, H. Liu, B. Jin, Q. Sheng, Q. Li, M. Cui, Y. Li, X. Lang and Q. Jiang, *ACS Appl. Nano Mater.*, 2023, **6**, 1161–1170.
199 X. Ou, Y. Yu, R. Wu, A. Tyagi, M. Zhuang, Y. Ding, I. H. Abidi, H. Wu, F. Wang and Z. Luo, *ACS Appl. Mater. Interfaces*, 2018, **10**, 5534–5542.
200 J. H. Lee, J. Kang, S. W. Kim, W. Halim, M. W. Frey and Y. L. Joo, *ACS Omega*, 2018, **3**, 16465–16471.
201 X. Qi, L. Huang, Y. Luo, Q. Chen and Y. Chen, *J. Colloid Interface Sci.*, 2022, **628**, 896–910.
202 L. Wang, Z. Yang, H. Nie, C. Gu, W. Hua, X. Xu, X. Chen, Y. Chen and S. Huang, *J. Mater. Chem. A*, 2016, **4**, 15343–15352.
203 H. Li, Y. Zhou, M. Zhao, B. Jin, Z. Wen, H. Xie, S. Dou and Q. Jiang, *Adv. Energy Mater.*, 2020, **10**, 1–11.
204 F. Ma, K. Srinivas, X. Zhang, Z. Zhang, Y. Wu, D. Liu, W. Zhang, Q. Wu and Y. Chen, *Adv. Funct. Mater.*, 2022, 1–14, DOI: **10.1002/adfm.202206113**.
205 L. Gai, C. Zhao, Y. Zhang, Z. Hu and Q. Shen, *Carbon Energy*, 2022, **4**, 142–154.
206 E. Jing, L. Chen, S. Xu, W. Tian, D. Zhang, N. Wang, Z. Bai, X. Zhou, S. Liu, D. Duan and X. Qiu, *J. Energy Chem.*, 2021, **64**, 574–582.
207 P. Wang, B. Xi, Z. Zhang, M. Huang, J. Feng and S. Xiong, *Angew. Chem.*, 2021, **133**, 15691–15699.

208 W. Jing, J. Zu, K. Zou, X. Dai, Y. Song, J. Han, J. Sun, Q. Tan, Y. Chen and Y. Liu, *J. Mater. Chem. A*, 2022, **10**, 4833–4844.
209 W. Jing, K. Zou, X. Dai, M. Shi, J. Sun, D. Zhu, S. Guo, Y. Chen and Y. Liu, *J. Colloid Interface Sci.*, 2021, **601**, 305–316.
210 Z. Cheng, Y. Chen, Y. Yang, L. Zhang, H. Pan, X. Fan, S. Xiang and Z. Zhang, *Adv. Energy Mater.*, 2021, **11**, 1–9.
211 P. Cheng, P. Guo, K. Sun, Y. Zhao, D. Liu and D. He, *J. Membr. Sci.*, 2021, **619**, 118780.
212 P. Cheng, P. Guo, D. Liu, Y. Wang, K. Sun, Y. Zhao and D. He, *J. Alloys Compd.*, 2019, **784**, 149–156.
213 K. Xu, X. Liang, L. L. Wang, Y. Wang, J. F. Yun, Y. Sun and H. F. Xiang, *Rare Met.*, 2021, **40**(10), 2810–2818.
214 J. Wang, Z. Shi, Y. Luo, D. Wang, H. Wu, Q. Li, S. Fan, J. Li and J. Wang, *Nanoscale*, 2021, **13**, 6863–6870.
215 Y. Zhao, J. Liu, Y. Zhou, X. Huang, Q. Liu, F. Chen, H. Qin, H. Lou, D. Y. W. Yu and X. Hou, *ACS Appl. Mater. Interfaces*, 2021, **13**, 41698–41706.
216 T. Xiao, Q. Chen, W. Zhong, M. Yang, F. Cai, W. Liu, M. Ren and Y. Wang, *J. Alloys Compd.*, 2022, **907**, 164486.
217 Y. Liu, X. Zhao, S. Li, Q. Zhang, K. Wang and J. Chen, *Chem. Res. Chin. Univ.*, 2022, **38**, 147–154.
218 C. Chen, Q. Jiang, H. Xu, Y. Zhang, B. Zhang, Z. Zhang, Z. Lin and S. Zhang, *Nano Energy*, 2020, **76**, 105033.
219 C. Shen, Y. Li, M. Gong, C. Zhou, Q. An, X. Xu and L. Mai, *ACS Appl. Mater. Interfaces*, 2021, **13**, 60046–60053.
220 P. Li, J. Deng, J. Li, L. Wang and J. Guo, *Ceram. Int.*, 2019, **45**, 13219–13224.
221 J. He, Z. Gao and X. Li, *Jom*, 2021, **73**, 2516–2524.
222 X. Fan, Y. Wang, M. Zeng, H. He, J. Huang, Z. Feng, J. Li, Z. Liang and T. Zhou, *J. Alloys Compd.*, 2022, **894**, 162556.
223 Q. X. Shi, C. Chang, H. J. Pei, X. Guan, L. L. Yin, X. L. Xie and Y. S. Ye, *Electrochim. Acta*, 2021, **367**, 137418.
224 X. Hu, T. Huang, S. Wang, S. Lin, Z. Feng, L. H. Chung and J. He, *Electrochim. Acta*, 2021, **398**, 139317.
225 N. Li, W. Cao, Y. Liu, H. Ye and K. Han, *Colloids Surf., A*, 2019, **573**, 128–136.
226 Z. T. Shao, L. L. Wu, Y. Yang, X. Z. Ma, L. Li, H. F. Ye and X. T. Zhang, *New Carbon Mater.*, 2021, **36**, 219–226.
227 M. Luo, Y. Bai, R. Sun, M. Qu, M. Wang, Z. Yang, Z. Wang, W. Sun and K. Sun, *J. Energy Chem.*, 2022, **73**, 407–415.
228 J. Zhang, Y. Cheng, H. Chen, Y. Wang, Q. Chen, G. Hou, M. Wen and Y. Tang, *ACS Appl. Mater. Interfaces*, 2022, **14**, 16289–16299.
229 Z. Li, L. Tang, X. Liu, T. Song, Q. Xu, H. Liu and Y. Wang, *Electrochim. Acta*, 2019, **310**, 1–12.
230 X. Yu, W. Chen, J. Cai, X. Lu and Z. Sun, *J. Colloid Interface Sci.*, 2022, **610**, 407–417.
231 Z. Gao, Z. Xue, Y. Miao, B. Chen, J. Xu, H. Shi, T. Tang and X. Zhao, *J. Alloys Compd.*, 2022, **906**, 164249.
232 L. Zhan, X. Zhou, J. Luo, X. Fan and X. Ning, *Int. J. Hydrogen Energy*, 2022, **47**, 27671–27679.
233 X. Qian, F. Li and L. Jin, *Microporous Mesoporous Mater.*, 2022, **329**, 111558.
234 X. Wu, S. Li, S. Yao, M. Liu, S. Pang, X. Shen, T. Li and S. Qin, *Int. J. Energy Res.*, 2021, **45**, 4331–4344.
235 T. Wang, Y. Liu, X. Zhang, J. Wang, Y. Zhang, Y. Li, Y. Zhu, G. Li and X. Wang, *ACS Appl. Mater. Interfaces*, 2021, **13**, 56085–56094.
236 Y. Gong, Y. Wang, Z. Fang, S. Zhao, Y. shi He, W. Zhang, J. Mu, L. Zhang and Z. F. Ma, *Chem. Eng. J.*, 2022, **446**, 136943.
237 J. Liu, K. Li, Q. Zhang, X. Zhang, X. Liang, J. Yan, H. H. Tan, Y. Yu and Y. Wu, *ACS Appl. Mater. Interfaces*, 2021, **13**, 45547–45557.
238 S. K. Kannan, H. Hareendrakrishnakumar, J. Joseph and M. G. Joseph, *Energy Fuels*, 2022, **36**, 8460–8470.
239 Q. Liu, X. Han, Q. Dou, P. Xiong, Y. Kang, B. K. Kim and H. S. Park, *Int. J. Energy Res.*, 2022, **46**, 9634–9642.
240 R. Ponraj, A. G. Kannan, J. H. Ahn, J. H. Lee, J. Kang, B. Han and D. W. Kim, *ACS Appl. Mater. Interfaces*, 2017, **9**, 38445–38454.
241 F. Wang, Z. Yang and C. Y. Tang, *ACS ES&T Engg.*, 2022, **2**, 2023–2033.
242 S. Sun, L. Han, J. Hou, Y. Yang, J. Yue, G. Gu, C. Yang, J. Li and Z. Zhang, *J. Colloid Interface Sci.*, 2022, **628**, 1012–1022.
243 P. Xie, B. Zhang, Y. Zhou, P. Li and X. Tian, *Electrochim. Acta*, 2021, **395**, 139181.
244 Z. Zhao, W. Yin, H. Li, Y. Jiao, D. Lei, Y. Li, J. Guo, W. Bai and M. Xiang, *Microporous Mesoporous Mater.*, 2022, **337**, 111946.
245 P. Zeng, L. Huang, Y. Han, X. Zhang, R. Zhang and Y. Chen, *ChemElectroChem*, 2018, **5**, 375–382.
246 D. Zhao, X. Qian, L. Jin, X. Yang, S. Wang, X. Shen, S. Yao, D. Rao, Y. Zhou and X. Xi, *RSC Adv.*, 2016, **6**, 13680–13685.
247 L. Jin, Z. Fu, X. Qian, B. Huang, F. Li, Y. Wang and X. Shen, *Microporous Mesoporous Mater.*, 2021, **316**, 110927.
248 C. Liao, X. Mu, L. Han, Z. Li, Y. Zhu, J. Lu, H. Wang, L. Song, Y. Kan and Y. Hu, *Energy Storage Mater.*, 2022, **48**, 123–132.
249 Y. C. Huang, Y. J. Yen, Y. H. Tseng and S. H. Chung, *Molecules*, 2021, **27**, 228.
250 L. Jin, Z. Fu, X. Qian, F. Li, Y. Wang, B. Wang and X. Shen, *Electrochim. Acta*, 2021, **382**, 138282.
251 J. He, G. Hartmann, M. Lee, G. S. Hwang, Y. Chen and A. Manthiram, *Energy Environ. Sci.*, 2019, **12**, 344–350.
252 S. Zhen, J. Huang, L. Peng, M. Zhang, K. Shi, G. Ma, A. Li and Y. Wang, *Energy Technol.*, 2021, **9**, 1–9.
253 H. Han, S. Niu, Y. Zhao, T. Tan and Y. Zhang, *Nanoscale Res. Lett.*, 2019, **14**, 1–8.
254 J. Huang, S. Dong and G. Xie, *Ionics*, 2022, **28**(9), 4129–4134.
255 W. Jiang, L. Dong, S. Liu, S. Zhao, K. Han, W. Zhang, K. Pan and L. Zhang, *Nanomater*, 2022, **12**, 1347.
256 X. Liu, S. Wang, H. Duan, Y. Deng and G. Chen, *J. Colloid Interface Sci.*, 2022, **608**, 470–481.
257 X. Shi, L. Yang, S. Li, Y. Wang, X. Chen, Z. Wu, Y. Zhong, Y. Chen, S. Gao, G. Wang, X. Guo and B. Zhong, *Electrochim. Acta*, 2021, **390**, 138829.
258 L. ying Wei, N. ping Deng, J. ge Ju, H. juan Zhao, G. Wang, H. ying Xiang, W. min Kang and B. wen Cheng, *Chem. Eng. J.*, 2021, **424**, 130346.
259 Y. Luo, H. Bai, B. Li, X. Song, J. Zhao, Y. Xiao, S. Lei and B. Cheng, *J. Alloys Compd.*, 2021, **879**, 160368.

260 P. Zeng, L. Huang, X. Zhang, R. Zhang, L. Wu and Y. Chen, *Chem. Eng. J.*, 2018, **349**, 327–337.
261 Z. Kong, Y. Lin, J. Hu, Y. Wang and L. Zhan, *Chem. Eng. J.*, 2022, **436**, 132719.
262 L. Liu, F. Yang, L. Ge, X. Wang, L. Cui and H. Yang, *Electrochim. Acta*, 2022, **401**, 139380.
263 F. Yang and K. Huang, *Mater. Res. Express*, 2021, **8**, 115002.
264 L. Zhu, J. Li, H. Xie and X. Shen, *Ionics*, 2022, **28**, 3207–3215.
265 Q. Li, Y. Liu, L. Yang, Y. Wang, Y. Liu, Y. Chen, X. Guo, Z. Wu and B. Zhong, *J. Colloid Interface Sci.*, 2021, **585**, 43–50.
266 J. R. Choi, E. Kim, B.-I. Park, I. Choi, B.-H. Park, S.-B. Lee, J. H. Lee and S. Yu, *J. Ind. Eng. Chem.*, 2022, **115**, 355–364.
267 X. Wang, L. Yang, R. Li, Y. Chen, Z. Wu, B. Zhong and X. Guo, *Appl. Surf. Sci.*, 2022, **602**, 154342.
268 L. Wu, H. Hou, J. Hu, B. Liu, X. Yang, S. Chen, L. Liu, S. Hu, J. Yang, S. Liang, K. Xiao and S. Yuan, *Microporous Mesoporous Mater.*, 2021, **317**, 111000.
269 X. Zhang, L. Chen, Z. Yang, X. Qiu and Z. Zheng, *Mater. Lett.*, 2021, **290**, 129512.
270 N. Díez, M. Sevilla and A. B. Fuertes, *ACS Appl. Energy Mater.*, 2020, **3**, 3397–3407.
271 B. Zheng, L. Yu, Y. Zhao and J. Xi, *Electrochim. Acta*, 2019, **295**, 910–917.
272 L. Han, S. Sun, Y. Yang, J. Yue and J. Li, *Appl. Surf. Sci.*, 2023, **610**, 155496.
273 B. Dang, D. Y. Gao, Y. Luo, Z. Zhang, J. Li and F. Wu, *J. Energy Storage*, 2022, **52**, 104981.
274 Y. Fan, Z. Niu, F. Zhang, R. Zhang, Y. Zhao and G. Lu, *ACS Omega*, 2019, **4**, 10328–10335.
275 J. Wang and J. Li, *J. Colloid Interface Sci.*, 2021, **584**, 354–359.
276 H. Chen, Y. Xiao, C. Chen, J. Yang, C. Gao, Y. Chen, J. Wu, Y. Shen, W. Zhang, S. Li, F. Huo and B. Zheng, *ACS Appl. Mater. Interfaces*, 2019, **11**, 11459–11465.
277 Y. Guo, M. Sun, H. Liang, W. Ying, X. Zeng, Y. Ying, S. Zhou, C. Liang, Z. Lin and X. Peng, *ACS Appl. Mater. Interfaces*, 2018, **10**, 30451–30459.
278 F. Wu, S. Zhao, L. Chen, Y. Lu, Y. Su, Y. Jia, L. Bao, J. Wang, S. Chen and R. Chen, *Energy Storage Mater.*, 2018, **14**, 383–391.
279 B. Ma, X. Zhang, X. Deng, S. Huang, M. Xiao, S. Wang, D. Han and Y. Meng, *Polymers*, 2021, **13**, 4210.
280 Z. Hu, Y. Wang and D. Zhao, *Chem. Soc. Rev.*, 2021, **50**, 4629–4683.
281 Y. Su, W. Wang, W. Wang, A. Wang, Y. Huang and Y. Guan, *J. Electrochem. Soc.*, 2022, **169**, 030528.
282 H. G. Jin, M. Wang, J. X. Wen, S. H. Han, X. J. Hong, Y. P. Cai, G. Li, J. Fan and Z. S. Chao, *ACS Appl. Mater. Interfaces*, 2021, **13**, 3899–3910.
283 X. Qian, J. Cheng, L. Jin, Y. Wang, B. Huang and J. Chen, *Colloids Surf., A*, 2022, **648**, 129036.
284 X. Qian, Y. Wang, L. Jin, J. Cheng, J. Chen and B. Huang, *J. Electroanal. Chem.*, 2022, **907**, 116029.
285 Y. Chen, L. Zhang, H. Pan, J. Zhang, S. Xiang, Z. Cheng and Z. Zhang, *J. Mater. Chem. A*, 2021, **9**, 26929–26938.
286 X. Wu, C. Zhou, C. Dong, C. Shen, B. Shuai, C. Li, Y. Li, Q. An, X. Xu and L. Mai, *Nano Res.*, 2022, **15**, 8048–8055.
287 S. H. Kim, J. S. Yeon, R. Kim, K. M. Choi and H. S. Park, *J. Mater. Chem. A*, 2018, **6**, 24971–24978.
288 S. Y. Ding and W. Wang, *Chem. Soc. Rev.*, 2012, **42**, 548–568.
289 Y. Zhu, J. Yang, X. Qiu, M. Li, G. He, Q. Wang, Z. Xie, X. Li and H. Yu, *ACS Appl. Mater. Interfaces*, 2021, **13**, 60373–60383.
290 J. Zhao, G. Yan, X. Zhang, Y. Feng, N. Li, J. Shi and X. Qu, *Chem. Eng. J.*, 2022, **442**, 136352.
291 T. S. Sahu, V. G. Abhijitha, I. Pal, S. Sau, M. Gautam, B. R. K. Nanda and S. Mitra, *Small*, 2022, **18**, 2203222.
292 K. Sun, C. Wang, Y. Dong, P. Guo, P. Cheng, Y. Fu, D. Liu, D. He, S. Das and Y. Negishi, *ACS Appl. Mater. Interfaces*, 2022, **14**, 4079–4090.
293 Q. X. Shi, C. Y. Yang, H. J. Pei, C. Chang, X. Guan, F. Y. Chen, X. L. Xie and Y. S. Ye, *Chem. Eng. J.*, 2021, **404**, 127044.
294 Y. Cao, H. Wu, G. Li, C. Liu, L. Cao, Y. Zhang, W. Bao, H. Wang, Y. Yao, S. Liu, F. Pan, Z. Jiang and J. Sun, *Nano Lett.*, 2021, **21**, 2997–3006.
295 M. Zhen, K. Jiang, S. Q. Guo, B. Shen and H. Liu, *Nano Res.*, 2021, **15**(2), 933–941.
296 J. Lin, K. Zhang, Z. Zhu, R. Zhang, N. Li and C. Zhao, *ACS Appl. Mater. Interfaces*, 2020, **12**, 2497–2504.
297 L. Peng, Z. Yu, M. Zhang, S. Zhen, J. Shen, Y. Chang, Y. Wang, Y. Deng and A. Li, *Nanoscale*, 2021, **13**, 16696–16704.
298 X. Wang, L. Yang, Y. Wang, Q. Li, C. Chen, B. Zhong, Y. Chen, X. Guo, Z. Wu, Y. Liu, Y. Liu and Y. Sun, *J. Colloid Interface Sci.*, 2022, **606**, 666–676.
299 P. Cheng, D. Cao, K. Sun, Y. Li, Y. Fu, Y. Zhao, D. Liu and D. He, *J. Alloys Compd.*, 2021, **868**, 159131.
300 S. Wang, P. Zhang, H. Tan, X. Fan and K. Huang, *J. Power Sources*, 2019, **419**, 106–111.
301 X. Wu, S. Yao, M. Liu, S. Pang, X. Shen, T. Li and S. Qin, *Ionics*, 2021, **27**, 2397–2408.
302 W. Sun, X. Sun, Q. Peng, H. Wang, Y. Ge, N. Akhtar, Y. Huang and K. Wang, *Nanoscale Adv.*, 2019, **1**, 1589–1597.
303 S. Hu, M. Yi, H. Wu, T. Wang, X. Ma, X. Liu and J. Zhang, *Adv. Funct. Mater.*, 2022, **32**, 1–12.
304 H. Shao, W. Wang, H. Zhang, A. Wang, X. Chen and Y. Huang, *J. Power Sources*, 2018, **378**, 537–545.
305 Z. Huang, M. Yang, J. Qi, P. Zhang, L. Lei and Q. Du, *Chem. Eng. J.*, 2020, **387**, 1–10.
306 Y. Zhu, Y. Zuo, X. Jiao, R. Manjunatha, E. R. Ezeigwe, W. Yan and J. Zhang, *Carbon Energy*, 2022, 1–13.
307 Q. Liu, X. Han, Q. Dou, P. Xiong, Y. Kang, S. W. Kang, B. K. Kim and H. S. Park, *Batteries Supercaps*, 2021, **4**, 1843–1849.
308 S. Liu, Z. Zhou and D. Liu, *Ceram. Int.*, 2019, **45**, 14415–14419.
309 B. Moorthy, S. Kwon, J. H. Kim, P. Ragupathy, H. M. Lee and D. K. Kim, *Nanoscale Horizons*, 2019, **4**, 214–222.
310 G. Liu, Q. Zeng, Z. Fan, S. Tian, X. Li, X. Lv, W. Zhang, K. Tao, E. Xie and Z. Zhang, *Chem. Eng. J.*, 2022, **448**, 137683.

311 H. Li, L. Sun, Y. Zhao, T. Tan and Y. Zhang, *Appl. Surf. Sci.*, 2019, **466**, 309–319.
312 Z. A. Ghazi, X. He, A. M. Khattak, N. A. Khan, B. Liang, A. Iqbal, J. Wang, H. Sin, L. Li and Z. Tang, *Adv. Mater.*, 2017, **29**, 1–6.
313 Z. Li, F. Zhang, L. Tang, Y. Tao, H. Chen, X. Pu, Q. Xu, H. Liu, Y. Wang and Y. Xia, *Chem. Eng. J.*, 2020, **390**, 124653.
314 Z. Liu, Z. Hu, X. Jiang, Y. Zhang, X. Wang and S. Zhang, *Electrochim. Acta*, 2022, **422**, 140496.
315 X. Yu, Y. Yang, L. Si, J. Cai, X. Lu and Z. Sun, *J. Colloid Interface Sci.*, 2022, **627**, 992–1002.
316 J. Song, D. Su, X. Xie, X. Guo, W. Bao, G. Shao and G. Wang, *ACS Appl. Mater. Interfaces*, 2016, **8**, 29427–29433.
317 Y. H. Liu, L. X. Li, A. Y. Wen, F. F. Cao and H. Ye, *Energy Storage Mater.*, 2023, **55**, 652–659.
318 P. Li, H. Lv, Z. Li, X. Meng, Z. Lin, R. Wang and X. Li, *Adv. Mater.*, 2021, **33**, 2007803.
319 R. Gao, Z. Wang, S. Liu, G. Shao and X. Gao, *Int. J. Miner. Metall. Mater.*, 2022, **29**, 990–1002.
320 Z. Wang, X. Xu, Z. Liu, D. Zhang, J. Yuan and J. Liu, *Chem. – A Eur. J.*, 2021, **27**, 13494–13512.
321 D. Yang, C. Zhang, J. J. Biendicho, X. Han, Z. Liang, R. Du, M. Li, J. Li, J. Arbiol, J. Llorca, Y. Zhou, J. R. Morante and A. Cabot, *ACS Nano*, 2020, **14**, 15492–15504.
322 W. Luo, Y. Wang, E. Hitz, Y. Lin, B. Yang and L. Hu, *Adv. Funct. Mater.*, 2017, **27**, 1–19.
323 Y. Fan, D. Liu, M. M. Rahman, T. Tao, W. Lei, S. Mateti, B. Yu, J. Wang, C. Yang and Y. Chen, *ACS Appl. Energy Mater.*, 2019, **2**, 2620–2628.
324 W. Luo, L. Zhou, K. Fu, Z. Yang, J. Wan, M. Manno, Y. Yao, H. Zhu, B. Yang and L. Hu, *Nano Lett.*, 2015, **15**, 6149–6154.
325 P. J. H. Kim, J. Seo, K. Fu, J. Choi, Z. Liu, J. Kwon, L. Hu and U. Paik, *NPG Asia Mater.*, 2017, **9**, e375.
326 H. S. Kim, H. J. Kang, H. Lim, H. J. Hwang, J. W. Park, T. G. Lee, S. Y. Cho, S. G. Jang and Y. S. Jun, *Nanomaterials*, 2021, **11**, 471.
327 P. Zhou, D. Yao, H. Liang, Y. Xia and Y. P. Zeng, *Ceram. Int.*, 2022, **49**, 1381–1389.
328 Q. Shen, L. Huang, G. Chen, X. Zhang and Y. Chen, *J. Alloys Compd.*, 2020, **845**, 155543.
329 W. Yao, C. Tian, C. Yang, J. Xu, Y. Meng, I. Manke, N. Chen, Z. Wu, L. Zhan, Y. Wang and R. Chen, *Adv. Mater.*, 2022, **34**, 1–13.
330 X. Kang, Z. Jin, H. Peng, Z. Cheng, L. Liu, X. Li, L. Xie, J. Zhang and Y. Dong, *J. Colloid Interface Sci.*, 2023, **637**, 161–172.
331 F. Ma, X. Zhang, K. Sriniva, D. Liu, Z. Zhang, X. Chen, W. Zhang, Q. Wu and Y. Chen, *J. Mater. Chem. A*, 2022, **10**, 8578–8590.
332 H. Y. Zhang, R. Q. Dai, S. Zhu, L. Z. Zhou, Q. J. Xu and Y. L. Min, *Chem. Eng. J.*, 2022, **429**, 132454.
333 B. Guan, Y. Zhang, L. Fan, X. Wu, M. Wang, Y. Qiu, N. Zhang and K. Sun, *ACS Nano*, 2019, **13**, 6742–6750.
334 A. E. Shrshr, Y. Dong, M. A. Al-Tahan, X. Kang, H. Guan, X. Zheng and J. Zhang, *J. Alloys Compd.*, 2022, **910**, 164917.
335 Z. Guo, Y. Zhao, Y. Miao, D. Wang and D. Zhang, *ACS Appl. Energy Mater.*, 2022, **5**, 11844–11852.
336 Y. Yuan, F. Wu, G. Chen, Y. Bai and C. Wu, *J. Energy Chem.*, 2019, **37**, 197–203.
337 Y. Chen, W. Zhang, D. Zhou, H. Tian, D. Su, C. Wang, D. Stockdale, F. Kang, B. Li and G. Wang, *ACS Nano*, 2019, **13**, 4731–4741.
338 Z. Wu, S. Chen, L. Wang, Q. Deng, Z. Zeng, J. Wang and S. Deng, *Energy Storage Mater.*, 2021, **38**, 381–388.
339 X. Wang, N. Deng, Y. Liu, L. Wei, H. Wang, Y. Li, B. Cheng and W. Kang, *Chem. Eng. J.*, 2022, **450**, 138191.
340 Z. Ren, Z. Zhao, K. Zhang, X. Wang and Y. Wang, *ChemElectroChem*, 2021, **8**, 1531–1536.
341 X. Zhang, X. Lv, C. Wei and J. G. Wang, *Appl. Surf. Sci.*, 2021, **568**, 150952.
342 Y. Tian, G. Li, Y. Zhang, D. Luo, X. Wang, Y. Zhao, H. Liu, P. Ji, X. Du, J. Li and Z. Chen, *Adv. Mater.*, 2020, **32**, 1–11.
343 Y. Li, W. Wang, B. Zhang, L. Fu, M. Wan, G. Li, Z. Cai, S. Tu, X. Duan, Z. W. Seh, J. Jiang and Y. Sun, *Nano Lett.*, 2021, **21**, 6656–6663.
344 J. Liu, J. Wang, L. Zhu, X. Chen, G. Yi, Q. Ma, S. Sun, N. Wang, X. Cui, Q. Chai, J. Feng and W. Yan, *J. Mater. Chem. A*, 2022, **10**, 14098–14110.
345 S. Luiso, M. J. Petrecca, A. H. Williams, J. Christopher, O. D. Velev, B. Pourdeyhimi and P. S. Fedkiw, *ACS Appl. Polym. Mater.*, 2022, **4**, 3676–3686.
346 G. Sun, S. Jiang, X. Feng, X. Shi, X. Zhang, T. Li, N. Chen, L. Hou, S. Qi and D. Wu, *J. Membr. Sci.*, 2022, **645**, 120208.
347 M. Guo, H. Zhu, P. Wan, F. Xu, C. Wang, S. Lu, Y. Zhang, H. Fan and J. Xu, *Adv. Fiber Mater.*, 2022, **2022**, 1–14.
348 X. Niu, J. Li, J. Song, Y. Li and T. He, *ACS Appl. Energy Mater.*, 2021, **4**, 11080–11089.
349 S. Kim, M. S. Kwon, J. H. Han, J. Yuk, J. Y. Lee, K. T. Lee and T. H. Kim, *J. Power Sources*, 2021, **482**, 228907.
350 S. Choudhury, M. Azizi, I. Raguzin, M. Göbel, S. Michel, F. Simon, A. Willomitzer, V. Mechtcherine, M. Stamm and L. Ionov, *Phys. Chem. Chem. Phys.*, 2017, **19**, 11239–11248.
351 Y. Feng, G. Wang, W. Kang, N. Deng and B. Cheng, *Electrochim. Acta*, 2021, **365**, 137344.
352 X. Zhu, Y. Ouyang, J. Chen, X. Zhu, X. Luo, F. Lai, H. Zhang, Y. E. Miao and T. Liu, *J. Mater. Chem. A*, 2019, **7**, 3253–3263.
353 Y. Wang, Z. Zhang, L. Dong and Y. Jin, *J. Membr. Sci.*, 2020, **595**, 117581.
354 Y. Yang, H. Xu, S. Wang, Y. Deng, X. Qin, X. Qin and G. Chen, *Electrochim. Acta*, 2019, **297**, 641–649.
355 M. S. Kiai, O. Eroglu and H. Kizil, *J. Appl. Polym. Sci.*, 2020, **137**, 1–9.
356 D. Huang, C. Liang, L. Chen, M. Tang, Z. Zheng and Z. Wang, *J. Mater. Sci.*, 2021, **56**, 5868–5877.
357 L. Y. Yang, J. H. Cao, B. R. Cai, T. Liang and D. Y. Wu, *Electrochim. Acta*, 2021, **382**, 138346.
358 L. Zhang, T. Qian, X. Zhu, Z. Hu, M. Wang, L. Zhang, T. Jiang, J. H. Tian and C. Yan, *Chem. Soc. Rev.*, 2019, **48**, 5432–5453.
359 S. Ai, M. Xiao, J. Chen, P. Wang, N. Li, J. He, W. L. Song and H. Sen Chen, *Energy Technol.*, 2022, **10**, 2200017.
360 I. Dienwiebel, M. Winter and M. Borner, *J. Phys. Chem. C*, 2022, **126**, 11016–11025.

361 Y. Deng, Y. Pan, Z. Zhang, Y. Fu, L. Gong, C. Liu, J. Yang, H. Zhang and X. Cheng, *Adv. Funct. Mater.*, 2022, **32**, 2106176.
362 J. Zhao, G. Zhou, K. Yan, J. Xie, Y. Li, L. Liao, Y. Jin, K. Liu, P. C. Hsu, J. Wang, H. M. Cheng and Y. Cui, *Nat. Nanotechnol.*, 2017, **12**, 993–999.
363 R. Mori, *J. Solid State Electrochem.*, 2023, DOI: **10.1007/s10008-023-05387-z**.
364 Y. Wang, Z. Zhang, M. Haibara, D. Sun, X. Ma, Y. Jin, H. Munakata and K. Kanamura, *Electrochim. Acta*, 2017, **255**, 109–117.
365 C. Choi and D. W. Kim, *J. Power Sources*, 2020, **448**, 1–11.
366 J. Cho, Y. K. Ahn, Y. J. Gong, S. Pyo, J. Yoo and Y. S. Kim, *Sustainable Energy Fuels*, 2020, **4**, 3051–3057.
367 J. Wu, S. Liu, J. Huang, Y. Cui, P. Ma, D. Wu and K. Matyjaszewski, *Macromolecules*, 2021, **54**, 2992–2999.
368 A. Kim, J. Hak Kim and R. Patel, *Bioresour. Technol.*, 2021, **345**, 126501.
369 S.-J. Tan, Y.-F. Tian, Y. Zhao, X.-X. Feng, J. Zhang, C.-H. Zhang, M. Fan, J.-C. Guo, Y.-X. Yin, F. Wang, S. Xin and Y.-G. Guo, *J. Am. Chem. Soc.*, 2022, **144**, 18240–18245.
370 Z. Wei, N. Zhang, T. Feng, F. Wu, T. Zhao and R. Chen, *Chem. Eng. J.*, 2022, **430**, 132678.
371 Y. Li, J. Zhang, C. Zhou, M. Ling, J. Lu, Y. Hou, Q. Zhang, Q. He, X. Zhan and F. Chen, *J. Alloys Compd.*, 2020, **826**, 154197.
372 B. Yu, Y. Fan, S. Mateti, D. Kim, C. Zhao, S. Lu, X. Liu, Q. Rong, T. Tao, K. K. Tanwar, X. Tan, S. C. Smith and Y. I. Chen, *ACS Nano*, 2021, **15**, 1358–1369.
373 J. Balach, H. K. Singh, S. Gomoll, T. Jaumann, M. Klose, S. Oswald, M. Richter, J. Eckert and L. Giebeler, *ACS Appl. Mater. Interfaces*, 2016, **8**, 14586–14595.
374 X. Liu, J. Zhao, J. Wang, Z. Le, P. Nie, H. Wang, T. Xu, G. Xu, L. Chang and M. Zhu, *J. Energy Storage*, 2022, **54**, 105324.
375 V. K. Bharti, A. D. Pathak, C. S. Sharma and M. Khandelwal, *Carbohydr. Polym.*, 2022, **293**, 119731.
376 W. D. Hsu, P. W. Yang, H. Y. Chen, P. H. Wu, P. C. Wu, C. W. Hu, L. Saravanan, Y. F. Liao, Y. T. Su, D. Bhalothia, T. Y. Chen and C. C. Chang, *Sci. Rep.*, 2021, **11**(1), 1–15.